THE XMAP215 FAMILY DRIVES MICROTUBULE POLYMERIZATION USING A STRUCTURALLY DIVERSE TOG ARRAY

Jaime Nicole Campbell

A dissertation submitted to the faculty of the University of North Carolina at Chapel Hill in partial fulfillment of the requirements for the degree of Doctor of Philosophy in the Department of Biochemistry and Biophysics.

Chapel Hill

2014

Approved by:

Kevin Slep

Dorothy Erie

William Marzluff

Edward Salmon

John Sondek

ABSTRACT

Jaime Nicole Campbell: The XMAP215 family drives microtubule polymerization using a structurally diverse TOG array
(Under the direction of Dr. Kevin C. Slep)

XMAP215 family members are potent microtubule (MT) polymerases, with mutants displaying reduced MT growth rates and aberrant spindle morphologies. XMAP215 proteins contain arrayed TOG domains that bind tubulin. Whether these TOG domains are functionally equivalent and how they collectively operate to drive polymerization remains unknown. Here, we present crystal structures of TOG4 from *Drosophila* Msps and human ch-TOG. These TOG4 structures architecturally depart from the structures of TOG domains 1 and 2, revealing a conserved domain bend that predicts a novel engagement with α-tubulin. *In vitro* assays show differential tubulin-binding affinities across the TOG array, as well as differential effects on MT nucleation and polymerization. We used *Drosophila* S2 cells depleted of endogenous Msps to assess the importance of individual TOG domains. While a TOG1-4 array largely rescues MT polymerization rates, mutating tubulin-binding determinants in any single TOG domain dramatically reduces rescue activity. Our work highlights the structurally diverse, yet positionally conserved TOG array that drives MT polymerization. XMAP215 family function in mitosis has been closely linked to a centrosomal binding factor, the TACC family of proteins. TACC family proteins have proven important structural components of the mitotic spindle apparatus. Disruption of TACC function causes disorganized and unstable spindle microtubules leading to multiple biological

consequences including chromosome instability, developmental problems, and cancer (reviewed in Thakur et al., 2013). The mechanism in which TACC family proteins functions at the centrosome is still poorly understood. Our study aims to further the field of centrosome biology by understanding how members of the TACC family are interacting with its binding partners, specifically XMAP215 family members. Here we have identified a minimal domain of the *Drosophila* TACC family member, DTACC, that confers TACC dimerization, localizes to spindle poles in mitosis and tracks along the MT plus-end potentially through an interaction with the XMAP215 family member Msps in interphase. Mutational analysis has identified specific residues within this minimal domain important for Msps binding and to centrosome localization. Further analysis to structurally characterize the DTACC-Msps interaction is ongoing in the lab.

ACKNOWLEDGEMENTS

First and foremost, I would like to thank my advisor, Dr. Kevin Slep. The past five years have been challenging yet amazingly rewarding. I would not be the scientist I am today without your guidance and example to follow. Thank you for having patience with me over the past six years and for molding me into a well-rounded scientist. I would like to thank my committee members: Dr. Dorothy Erie, Dr. Bill Marzluff, Dr. Ted Salmon, and Dr. John Sondek. Your guidance and knowledge pushed me to think more critically about my science and I enjoyed sharing my work with you each year. I would also like to thank Dr. Barry Lentz and the Molecular and Cellular Biophysics program, Dr. Ashitosh Tripothy at the UNC Macromolecular Interactions Facility and Dr. Michael Miley at the UNC Crystallography Core.

A huge thank you is needed to the members of the Slep lab for making it such a wonderful place to work. To my lab ladies, thanks for the constant support, sugar boosts and comic relief! I couldn't have done it without you! Special thanks go to Erin Romes and Alyssa Manning for the hours of moral support and an ear to listen when needed.

To Mom, Dad, Jake, Jennifer, Jodie and my soon-to-be husband Tom: thank you for supporting me through my extensive time pursuing this degree. Your encouragement and constant praise kept me going in hard times and made good times that much more enjoyable. Without you, I would not have achieved this wonderful goal of earning a Ph.D. I love you all more than words can describe!

PREFACE

The work in Chapter 2 is a methods book chapter written with my graduate advisor, Kevin Slep. This work was published in Methods in molecular biology in 2011. The authors would like to thank Dr. Stephen Rogers for advice. This work was supported by a Basil O'Connor Research Starter Grant from the March of Dimes.

Campbell, J.N., and Slep, K.C. (2011). αβ-Tubulin and Microtubule binding assays. Methods in Molecular Biology, *777*, 87-97.

The work in Chapter 3 is a manuscript that is currently under revision. Josh Currie developed the cellular EB1 comet velocity assay and cloned the Msps 498-1080 WT construct. Kevin Slep crystallized and collected Msps TOG4 diffraction data while I built the model and refined the structure. Amy Howard assisted on the CD experiments and Msps 498-1080 cellular assay.

Campbell, J.N., Howard A.E., Currie, J.D., Rogers, S.L., and Slep, K.C. (submitted August 2013: currently in revision). The XMAP215 family drives microtubule polymerization using a structurally diverse TOG array. Molecular Biology of the Cell.

The work in Chapter 4 was done as a collaborative effort over the past four years with the undergraduate students Rebekah Shaw and Tanner Fader under my supervision. I designed initial truncation constructs with the guidance of Dr. Kevin Slep. Rebekah Shaw performed the cloning and S2 cellular expression under my guidance. I performed all imaging. Tanner Fadero helped design, clone and express all mutational constructs presented.

Rebekah Shaw and Tanner Fadero cloned all DTACC constructs for expression and I purified the proteins. I also cloned, expressed, and purified Msps constructs for this work. SEC-MALS experiments were performed with the assistance of Rebecca Adikes. A manuscript detailing this work is currently being drafted for publication.

TABLE OF CONTENTS

LIST OF TABLES

LIST OF FIGURES

LIST OF ABBREVIATIONS AND SYMBOLS

Å	Angstrom
ARNT	aryl hydrocarbon receptor nuclear translocator
ATP	adenosine triphosphate
β-ME	beta-mercaptoethanol
$CaCl_2$	calcium chloride
CD	circular dichroism
ch-TOG	colonic and hepatic tumor-overexpressed gene
CLASP	CLIP170 associated protein
CLIP170	cytoplasmic linker protein 170
cm	centimeter
CPEB	cytoplasmic polyadenylation element binding protein
$CuSO_4$	copper sulfate
Da	Dalton
DARPin	designed ankryin repeat protein
DMSO	dimethyl sulfoxide
dsRNA	double-stranded RNA
DTACC	*Drosophila* transforming acidic coiled-coil
DTT	dithiothreitol
EB1	end binding protein 1
eGFP	enhanced green fluorescent protein
FBS	fetal bovine serum

FOG-1	Friend of GATA-1
GDP	guanosine diphosphate
GFP	green fluorescent protein
GMPCPP	guanosine-5'-[(α,β)-methyleno]triphosphate
GTP	guanosine triphosphate
HAT	histone acetyltransferase
HCl	hydrochloric acid
HEAT	*H*untingtin, *e*longation factor 3, protein phosphatase 2*A*, *t*arget of rapamycin 1
HR	HEAT repeat
IPTG	isopropyl β-D-1-thiogalactopyranoside
KCl	potassium chloride
kDa	kilo Dalton
KOH	potassium hydroxide
L	liter v. leucine
LSM7	like-SM7
M	molar
MAP	microtubule associated protein
MAP2c	microtubule associated protein 2c
mdeg	millidegrees
mg	milligram
$MgCl_2$	magnesium chloride
min	minute
ml	milliliter

ML	maximum-likelihood
MLHL	phased maximum-likelihood
mM	millimolar
MPa	megapascal
Msps	Minispindles
MTBD	microtubule binding domain
MT	microtubule
MWCO	molecular weigh cut off
NaCl	sodium chloride
NaN_3	sodium azide
Ni^{2+}-NTA	nickel nitrilotriacetic acid
nm	nanometer
PAGE	polyacrylamide gel electrophoresis
PBS	phosphate buffer saline
PCM	pericentriolar material
PEG	polyethylene glycol
rmsd	root-mean-square deviation
RAR	retinoic acid receptor
res	residues
rmsd	root-mean-square deviation
RNAi	RNA interference
rpm	rotations per minute
SAD	single-wavelength anomalous diffraction

SASA	solvent accessible surface area
SDS	sodium dodecyl sulfate
SEC-MALS	size exclusion chromatography coupled with multi-angle light scattering
SeMet	selenomethionine
SPAZ	Ser-Proline Azu-1 motif
SPD	Serine-Proline-Glutamate repeat region
STAT5	signal transducer and activator or transcription 5
TACC	transforming acidic coiled-coil
TOG	tumor-overexpressed gene
TR	thyroid hormone receptors
tRFP	tag red fluorescent protein
tRFP	tagRFP
µg	microgram
µl	microliter
µM	micromolar
µm	micron
UTR	untranslated region
UV	ultraviolet
WT	wild type
XMAP215	*Xenopus* microtubule associated protein 215
+TIP	microtubule plus-end tracking protein

CHAPTER 1: INTRODUCTION

Microtubules are dynamic polymers composed of αβ-tubulin that facilitate many fundamental cellular functions

Microtubules (MTs) are filamentous cytoskeletal polymers that facilitate directed cell migration, establish cell polarity, serve as intracellular transport tracks, and form the bipolar mitotic spindle. MTs can self-organize by the polymerization of highly polarized αβ-tubulin heterodimers in a head-to-tail fashion, resulting in structurally polar protofilaments. Approximately thirteen protofilaments interact laterally creating a hollow, tube-like polymer (Figure 1-1). The polarity of the αβ-tubulin heterodimer is echoed in the structure of the polymer; polymerization predominately occurs at the plus-end where the β subunit is exposed while polymerization is slower at the minus end where the α-subunit is exposed (Desai and Mitchison, 1997; Howard and Hyman, 2003). Polymerization, however, is not static; MTs exhibit a rapid switching between phases of polymerization and depolymerization termed dynamic instability. As a result, events of catastrophe (the transition from polymerization to depolymerization), rescue (the transition from depolymerization to polymerization), and pause are staples of MT dynamics (Mitchison and Kirschner, 1984). Dynamic instability is required for the rapid reorganization of the MT cytoskeleton at the onset of mitosis and is directly observed in the search-and-capture of kinetochores during mitosis (Desai and Mitchison, 1997; Kirschner and Mitchison, 1986; Hayden et al., 1990).

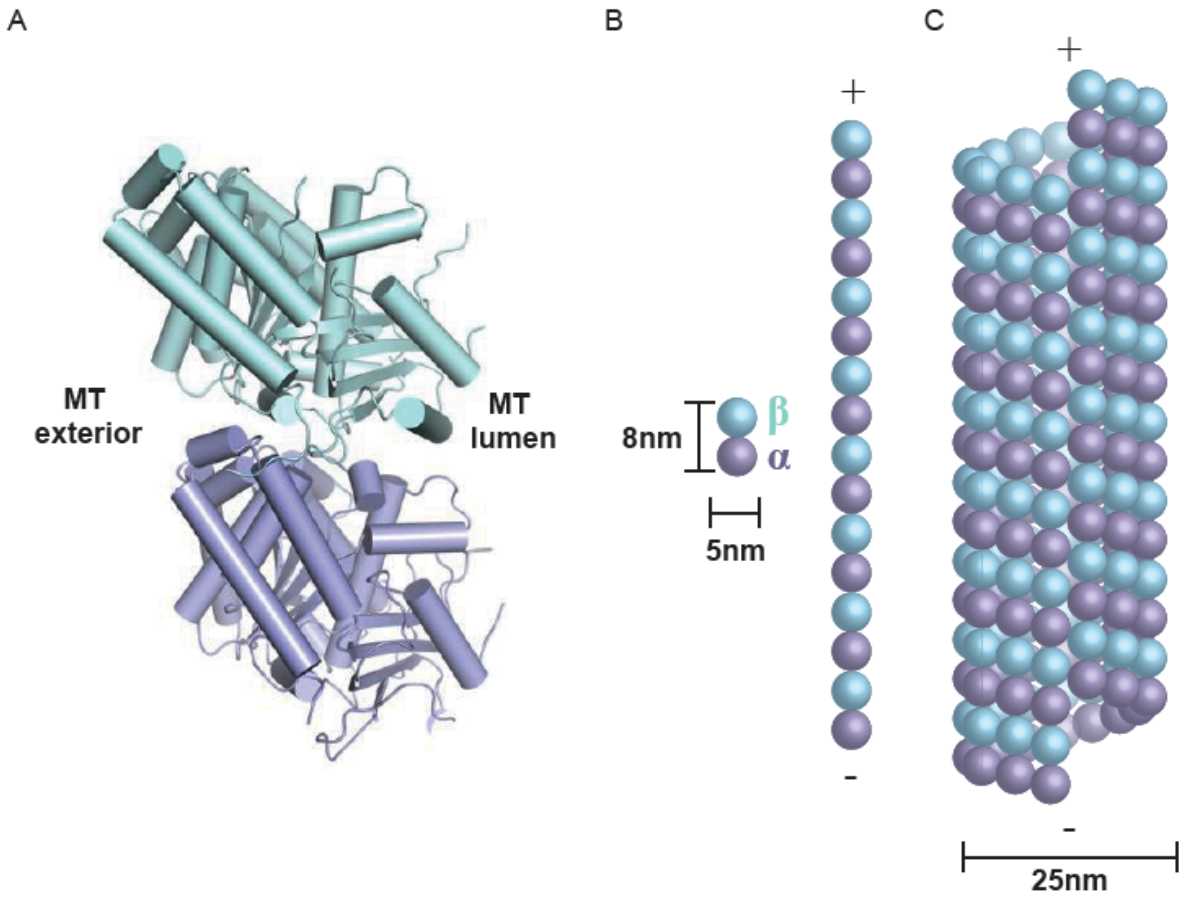

Figure 1-1. **The structure of a microtubule.** (A) The crystal structure of the αβ-tubulin heterodimers (1JFF). (B) Tubulin heterodimers interact longitudinally to form protofilaments. (C) Thirteen protofilaments interact laterally to form a hollow tube-like structure with a 25nm diameter. Plus- and minus-ends of the protofilament and MT are labeled and MT lattice is B-form.

Complete understanding of how MT dynamics are regulated is still unknown. Studies have suggested that the stability of MTs is dependent upon nucleotide hydrolysis, which could account for inherent catastrophe and rescue events observed. Tubulin heterodimers are GTPases that have two GTP binding sites, a non-exchangeable site on α-tubulin that is buried within the α-β interface and an exchangeable site on β-tubulin (Weisenbuer et al., 1976, Spiegelman et al., 1977, David-Pfeuty et al., 1977, MacNeal and Purich, 1978). The GTPase active site found at the β-tubulin GTP site is completed when the α-tubulin subunit of a new heterodimer is incorporated into the MT lattice and interacts longitudinally with the

β-tubulin exchangeable site. Once the active site is complete, GTP can be hydrolyzed into GDP. Non-polymerized tubulin is found mainly in a GTP state, where the β subunit is bound to GTP and the heterodimer is in a bent conformation and GTP hydrolysis occurs at an extremely slow rate (David-Pfeuty et al., 1977, Caplow and Shanks, 1990). Upon incorporation into the MT lattice, tubulin undergoes a conformational change that results in a straight conformation amenable to incorporation into the lattice. Incorporation also activates hydrolysis by completing the GTP active site on β-tubulin, resulting in GTP hydrolysis to GDP and a MT containing predominantly GDP-bound tubulin. GDP tubulin is highly unstable and will depolymerize rapidly. Studies have proposed a 'cap' of GTP tubulin found at the growing plus end of the microtubule that allows sufficient stabilization of the plus-end to facilitate growth and prevent depolymerization (Mitchison and Kirschner, 1984; Chen and Hill, 1985; Kirschner and Mitchison, 1986; Carlier, 1989; Caplow, 1992; Caplow and Shanks, 1995). Tubulin bound to a non-hydrolysable form of GTP (GMPCPP) has been shown to polymerize into stable microtubules that exhibit little to no dynamics (Drechsel and Kirschner, 1994).

Though the GTP cap hypothesis describes a mechanism to switch between phases of polymerization and depolymerization, it does not fully describe the rapid dynamics MTs exhibit *in vivo*. Specifically, it does not account for the rates at which polymerization and depolymerization occur or the frequencies in which catastrophe and rescue occur. MT dynamics have been reconstituted *in vitro* with pure tubulin and GTP (Desai and Mitchison, 1997; Horio and Hotani, 1986; Mitchison and Kirschner, 1984). The rates observed *in vitro* are much slower and transitions between dynamic phases were less frequent than *in vivo* (Kinoshita et al., 2001). This difference is accounted for by an array of microtubule-

associated proteins (MAPs) that regulate MT dynamics *in vivo*. MAPs include proteins that promote polymerization, stabilization, pause or depolymerization (Olmstead, 1986; Belmont and Mitchison, 1996; Sousa et al., 2007). An outstanding question in the cytoskeletal field is to mechanistically understand how these MAPs regulate dynamics *in vivo*.

Microtubule associated proteins (MAPs) regulate MT dynamics

MT associated proteins (MAPs) regulate the rates of polymerization, depolymerization, and the transitions between these states in space and time to facilitate cytoskeletal restructuring, as required during migration or mitotic spindle formation. Determining how MAPs mechanistically regulate MT dynamics is a key area of research in the cytoskeletal field.

One class of MAPs is those that promote MT depolymerization or destabilization. Katanin is an ATPase identified by the Vale lab that binds to and directly severs MTs. The activity of Katanin is dependent upon ATP hydrolysis and the severing events result in rapid disassembly of microtubules (McNally and Vale, 1993). Another example of a destabilizing MAP is the phospho-protein, stathmin. When bound to MTs, stathmin forms a long coiled-coil that binds along multiple tubulin heterodimers, creating curved structure that can promote catastrophe or prevent free tubulin from incorporating into the MT lattice (Belmont and Mitchison, 1996; Ravelli, 2004, Clement et al., 2005). Motor proteins can also promote MT depolymerization. For example, kinesin-13 and kinesin-8 family members destabilize MTs by removing the GTP-cap at the MT plus-end (Howard and Hyman, 2007). An opposing class of MAPs works to promote MT polymerization. A potent member of this class of MAPs is the XMAP215 family, discussed in detail below. The neuronal MAP tau

promotes MT polymerization by opposing kinesin function and subsequently preventing catastrophe (Noetzel et al., 2005).

Microtubule plus end tracking proteins (+TIPs) are a specific class of MAPs that includes the proteins EB1, XMAP215, cytoplasmic linker protein 170 (CLIP170), and CLIP170 associated proteins (CLASPs) that localize to the growing plus-ends of MTs. +TIPS are vital for plus-end dynamics: the loss of for example EB1 results in loss of dynamic MTs (Rogers et al., 2002). EBs are major binding hubs at the plus-end and are necessary for the recruitment of a majority of +TIPs as well as MT dynamics (Rogers et al., 2002). EBs recognize the interface of four tubulin heterodimers (spanning two protofilaments) and bind close to the GTP hydrolysis site of tubulin, specifically recognizing the tubulin nucleotide state that is mimicked by GTPγS. This EB binding interface on MTs could account for recognition of MT structural changes in GTP-hydrolysis dependent manner (Maurer, et al., 2012). EB1 mediates recruitment of other +TIPs by binding SxIP motif proteins or CAP-Gly domain containing proteins (Honnappa et al., 2002; Slep et al, 2007). SxIP motif proteins such as MACF2 bind EB1 along its dimerization domain. EB1 interacts with CAP-Gly domain proteins including the EEY tail of CLIP170 and $p150^{glued}$ EB1. In addition to EEY tail binding, the CAP-Gly domain of $p150^{glued}$ has a second binding site at the four-helix bundle formed by EB1 dimerization.

XMAP215 family members associate with the MT plus-end and promote MT polymerization

XMAP215 family proteins are master MT polymerases that promote MT growth and are critical for mitotic spindle structure and dynamics (Gard and Kirschner, 1987; Vasquez et al., 1994; Cullen et al., 1999; Tournebize et al., 2000; Kosco et al., 2001; Kawamura and

Wasteneys, 2008; Kronja et al., 2009; Cassimeris et al., 2009; Zanic et al., 2013). The XMAP215/Dis1 family of proteins is highly conserved across many species including plants, animals, and fungi (Al-Bassam et al, 2007, Gard et al, 2004). Its name stems from the two original members, XMAP215, isolated from *X. laevis* egg extract and Dis1, identified in *S. pombe* (Gard and Kirschner, 1987; Ohkura et al, 1988). Members of this protein family have been shown to localize to the plus-end of MTs, the MT lattice, the kinetochore and centrosomes (Gard and Kirschner, 1987, Vasques et al, 1994). XMAP215/Dis1 family members stabilize MTs (Ohkura et al., 2001) and regulate microtubule dynamics. When added *in vitro* to purified centrosomes, tubulin and GTP, XMAP215 increases MT polymerization rates 10-fold (Gard and Kirschner, 1987). Depletion of the *Drosophila* XMAP215 member Minispindles (Msps) in cell culture results in disrupted, shortened spindle poles, which can lead to aberrant cell division resulting in aneuploidy and cell death (Brittle and Ohkura, 2005).

Multiple models for the XMAP215/Dis1 tubulin polymerization mechanism have been proposed. Early models predicted XMAP215 proteins act as a template, where multiple tubulin heterodimers are added at once to the MT plus-end (Cassimeris et al., 2001; Kerssemakers et al., 2006). In contrast to this model, single molecule studies have shown XMAP215 to be a processive polymerase, directly adding tubulin heterodimers to the plus end (Brouhard et al., 2008). This study led to a non-templating model where XMAP215 'surfs' along the MT plus end, adding one tubulin heterodimer at a time (Brouhard et al., 2008). How XMAP215 family members potentiate MT polymerization remains unknown.

TOG domains bind tubulin and promote MT polymerization

All XMAP215 family members have an N-terminal TOG domain array and a C-terminal region that links XMAP215 members to other MAPs (Figure 1-2) (Spittle et al., 2000; Lee et al., 2001; van der Vaart et al., 2011, Hsu and Toda, 2011; Li et al., 2011). TOG domains range in size from 220-250 amino acids (Charrasse et al., 1998; Slep, 2009; Al-Bassam and Chang, 2011). While the XMAP215 C-terminal domain differs between yeast and higher eukaryotes, the N-terminal TOG array feature is conserved and can promote MT polymerization in cell culture (Currie et al., 2011). Yeast members Stu2 and Dis1 have two N-terminal TOG domains and a C-terminal coiled coil domain that facilitates dimerization (Gard et al., 2004; Al-Bassam et al., 2006). In contrast, higher eukaryotic XMAP215 members are monomeric and contain a pentameric TOG array. TOG domains are bridged by linkers that are 60-100 amino acids in length and have no predicted secondary structure but contain basic residues that promote MT association (Widlund et al., 2011;Currie et al., 2011).

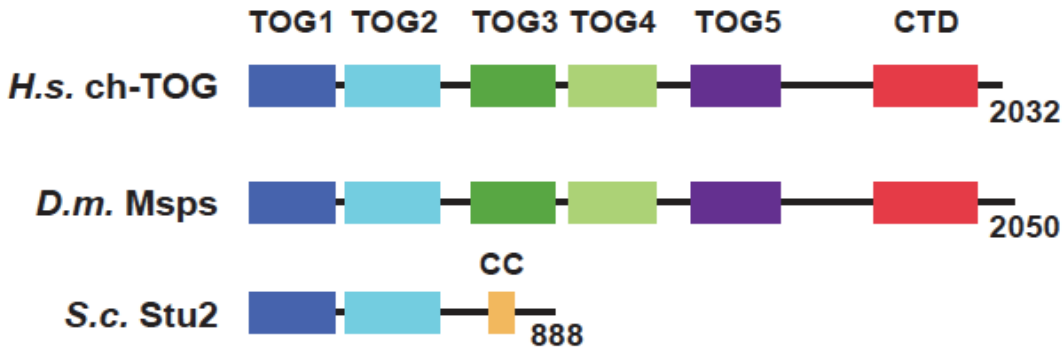

Figure 1-2. XMAP215 family member structural organization. Higher eukaryotes contain five arrayed TOG domains (blues, greens, and purple boxes) and a conserve C-terminal domain (red box). Yeast homologs have two arrayed TOG domains adjacent to a coiled-coil (yellow box) that facilitates dimerization resulting in a functional number of four TOG domains.

TOG domain structures determined to date reveal a series of six *H*untingtin,

*e*longation factor 3, protein phosphatase 2*A*, *t*arget of rapamycin 1 (HEAT) repeats (HR) that form a 60 Å oblong structure (Al-Bassam et al., 2007; Slep and Vale, 2007). The intra-HEAT loops on one face are highly conserved. A recent low-resolution structure of Stu2 TOG1 in complex with a polymerization-blocked mutant αβ-tubulin heterodimer confirmed that the intra-HEAT loop TOG face is the tubulin-interaction surface (Ayaz et al., 2012). In this structure, the first four N-terminal HRs engage β-tubulin while the final two HRs engage α-tubulin, collectively binding αβ-tubulin in a curved conformation thought to be its free, unpolymerized state (Rice et al., 2008; Pecqueur et al., 2012). While TOG domain structures determined to date have provided insight into the XMAP215 mechanism, these studies have only reported structures of TOG1, TOG2 and TOG3 from three diverse species: *S. cerevisiae* Stu2 TOG1 and TOG2, *Drosophila* Msps TOG2, and *C. elegans* Zyg9 TOG3 (Ayaz *et al*., 2012; Slep and Vale, 2007; Al-Bassam *et al.,* 2007). Zyg9 contains a trimeric TOG array that has diverged from other XMAP215 members. While Zyg9's TOG3 sequence is divergent, it is most closely related to TOG5 from XMAP215 family members that contain a pentameric TOG array, but whether Zyg9 TOG3 is functionally and structurally similar to TOG5 remains to be determined (Al-Bassam and Chang, 2011). TOG1 and TOG2 from *S. cerevisiae, S. pombe*, and *Drosophila* can bind tubulin heterodimers as assayed by gel filtration (Al-Bassam et al., 2006; Slep and Vale, 2007; Al-Bassam et al., 2012; Ayaz et al., 2012), but determining how the TOG array promotes MT polymerization requires knowledge of the TOG array's tubulin-binding stoichiometry. Determination of this stoichiometry is complicated by XMAP215-tubulin association and dissociation rates that are tuned to afford rapid, processive polymerization activity. Accordingly, studies to date have calculated quite different stoichiometries for XMAP215 members in complex with tubulin (Al-Bassam et al.,

2006; Kerssemakers, et al., 2006; Slep and Vale, 2007; Brouhard et al., 2008; Ayaz et al., 2012). Models derived from these studies range from a wrap-around model in which functional XMAP215 molecules, either a Stu2 dimer or a XMAP215 monomer, use their TOG array(s) to encapsulate a single tubulin heterodimer and deliver it to the MT plus end, versus a templating model in which each TOG domain in the array uses similar tubulin-binding determinants to interact cooperatively with an array of tubulin heterodimers. Key to distinguishing these models is a determination of the structure, tubulin-binding, and MT polymerization activities of each TOG domain within the array. The structures of yeast TOG1, TOG2, *Drosophila* TOG2, and *C. elegans* TOG3 show a conserved TOG structure with little deviation in domain architecture within or across species. However, we lack a structural and functional characterization of the remaining TOG domains in the higher eukaryotic pentameric TOG array (TOG3, 4, and 5), and we do not know whether these TOG domains are equivalent to TOGs 1 and 2 or structurally and functionally distinct.

For my thesis work, I have investigated how the arrayed TOG domains in the XMAP215 family collectively promote MT polymerization, comparing and contrasting the functional and structural properties of TOG domains in the array. We carried out structural, biochemical and cellular studies on the *Drosophila* XMAP215 family member, Msps, and supported our structural findings with a parallel investigation of the human member, ch-TOG. We report the first structures of TOG4 from both Msps and ch-TOG, revealing a TOG domain architecture quite distinct from TOG1 and TOG2. We find that the full TOG array is required for Msps polymerization activity and that it uses architecturally distinct, yet positionally conserved TOG domains, each with different tubulin-binding affinities and MT nucleation activities to drive MT polymerization *in vivo*. ch-TOG, the human homolog in the

XMAP215 family, localizes to MTs through an interaction with SLAIN2, which itself binds EB1 and has EB1-dependent MT plus-end localization. This interaction network greatly enhances MT polymerization rates (van der Vaart et al., 2011). SLAIN also interacts with CLASP and CLIP170. In *Drosophila*, the functional homolog of SLAIN2 is Sentin. Sentin is necessary for Msps plus-end localization and links Msps to EB1 (Li et al., 2011). When depleted of Sentin, *Drosophila* S2 cells mimic EB1 and Msps depletion; MTs are less dynamics and spindles are shorter. MT dynamics were reconstituted *in vitro* with Msps, Sentin and EB1, showing a cooperative, synergistic mechanism of action (Li et al., 2011).

Metazoan XMAP215 family members contain a conserved C-terminal domain that confers plus-end and centrosome localization

Higher eukaryotic members of the XMAP215 family contain a conserved helical domain at the C-terminus (Figure 1-2). Largely uncharacterized, the conserved C-terminal domain is a factor-binding hub that confers localization to specific sub-cellular components. Plus-end localization relies on the C-terminal domain; truncations constructs where the C-terminus has been removed no longer track along growing MT plus-ends but have a dispersed, cytoplasmic localization. The conserved C-terminal domain also interacts with centrosomal proteins from the TACC family of proteins (Lee et al., 2001; Lauffart, 2002) Secondary structure analysis along with NMR analysis suggests the conserved C-terminal domain to contain a putative TOG6 domain followed by two consecutive helices (Hood et al., 2013). Residues C-terminal of the predicted TOG6 domain has been implicated in binding to the TACC domain of TACC3 (Thakur, 2013). This interaction is crucial for the stability of centrosomes, the polymerization of MTs from centrosomes, and ultimately the integrity of the bipolar spindle (Barros et al., 2005; Peset et al., 2005; Gergely et al., 2003).

The TACC family: conserved centrosomal proteins important for mitotic spindle integrity.

Cell division is a highly organized process in which the genome is replicated and equally partitioned into two daughter cells. At the onset of mitosis, the entire microtubule network must completely reorganize to form the bipolar mitotic spindle. Dynamic microtubules are nucleated from two centrosomes at opposing ends of the cell to form the bipolar spindle. Centrosomes are the major microtubule organizing centers in metazoans that nucleate, stabilize and anchor both astral and spindles MTs during mitosis. These organelles are composed of a pair of orthogonally positioned centrioles surrounded by a dense matrix of over 150 scaffolding and regulatory proteins termed pericentriolar material (PCM). Centrioles are microtubule-based structures that exhibit 9-fold symmetry. Centriole duplication is highly regulated; over duplication can lead to aneuploidy, chromosome instability and cancer (reviewed in Brownlee and Rogers, 2013). The minus ends of the microtubules are anchored at the centrosomes while the dynamic plus ends are free to search the cytoplasm and capture chromosomes at the kinetochore. In addition to centriole over duplication, aberrant spindle formation can lead to the miss-segregation of chromosomes, resulting in chromosome instability, cell cycle arrest, developmental defects and apoptosis.

One particular family of centrosomal proteins found to be important for spindle formation and MT stability is the TACC family. TACC proteins were initially identified in a screen of genes amplified in cancer. *TACC1* was identified as a gene implicated in tumor formation as a result of the 8p11 over-amplification in human breast cancer cells (Still et al., 1999). Subsequent studies suggest expression is reduced in other cancer tissue type (Conte et al., 2003, Lauffart et al., 2003). The name *T*ransforming *A*cidic *C*oiled-*C*oil 1 (TACC1) hails from its ability to transform cells, its acidic charge, and the predicted coiled-coil secondary

structure of the C-terminus. Humans have three isoforms of TACC; TACC1 and TACC2 have been implicated in breast cancer and tumorigenesis, while TACC3 has been implicated in multiple myeloma (Still et al., 1999). TACC proteins are conserved from yeast to humans including *S. pombe* (Alp7) *C. elegans* (TAC-1), *D. melanogaster* (DTACC), *X. laevis* (Maskin), and humans (TACC1, TACC2, and TACC3) (Figure 1-3, reviewed in Peset and Vernos, 2008).

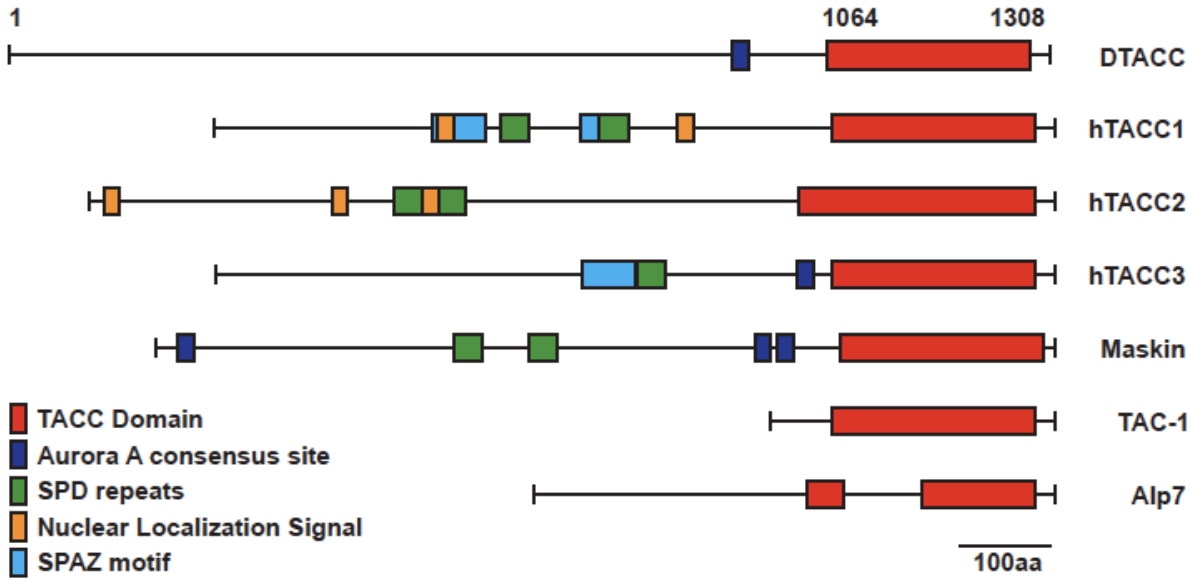

Figure 1-3. Domain architecture of the TACC family proteins. TACC proteins have conserved 200 amino acid C-terminal TACC domains (red) and divergent N-terminal regions. The variable N-terminal region contain domains including Aurora A phosphorylation sites (blue), Ser-Pro-Glu repeat regions (SPD, green), nuclear localization signals (yellow), and Ser-Pro Azu-1 motifs (SPAZ, light blue). Adapted from Peset and Vernos, 2008.

TACC members contain a conserved 200 amino acid TACC domain

The defining feature the TACC family is the presence of a 200 amino acid conserved domain at the C-terminus predicted to be a coiled coil by secondary structure analysis. The N-termini of TACC family homologs are divergent and contain a range of domains (SPD repeats, Ser-Pro Azu-1 motifs, nuclear localization signals, and Aurora A phosphorylation

sites) that contribute to non-mitotic functions (reviewed in Peset and Vernos, 2008). The *C. elegans* homolog is the smallest member of the family (TAC-1) containing only the conserved C-terminal TACC domain (Srayko et al., 2003). The TACC domain alone is sufficient for centrosome localization (Gergely et al., 2000a; Peset et al., 2005). Other localization patterns observed for TACC family proteins are spindle and astral MT decoration as well as nuclear localization in interphase depending on the species and/or isoform (reviewed in Peset and Vernos, 2008).

TACC members have evolved divergent, non-mitotic function

TACC proteins have evolved non-mitotic functions including roles in transcription and the processing of mRNA. Maskin, the *Xenopus* TACC family member, interacts with cytoplasmic polyadenylation element binding protein (CPEB), a known mRNA regulator and eIF-4E, a translation initiation factor. The Maskin-CPEB interaction prevents activation of CPE-containing mRNAs while the Maskin-eIF-4E interaction represses translation (Stebbins-Boaz et al., 1999). Human TACC1 has binding partners that play roles in mRNA processing such as like-SM7 (LSM7) and SmG (Conte et al., 2002). TACC1 has also been associated by yeast two hybrid with nuclear receptors that contribute to transcriptional regulation including, for example, thyroid hormone receptor (TRs), retinoic acid receptor α (RARα) (Guyot et al., 2010). In addition to TACC1's involvement in transcriptional regulation, TACC2, like TACC1, interacts with GAS41 through SPD repeats in the N-terminal region (Lauffart et al, 2002; Lauffart et al., 2003). TACC2 has also been shown through a yeast two-hybrid screen to interact with hGCN5L2, a histone acetyltranferase (HAT) involved in tumor suppression (Gangisetty et al., 2004). The third human homolog, TACC3, is also implicated

in transcription regulation; TACC3 was identified as a binding partner of transcription factors signal transducer and activator of transcription 5 (STAT5), Friend of GATA-1 (FOG-1), and aryl hydrocarbon receptor nuclear translocator (ARNT) (Piekorz et al., 2002; Garriga-Canut et al., 2004; Sadek et al., 2000). Though TACC proteins have been implicated in many instances of transcription regulation, there is little to no conservation of biological function observed across species in these processes and little is known about the mechanism of action.

The TACC domain functions to stabilize MTs in mitosis

TACC function of stabilizing spindle microtubules during mitosis varies only slightly between species. Alp7 in *S. pombe* is required for bipolar spindle formation and is essential for Alp14, the *S. pombe* XMAP215 homolog, localization to spindle pole bodies and mitotic spindles (Sato et al., 2004). Alp7 loss gives a growth defect due to aberrant spindle formation (Sato et al, 2003). TAC-1 depleted *C. elegans* embryos have defects in pronuclear migration during embryogenesis (the first process in *C. elegans* development that requires MTs) and have short MTs and spindles. TAC-1 is also required for sufficient enrichment of Zyg-9, the XMAP215 homolog in *C. elegans*, to the spindle pole (Le Bot et al, 2003; Bellanger and Gonczy, 2003; Srayko, 2003). *Drosophila* DTACC is essential in early embryonic development; mutations in DTACC lead to female sterility while decreased levels of DTACC arrests most embryos (50-70%) in the first mitotic division. Embryos that progress past this point (30-50%) died in embryogenesis due to an accumulation of significant mitotic defects. Injecting DTACC antibodies into syncytial embryos disrupted MT stability and caused short spindle and astral MTs (similar to a Msps depletion)(Gergely et al., 2000a). The *Xenopus* homolog Maskin has been implicated in bipolar spindle integrity, anchoring MTs at the

centrosome, MT length at the centrosome, and XMAP215 localization (Groisman et. al, 2000, O'Brien et al., 2005; Kinoshita et al., 2005; Peset et al., 2005; Albee and Wiese, 2008). TACC1 depletion in HeLa cells had no affect on cell cycle but caused multipolar spindles and abnormal cell division (Conte et al., 2003). In late mitosis, TACC1 localizes to the midzone and midbody in anaphase and cytokinesis, respectively (Delaval et al., 2004). TACC3 is important for stabilizing spindles by recruiting ch-TOG and clatherin to the spindle microtubules. This complex stabilizes K-fibers by bundling adjacent MTs and is regulated by Aurora A kinase (Hood and Royal, 2011; Foraker et al., 2012; Cheeseman et al., 2013).

The TACC domain facilitates binding to XMAP215 family members and other centrosomal proteins

Much of TACC protein family members' function in mitosis is dependent on the evolutionarily conserved interaction with the C-terminus of the XMAP215 family. This interaction is necessary for mitotic spindle stability during cell division (Bellanger and Gonczy, 2003; Srayko et al., 2003; Sato et al., 2004; Conte et al., 2003; O'Brien et al., 2005; Kinoshita et al., 2005; Peset et al., 2005; Lee et al., 2001). This interaction was first reported between *Drosophila* proteins DTACC and Msps where reduction of DTACC resulted in a loss of Msps at the centrosome and instability in spindle MTs (Lee et al., 2001). Structural studies of this interaction are lacking, however recent studies on TACC3 have focused on further elucidating the means of interaction. In 2011, the Royale lab showed a TACC3-clathrin-ch-TOG complex is important for stabilizing K-fibers at the spindle poles (Booth et al., 2011). The Royale lab went on to show that the clathrin-TACC3 interaction is necessary for proper centrosome localization and that complex formation is dependent on the

phosphorylation of Aurora A. This group showed that a predicted 3 amino acid 'stutter' within residues 654-713 in the coiled-coil of TACC3 were required to bind to a putative TOG6 domain (residues 1591-1850) in ch-TOG (Hood et al., 2013). An additional study that showed TACC3 can be functional broken into two sub-domains (CC1 and CC2). CC1 (containing the previously described 'stutter' sequence) interacts with ch-TOG. CC2, or the second half of the TACC domain interacts with a central repeat region in the variable N-terminal domain demonstrating a potential inter-molecular regulatory mechanism (Thakur et al., 2013). Contrary to previous studies, Thakur et al. reported that TACC3-ch-TOG complex formation is independent of Aurora A kinase activity suggesting phosphorylation is necessary for recruitment instead (Barros et al., 2005; Hood et al., 2013). Together, these data are beginning to shed light on the structural mechanism of how TACC and ch-TOG contribute to spindle and MT stability in mitosis.

Here we have identified a minimal domain of that *Drosophila* TACC family member, DTACC, that confers TACC dimerization, localizes to spindle poles in mitosis and tracks along the MT plus-end presumably through the interaction with the XMAP215 family member Msps in interphase. Mutational analysis has identified specific residues within this minimal domain important for Msps binding and centrosome localization. Further analysis to structurally characterize the DTACC-Msps interaction is ongoing in the lab.

REFERENCES

1. Al-Bassam, J., van Breugel, M., Harrison, S.C., and Hyman, A. (2006). Stu2p binds tubulin and undergoes an open-to-closed conformational change. The Journal of Cell Biology *172*, 1009-1022.

2. Al-Bassam, J., Larsen, N. A., Hyman, A. A., and Harrison, S. C. (2007). Crystal structure of a TOG domain: Conserved features of XMAP215/Dis1-family TOG domains and implications for tubulin binding. Structure, *15*(3), 355-362.

3. Al-Bassam, J., and Chang, F. (2011). Regulation of microtubule dynamics by TOG-domain proteins XMAP215/Dis1 and CLASP. Trends in Cell Biololgy *21*, 604-614.

4. Al-Bassam, J., Kim, H., Flor-Parra, I., Lal, N., Velji, H., and Chang, F. (2012). Fission yeast Alp14 is a dose-dependent plus end-tracking microtubule polymerase. Molecular Biology of the Cell *23*, 2878-2890.

5. Albee, A. J., and Wiese, C. (2008). Xenopus TACC3/Maskin is not required for microtubule stability but is required for anchoring microtubules at the centrosome. Molecular Biology of the Cell*, 19*(8), 3347-3356.

6. Andersen, J. S., Wilkinson, C. J., Mayor, T., Mortensen, P., Nigg, E. A., and Mann, M. (2003). Proteomic characterization of the human centrosome by protein correlation profiling. Nature*, 426*(6966), 570-574..

7. Ayaz, P., Ye, X., Huddleston, P., Brautigam, C.A., and Rice, L.M. (2012). A TOG:alphabeta-tubulin complex structure reveals conformation-based mechanisms for a microtubule polymerase. Science *337*, 857-860.

8. Barros, T. P., Kinoshita, K., Hyman, A. A., and Raff, J. W. (2005). Aurora A activates D-TACC-Msps complexes exclusively at centrosomes to stabilize centrosomal microtubules. The Journal of Cell Biology, *170*(7), 1039-1046.

9. Bellanger, J. M., and Gonczy, P. (2003). TAC-1 and ZYG-9 form a complex that promotes microtubule assembly in C. elegans embryos. Current Biology, *13*(17), 1488-1498.

10. Belmont, L. D., and Mitchison, T. J. (1996). Identification of a protein that interacts with tubulin dimers and increases the catastrophe rate of microtubules. Cell, *84*(4), 623-631.

11. Booth, D., G., Hood, F.E., Prior, I.A., and Royale, S.J. (2011). A TACC3/ch-TOG/clathrin complex stabilises kinetochore fibers by inter-microtubule bridging. The EMBO Journal, *30*, 906-919.

12. Brittle, A. L., and Ohkura, H. (2005). Mini spindles, the XMAP215 homologue, suppresses pausing of interphase microtubules in drosophila. The EMBO Journal, *24*(7), 1387-1396.

13. Brouhard, G. J., Stear, J. H., Noetzel, T. L., Al-Bassam, J., Kinoshita, K., Harrison, S. C., Howard, J., and Hyman, A. A. (2008). XMAP215 is a processive microtubule polymerase. Cell, *132*(1), 79-88.

14. Caplow, M. (1992). Microtubule dynamics. Current Opinion in Cell Biology*, 4*(1), 58-65.

15. Caplow, M., and Shanks, J. (1990). Mechanism of the microtubule GTPase reaction. The Journal of Biological Chemistry*, 265*(15), 8935-8941.

16. Caplow, M., and Shanks, J. (1996). Evidence that a single monolayer tubulin-GTP cap is both necessary and sufficient to stabilize microtubules. Molecular Biology of the Cell*, 7*(4), 663-675.

17. Carlier, M. F. (1989). Role of nucleotide hydrolysis in the dynamics of actin filaments and microtubules. International Review of Cytology*, 115*, 139-170.

18. Cassimeris, L., Gard, D., Tran, P. T., and Erickson, H. P. (2001). XMAP215 is a long thin molecule that does not increase microtubule stiffness. Journal of Cell Science*, 114*(Pt 16), 3025-3033.

19. Cassimeris, L., Becker, B., and Carney, B. (2009). TOGp regulates microtubule assembly and density during mitosis and contributes to chromosome directional instability. Cell Motility and the Cytoskeleton *66*, 535-545.

20. Charrasse, S., Schroeder, M., Gauthier-Rouviere, C., Ango, F., Cassimeris, L., Gard, D.L., and Larroque, C. (1998). The TOGp protein is a new human microtubule-associated protein homologous to the Xenopus XMAP215. Journal of Cell Science *111*(Pt 10), 1371-1383.

21. Cheeseman, L. P., Harry, E. F., McAinsh, A. D., Prior, I. A., & Royle, S. J. (2013). Specific removal of TACC3-ch-TOG-clathrin at metaphase deregulates kinetochore fiber tension. Journal of Cell Science*, 126*(Pt 9), 2102-2113.

22. Chen, Y. D., and Hill, T. L. (1985). Monte carlo study of the GTP cap in a five-start helix model of a microtubule. Proceedings of the National Academy of Sciences of the United States of America*, 82*(4), 1131-1135.

23. Clement, M. J., Jourdain, I., Lachkar, S., Savarin, P., Gigant, B., Knossow, M., Toma, F., Sobel, A., and Curmi, P. A. (2005). N-terminal stathmin-like peptides bind tubulin and impede microtubule assembly. Biochemistry, *44*(44), 14616-14625.

24. Conte, N., Charafe-Jauffret, E., Delaval, B., Adelaide, J., Ginestier, C., Geneix, J., Isnardon, D., Jacquemier, J., and Birnbaum, D. (2002). Carcinogenesis and translational controls: TACC1 is down-regulated in human cancers and associates with mRNA regulators. Oncogene, *21*(36), 5619-5630.

25. Conte, N., Delaval, B., Ginestier, C., Ferrand, A., Isnardon, D., Larroque, C., Prigent, C., Seraphin, B., Jacquemier, J., and Birnbaum, D. (2003). TACC1-chTOG-aurora A protein complex in breast cancer. Oncogene, *22*(50), 8102-8116

26. Cullen, C. F., Deak, P., Glover, D. M., and Ohkura, H. (1999). Mini spindles: A gene encoding a conserved microtubule-associated protein required for the integrity of the mitotic spindle in drosophila. The Journal of Cell Biology, *146*(5), 1005-1018.

27. Currie, J.D., Stewman, S., Schimizzi, G., Slep, K.C., Ma, A., and Rogers, S.L. (2011). The microtubule lattice and plus-end association of Drosophila Mini spindles is spatially regulated to fine-tune microtubule dynamics. Molecular Biology of the Cell *22*, 4343-4361.

28. David-Pfeuty, T., Erickson, H. P., and Pantaloni, D. (1977). Guanosine triphosphatase activity of tubulin associated with microtubule assembly. Proceedings of the National Academy of Sciences of the United States of America*, 74*(12), 5372-5376.

29. Delaval, B., Ferrand, A., Conte, N., Larroque, C., Hernandez-Verdun, D., Prigent, C., and Birnbaum, D. (2004). Aurora B -TACC1 protein complex in cytokinesis. Oncogene, *23*(26), 4516-4522.

30. Desai, A., and Mitchison, T. J. (1997). Microtubule polymerization dynamics. Annual Review of Cell and Developmental Biology, *13*, 83-117.

31. Drechsel, D. N., and Kirschner, M. W. (1994). The minimum GTP cap required to stabilize microtubules. Current Biology, *4*(12), 1053-1061.

32. Foraker, A. B., Camus, S. M., Evans, T. M., Majeed, S. R., Chen, C. Y., Taner, S. B., Correa, I.R., Doxsey, S.J., and Brodsky, F. M. (2012). Clathrin promotes centrosome integrity in early mitosis through stabilization of centrosomal ch-TOG. The Journal of Cell Biology, *198*(4), 591-605.

33. Gangisetty, O., Lauffart, B., Sondarva, G. V., Chelsea, D. M., and Still, I. H. (2004). The transforming acidic coiled-coil proteins interact with nuclear histone acetyltransferases. Oncogene, *23*(14), 2559-2563.

34. Gard, D. L., Becker, B. E., and Josh Romney, S. (2004). MAPping the eukaryotic tree of life: Structure, function, and evolution of the MAP215/Dis1 family of microtubule-associated proteins. International Review of Cytology, *239*, 179-272.

35. Gard, D. L., and Kirschner, M. W. (1987). A microtubule-associated protein from xenopus eggs that specifically promotes assembly at the plus-end. The Journal of Cell Biology, *105*(5), 2203-2215.

36. Garriga-Canut, M., and Orkin, S. H. (2004). Transforming acidic coiled-coil protein 3 (TACC3) controls friend of GATA-1 (FOG-1) subcellular localization and regulates the association between GATA-1 and FOG-1 during hematopoiesis. The Journal of Biological Chemistry, *279*(22), 23597-23605.

37. Gergely, F., Kidd, D., Jeffers, K., Wakefield, J. G., and Raff, J. W. (2000a). DTACC: A novel centrosomal protein required for normal spindle function in the early drosophila embryo. The EMBO Journal, *19*(2), 241-252.

38. Gergely, F., Karlsson, C., Still, I., Cowell, J., Killmartin, J., and Raff, J.W. (2000b). The TACC domain identifies a family of centrosomal proteins that can interact with microtubules. Proceeding of the National Academy of Science of the United States of American, *97*(26), 14352-14357.

39. Gergely, F., Draviam, V. M., and Raff, J. W. (2003). The ch-TOG/XMAP215 protein is essential for spindle pole organization in human somatic cells. Genes and Development, *17*(3), 336-341.

40. Groisman, I., Huang, Y.S., Mendez, R., Cao, Q., Theurkauf, W., and Richter, J.D. (2000). Cell, *103*(3), 435-447.

41. Guyot, R., Vincent, S., Bertin, J., Samarut, J., and Ravel-Chapuis, P. (2010). The transforming acidic coiled coil (TACC1) protein modulates the transcriptional activity of the nuclear receptors TR and RAR. BMC Molecular Biology, *11*, 3-2199-11-3.

42. Hayden, J. H., Bowser, S. S., and Rieder, C. L. (1990). Kinetochores capture astral microtubules during chromosome attachment to the mitotic spindle: Direct visualization in live newt lung cells. The Journal of Cell Biology, *111*(3), 1039-1045.

43. Hood, F. E., and Royle, S. J. (2011). Pulling it together: The mitotic function of TACC3. Bioarchitecture *1*(3), 105-109.

44. Hood, F. E., Williams, S. J., Burgess, S. G., Richards, M. W., Roth, D., Straube, A., Pfuhl, M., Bayliss, R., and Royle, S. J. (2013). Coordination of adjacent domains mediates TACC3-ch-TOG-clathrin assembly and mitotic spindle binding. The Journal of Cell Biology, *202*(3), 463-478.

45. Horio, T., and Hotani, H. (1986). Visualization of the dynamic instability of individual microtubules by dark-field microscopy. Nature, *321*(6070), 605-607.

46. Howard, J., and Hyman, A. A. (2003). Dynamics and mechanics of the microtubule plus end. Nature, *422*(6933), 753-758.

47. Howard, J., and Hyman, A. A. (2007). Microtubule polymerases and depolymerases. Current Opinion in Cell Biology, *19*(1), 31-35.

48. Hsu, K.S., and Toda, T. (2011). Ndc80 internal loop interacts with Dis1/TOG to ensure proper kinetochore-spindle attachment in fission yeast. Current Biology, *21*, 214-220.

49. Hyman, A. A., Salser, S., Drechsel, D. N., Unwin, N., and Mitchison, T. J. (1992). Role of GTP hydrolysis in microtubule dynamics: Information from a slowly hydrolyzable analogue, GMPCPP. Molecular Biology of the Cell, *3*(10), 1155-1167.

50. Kawamura, E., and Wasteneys, G.O. (2008). MOR1, the Arabidopsis thaliana homologue of Xenopus MAP215, promotes rapid growth and shrinkage, and suppresses the pausing of microtubules in vivo. Journal of Cell Science, *121*, 4114-4123.

51. Kerssemakers, J.W., Munteanu, E.L., Laan, L., Noetzel, T.L., Janson, M.E., and Dogterom, M. (2006). Assembly dynamics of microtubules at molecular resolution. Nature *442*, 709-712.

52. Kinoshita, K., Arnal, I., Desai, A., Drechsel, D. N., and Hyman, A. A. (2001). Reconstitution of physiological microtubule dynamics using purified components. Science, *294*(5545), 1340-1343.

53. Kinoshita, K., Noetzel, T. L., Pelletier, L., Mechtler, K., Drechsel, D. N., Schwager, A., Lee, M., Raff, J.W., and Hyman, A. A. (2005). Aurora A phosphorylation of TACC3/maskin is required for centrosome-dependent microtubule assembly in mitosis. The Journal of Cell Biology, *170*(7), 1047-1055.

54. Kirschner, M., and Mitchison, T. (1986). Beyond self-assembly: From microtubules to morphogenesis. Cell, *45*(3), 329-342.

55. Kirschner, M. W., and Mitchison, T. (1986). Microtubule dynamics. Nature, *324*(6098), 621.

56. Kosco, K.A., Pearson, C.G., Maddox, P.S., Wang, P.J., Adams, I.R., Salmon, E.D., Bloom, K., and Huffaker, T.C. (2001). Control of microtubule dynamics by Stu2p is essential for spindle orientation and metaphase chromosome alignment in yeast. Molecular Biology of the Cell, *12*, 2870-2880.

57. Kronja, I., Kruljac-Letunic, A., Caudron-Herger, M., Bieling, P., and Karsenti, E. (2009). XMAP215-EB1 interaction is required for proper spindle assembly and chromosome segregation in Xenopus egg extract. Molecular Biology of the Cell, *20*, 2684-2696.

58. Lauffart, B., Gangisetty, O., and Still, I. H. (2003). Molecular cloning, genomic structure and interactions of the putative breast tumor suppressor TACC2. Genomics, *81*(2), 192-201.

59. Lauffart, B., Howell, S. J., Tasch, J. E., Cowell, J. K., and Still, I. H. (2002). Interaction of the transforming acidic coiled-coil 1 (TACC1) protein with ch-TOG and GAS41/NuBI1 suggests multiple TACC1-containing protein complexes in human cells. The Biochemical Journal, *363*(Pt 1)*,* 195-200.

60. Le Bot, N., Tsai, M. C., Andrews, R. K., and Ahringer, J. (2003). TAC-1, a regulator of microtubule length in the C. elegans embryo. Current Biology*, 13*(17), 1499-1505.

61. Lee, M. J., Gergely, F., Jeffers, K., Peak-Chew, S. Y., and Raff, J. W. (2001). Msps/XMAP215 interacts with the centrosomal protein D-TACC to regulate microtubule behaviour. Nature Cell Biology, *3*(7), 643-649.

62. Li, W., Miki, T., Watanabe, T., Kakeno, M., Sugiyama, I., Kaibuchi, K., and Goshima, G. (2011). EB1 promotes microtubule dynamics by recruiting Sentin in Drosophila cells. The Journal of Cell Biology, *193*, 973-983.

63. MacNeal, R. K., and Purich, D. L. (1978). Stoichiometry and role of GTP hydrolysis in bovine neurotubule assembly. The Journal of Biological Chemistry, *253*(13), 4683-4687.

64. McNally, F. J., and Vale, R. D. (1993). Identification of katanin, an ATPase that severs and disassembles stable microtubules. Cell, *75*(3), 419-429.

65. Mitchison, T., and Kirschner, M. (1984). Dynamic instability of microtubule growth. Nature, *312*(5991), 237-242.

66. Noetzel, T. L., Drechsel, D. N., Hyman, A. A., and Kinoshita, K. (2005). A comparison of the ability of XMAP215 and tau to inhibit the microtubule destabilizing activity of XKCM1. Philosophical Transactions of the Royal Society of London. Series B, Biological Sciences, *360*(1455), 591-594.

67. Nogales, E., Wolf, S. G., and Downing, K. H. (1998). Structure of the alpha beta tubulin dimer by electron crystallography. Nature, *391*(6663), 199-203.

68. O'Brien, L. L., Albee, A. J., Liu, L., Tao, W., Dobrzyn, P., Lizarraga, S. B., and Wiese, C. (2005). The xenopus TACC homologue, maskin, functions in mitotic spindle assembly. Molecular Biology of the Cell, *16*(6), 2836-2847.

69. Ohkura, H., Adachi, Y., Kinoshita, N., Niwa, O., Toda, T., and Yanagida, M. (1988). Cold-sensitive and caffeine-supersensitive mutants of the schizosaccharomyces pombe dis genes implicated in sister chromatid separation during mitosis. The EMBO Journal, *7*(5), 1465-1473.

70. Ohkura, H., Garcia, M. A., and Toda, T. (2001). Dis1/TOG universal microtubule adaptors - one MAP for all? Journal of Cell Science, *114*(Pt 21), 3805-3812.

71. Olmsted, J. B. (1986). Microtubule-associated proteins. Annual Review of Cell Biology, *2*, 421-457.

72. Pecqueur, L., Duellberg, C., Dreier, B., Jiang, Q.Y., Wang, C.G., Pluckthun, A., Surrey, T., Gigant, B., and Knossow, M. (2012). A designed ankyrin repeat protein selected to bind to tubulin caps the microtubule plus end. Proceedings of the National Academy of Science fo the United States of America, *109*, 12011-12016.

73. Peset, I., and Vernos, I. (2008). The TACC proteins: TACC-ling microtubule dynamics and centrosome function. Trends in Cell Biology, *18*(8), 379-388.

74. Peset, I., Seiler, J., Sardon, T., Bejarano, L. A., Rybina, S., and Vernos, I. (2005). Function and regulation of Maskin, a TACC family protein, in microtubule growth during mitosis. The Journal of Cell Biology, *170*(7), 1057-1066.

75. Piekorz, R. P., Hoffmeyer, A., Duntsch, C. D., McKay, C., Nakajima, H., Sexl, V., Snyder, L., Rehg, J., and Ihle, J. N. (2002). The centrosomal protein TACC3 is essential for hematopoietic stem cell function and genetically interfaces with p53-regulated apoptosis. The EMBO Journal, *21*(4), 653-664.

76. Ravelli, R. B., Gigant, B., Curmi, P. A., Jourdain, I., Lachkar, S., Sobel, A., and Knossow, M. (2004). Insight into tubulin regulation from a complex with colchicine and a stathmin-like domain. Nature, *428*(6979), 198-202.

77. Rice, L.M., Montabana, E.A., and Agard, D.A. (2008). The lattice as allosteric effector: Structural studies of alpha beta- and gamma-tubulin clarify the role of GTP in microtubule assembly. Proceedings of the National Academy of Science of the United States of America, *105*, 5378-5383.

78. Rogers, S.L., Rogers, G.C., Sharp, D.J., and Vale, R.D. (2002). Drosophila EB1 is important for proper assembly, dynamics, and positioning of the mitotic spindle. The Journal of Cell Biology, *158*, 873-884.

79. Sadek, C. M., Jalaguier, S., Feeney, E. P., Aitola, M., Damdimopoulos, A. E., Pelto-Huikko, M., and Gustafsson, J. A. (2000). Isolation and characterization of AINT: A novel ARNT interacting protein expressed during murine embryonic development. Mechanisms of Development, *97*(1-2), 13-26.

80. Sato, M., Koonrugsa, N., Toda, T., Vardy, L., Tournier, S., and Millar, J. B. (2003). Deletion of Mia1/Alp7 activates Mad2-dependent spindle assembly checkpoint in fission yeast. Nature Cell Biology*, 5*(9), 764-6.

81. Sato, M., Vardy, L., Angel Garcia, M., Koonrugsa, N., and Toda, T. (2004). Interdependency of fission yeast Alp14/TOG and coiled coil protein Alp7 in microtubule localization and bipolar spindle formation. Molecular Biology of the Cell, *15*(4), 1609-1622.

82. Slep, K. C. (2009). The role of TOG domains in microtubule plus end dynamics. Biochemical Society Transactions, *37(Pt 5),* 1002-1006.

83. Slep, K. C., and Vale, R. D. (2007). Structural basis of microtubule plus end tracking by XMAP215, CLIP-170, and EB1. Molecular Cell, *27*(6), 976-991.

84. Sousa, A., Reis, R., Sampaio, P., and Sunkel, C. E. (2007). The drosophila CLASP homologue, Mast/Orbit regulates the dynamic behaviour of interphase microtubules by promoting the pause state. Cell Motility and the Cytoskeleton, *64*(8), 605-620.

85. Spiegelman, B. M., Penningroth, S. M., and Kirschner, M. W. (1977). Turnover of tubulin and the N site GTP in chinese hamster ovary cells. Cell, *12*(3), 587-600.

86. Spittle, C., Charrasse, S., Larroque, C., and Cassimeris, L. (2000). The interaction of TOGp with microtubules and tubulin. Journal Biological Chemistry *275*, 20748-20753.

87. Srayko, M., Quintin, S., Schwager, A., and Hyman, A. A. (2003). Caenorhabditis elegans TAC-1 and ZYG-9 form a complex that is essential for long astral and spindle microtubules. Current Biology*, 13*(17), 1506-1511.

88. Stebbins-Boaz, B., Cao, Q., de Moor, C. H., Mendez, R., and Richter, J. D. (1999). Maskin is a CPEB-associated factor that transiently interacts with elF-4E. Molecular Cell, *4*(6), 1017-1027.

89. Still, I. H., Hamilton, M., Vince, P., Wolfman, A., and Cowell, J. K. (1999). Cloning of TACC1, an embryonically expressed, potentially transforming coiled-coil containing gene, from the 8p11 breast cancer amplicon. Oncogene, *18*(27), 4032-4038.

90. Thakur, H. C., Singh, M., Nagel-Steger, L., Kremer, J., Prumbaum, D., Fansa, E. K., Ezzahoini, H., Nouri, K., Gremer, L., Abts, A., Schmitt, L., Raunser, S., Ahmadian, M.R., and Piekorz, R. P. (2014). The centrosomal adaptor TACC3 and the microtubule polymerase chTOG interact via defined C-terminal subdomains in an aurora-A kinase-independent manner. The Journal of Biological Chemistry, *289*(1), 74-88.

91. Thakur, H. C., Singh, M., Nagel-Steger, L., Prumbaum, D., Fansa, E. K., Gremer, L., Ezzohoini, H., Abts, A., Schmitt, L., Raunser, S., Ahmandian, M.R., and Piekorz, R. P. (2013). Role of centrosomal adaptor proteins of the TACC family in the regulation of microtubule dynamics during mitotic cell division. Biological Chemistry, *394*(11), 1411-1423.

92. Tournebize, R., Popov, A., Kinoshita, K., Ashford, A.J., Rybina, S., Pozniakovsky, A., Mayer, T.U., Walczak, C.E., Karsenti, E., and Hyman, A.A. (2000). Control of microtubule dynamics by the antagonistic activities of XMAP215 and XKCM1 in Xenopus egg extracts. Nature Cell Biology, *2*, 13-19.

93. van der Vaart, B., Manatschal, C., Grigoriev, I., Olieric, V., Gouveia, S.M., Bjelic, S., Demmers, J., Vorobjev, I., Hoogenraad, C.C., Steinmetz, M.O.*, et al.* (2011). SLAIN2 links microtubule plus end-tracking proteins and controls microtubule growth in interphase. The Journal of Cell Biology, *193*, 1083-1099.

94. Vasquez, R.J., Gard, D.L., and Cassimeris, L. (1994). XMAP from Xenopus eggs promotes rapid plus end assembly of microtubules and rapid microtubule polymer turnover. The Journal of Cell Biology, *127*, 985-993.

95. Weisenberg, R. C., and Deery, W. J. (1976). Role of nucleotide hydrolysis in microtubule assembly. Nature*, 263*(5580), 792-793.

96. Widlund, P.O., Stear, J.H., Pozniakovsky, A., Zanic, M., Reber, S., Brouhard, G.J., Hyman, A.A., and Howard, J. (2011). XMAP215 polymerase activity is built by combining multiple tubulin-binding TOG domains and a basic lattice-binding region. Proceedings of the National Academy of Science of the United States of America, *108*, 2741-2746.

97. Zanic, M., Widlund, P.O., Hyman, A.A., and Howard, J. (2013). Synergy between XMAP215 and EB1 increases microtubule growth rates to physiological levels. Nature Cell Biology *15*, 688-693.

CHAPTER 2: αβ-TUBULIN AND MICROTUBULE BINDING ASSAYS [1]

Summary

Dynamic instability is a hallmark of the microtubule cytoskeleton. In order to regulate microtubule dynamics *in vivo*, a varied host of microtubule-associated proteins are mobilized to promote microtubule nucleation, growth, stabilization, catastrophe, depolymerization, rescue and severing. To confer these various functions, cytoskeletal regulators have highly tuned affinities for tubulin, recognizing the unpolymerized αβ-tubulin heterodimer, the dynamic microtubule lattice, the stabilized microtubule lattice, or a combination therein. The protocols presented here assay for αβ-tubulin and microtubule binding using gel filtration and cosedimentation respectively.

Introduction

The microtubule is a polarized structure characterized by a minus end, the site of nucleation, and a plus end where the majority of dynamic growth and depolymerization occurs (Desai and Mitchison, 1997). GTP-bound αβ-tubulin is incorporated into the growing microtubule lattice while GDP-bound αβ-tubulin is released as microtubules depolymerize (Margolis, 1981). Regulators of microtubule dynamics recognize features of free αβ−tubulin and/or the microtubule lattice (Brouhard et al., 2008; Vitre et al., 2008,

[1] Campbell, J.N., and Slep, K.C. (2011). αβ-Tubulin and Microtubule binding assays. Methods in Molecular Biology, *777*, 87-97.

Roll-Mecak and Vale, 2008; Moores et al., 2002). To assay binding between a protein of interest and the various forms of αβ−tubulin (free versus lattice-bound) two methods are discussed: 1) gel filtration to detect αβ−tubulin binding and 2) co-sedimentation to detect binding between a protein of interest and static or dynamic microtubules.

Gel filtration assays use depolymerized, heterodimeric αβ-tubulin and are conducted at 4°C to prevent polymerization. In this assay, the elution profiles of tubulin

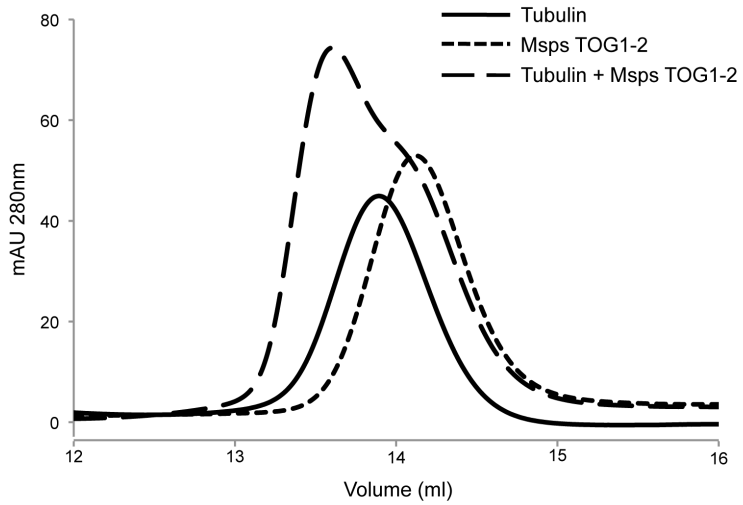

Figure 2-1. **Gel filtration binding assay showing the interaction between the first two TOG domains from *Drosophila* Minispindles (Msps) and αβ-tubulin**. αβ-tubulin, with a molecular weight of 110 kDa, elutes at 13.9 ml when run alone (solid line, injected amount = 50 µl of 20 µM tubulin). Msps TOG1-2, with a molecular weight of 57 kDa, elutes at 14.2 ml when run alone (short dashed line, injected amount = 50 µl of 40 µM Msps TOG1-2). When 20 µM tubulin is incubated with 40 µM Msps and run over gel filtration, a peak elutes at 13.6 ml, earlier than either individual component elutes, indicative of complex formation (long dashed line, injected amount = 50 µl) (Slep and Vale, 2007). Excess Msps creates a right shoulder to the complex peak. A Superdex 200 10/300 GL column was used.

alone, the tubulin-binding protein alone and a mixture of tubulin and the tubulin-binding protein are compared (Figure 2-1). The size exclusion chromatographic step separates proteins and protein complexes based on their relative size and shape. Larger proteins

and protein complexes elute earlier than smaller proteins or protein complexes. A shift in the elution profile of the components to a higher molecular weight as compared to the summated elution profiles of the individual components is indicative of complex

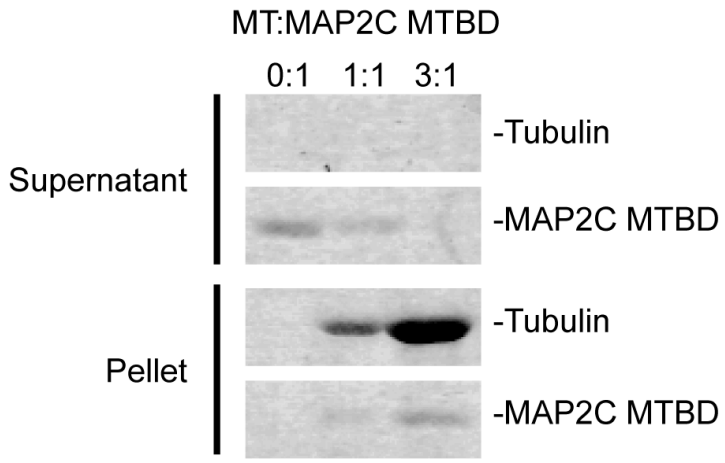

formation. The relative stoichiometric shift can be monitored through fractionation and SDS-PAGE analysis.

Figure 2-2. **The microtubule-binding domain of MAP2C (MAP2C MTBD) cosediments with taxol-stabilized microtubules (MT).** 6 μM MAP2C MTBD was incubated alone and in the presence of 6 and 18 μM taxol-stabilized microtubules representing 0:1, 1:1 and 3:1 MT:MAP2C MTBD ratios respectively. Incubated samples were centrifuged over a 40% glycerol cushion and the supernatant and pellet fractions analyzed by SDS-PAGE and Coomassie staining. All tubulin sedimented to the pellet fraction. MAP2C is present in the supernatant in the absence of taxol-stabilized microtubules but cosediments as the concentration of taxol-stabilized microtubules is increased.

Microtubule co-sedimentation assays are used to determine if a protein has microtubule-binding properties. A centrifugation step pellets taxol-stabilized microtubules or dynamic microtubules through a 40% glycerol cushion. Proteins that bind the microtubule are carried through the glycerol cushion and co-sediment with the microtubules. Proteins that fail to bind the microtubule remain layered above the

glycerol cushion. SDS-PAGE analysis of the supernatant and pellet fractions is used to assay microtubule binding activity. When examining dynamic microtubules, the relative portion of polymerized tubulin in the pellet versus non-polymerized tubulin in the supernatant can be assayed to determine the effect a microtubule regulator has on polymerization.

Materials

Gel filtration tubulin binding assay

1. Purified αβ-tubulin (bovine or porcine) at a concentration of 20 μM or higher (Cytoskeleton, Inc., Denver, CO). (See Note 1).
2. Purified tubulin-binding protein at a concentration of 20 μM or higher.
3. Amicon Ultra centrifugal filters (Millipore, Billerica, MA), 5 or 15 ml capacity.
4. Protein denaturation solution: 6.67 M guanidinium hydrochloride, 22.2 mM phosphate buffer pH 6.5 (for 100 ml solution, add 21.4 g monosodium phosphate, monohydrate and 17.9 g disodium phosphate, heptahydrate). Filter using a 0.22 μm filter.
5. Running buffer: 20 mM Pipes, 200 mM KCl, 1 mM $MgCl_2$, 50 μM GTP (Sigma, St. Louis, MO), 0.1% β-Mercaptoethanol (v/v), adjust pH to 6.5 using KOH. Filter the running buffer using a 0.22 μm filter. (See Note 2).
6. Superdex 200 10/300 GL gel filtration column (GE Healthcare, Piscataway, NJ). (See Note 3).

Taxol-stabilized microtubule cosedimentation assay

1. Materials 1-4 from section 2.1.
2. 2 x BRB80 buffer: 160 mM K-Pipes, 2 mM $MgCl_2$, 2mM EGTA, adjust pH to 6.8 using KOH.
3. GTP stock: 100 mM GTP (Sigma).
4. DTT stock: 1M Dithiothreitol (Sigma).
5. Taxol stock solutions: 20 μM, 200 μM and 2 mM Paclitaxel (Sigma) in DMSO (Sigma). A master stock solution at 100 mM can be prepared in DMSO and stored at -20°C.
6. 7 x 20 mm polycarbonate ultracentrifuge tubes (Beckman Coulter, Inc., Brea, CA, item 343775).
7. Taxol-glycerol cushion solution: 1 x BRB80 buffer supplemented with 40% glycerol and 20 μM taxol. (See Note 4).

Dynamic microtubule cosedimentation assay

1. Materials 1-6 from section 2.2.
2. DMSO (Sigma).
3. GTP-glycerol cushion solution: 1 x BRB80 buffer supplemented with 40% glycerol and 1 mM GTP. (See Note 4).

SDS-polyacrylamide gel electrophoresis (SDS-PAGE)

1. 5 x SDS gel loading buffer: 250 mM Tris-HCl pH 6.8, 10% SDS (w/v), 50% glycerol, 0.02% bromophenol blue (w/v) and 10% beta-mercaptoethanol (v/v). Solid SDS is a respiratory irritant and a mask should be worn when handling it.

2. Molecular weight markers: PageRuler Plus Prestained Protein Ladder (Fermentas Life Sciences, Burlington, Ontario).
3. SDS-Polyacrylamide Tris-HCl gel: 15% resolving gel or a 10-20% linear gradient gel (BioRad, Hercules, CA). (See Note 5).
4. Tris-glycine SDS running buffer: 25 mM Tris, 192 mM glycine, 0.1% SDS, pH 8.3.
5. Coomassie stain: 0.1% Coomassie blue (w/v), 10% acetic acid (v/v) and 40% methanol (v/v).
6. Destain solution: 10% acetic acid (v/v) and 20% methanol (v/v).
7. Kimwipes (Fisher Scientific)

Methods

αβ-Tubulin gel filtration binding assays

1. In order to maintain αβ-tubulin in a heterodimeric, non-polymerized, non-aggregated state, it is important to carry out all steps in this protocol at 4°C.
2. Independently exchange stocks of tubulin and the tubulin binding protein into running buffer at 4˚C. This may be achieved through a 10-fold dilution of the protein stock into running buffer followed by a concentration step using an Amicon Ultra centrifugal filter (Millipore), concentrating to the original volume by centrifugation at 3000 x g, then repeating the dilution, concentration step a second time. Use a centrifugal filter with a nominal molecular weight limit that is less than half the protein's molecular weight.

3. Centrifuge the exchanged protein stock solutions at 50,000 x g for 20 minutes at 4˚C to remove aggregates. Remove supernatant and transfer protein stocks to a clean tube.
4. Determine the concentration of tubulin and the tubulin binding protein using the protein's extinction coefficient at 280 nm. The extinction coefficient (ε_{280}) of GTP-bound αβ-tubulin is 115,000 $M^{-1}cm^{-1}$ (Budde et al., 2006). The extinction coefficient of the tubulin-binding protein can be calculated using the ExPASy ProtParam tool (http://ca.expasy.org/tools/protparam.html) or approximated using the equation ε_{280} = (# Tryptophan)(5690) + (#Tyrosine)(1280) + (# Cystine)(120) $M^{-1}cm^{-1}$ (Gill and von Hippel, 1989). The ε_{280} of any cofactors should be added to the extinction coefficient in accord with binding stoichiometry. To each of three 1.5 ml tubes, add 90 µl of protein denaturation solution and 8 µl of water. To the first tube, add 2 µl of running buffer. To the second tube add 2 µl of concentrated tubulin. To the third tube, add 2 µl of concentrated tubulin-binding protein. Mix the contents of each tube. Place the contents of tube one into a 100 µl, 1 cm path length quartz cuvette and blank a spectrophotometer at 280 nm against this solution. Once the spectrophotometer is blanked, measure the A_{280} of the denatured tubulin and tubulin-binding protein solutions respectively. The A_{280} measurement should be in the range of 0.05 to 1.00 AU. The volume of protein diluted into denaturation solution can be adjusted to obtain an A_{280} value in this range. Calculate the amount of protein in the stock solution using the Beer-Lambert Law for a 50-fold dilution: protein concentration = $(A_{280})(50)/(\varepsilon_{280}\ M^{-1}cm^{-1})(1\ cm)$.

5. Insert the chromatography system's pump A lead into the running buffer and exchange pump A into running buffer.
6. Pre-clean a 50 µl injection loop by flushing with 10 ml of running buffer. Attach the loop to the injection valve.
7. Without a column attached, flush the system with 10 ml of running buffer by setting a flow rate on pump A of 1 ml/min. After 10 ml of running buffer have flowed through the system, reduce the flow to 0.1 ml/min and set the system pressure limit at 1 MPa. Attach the Superdex 200 10/300 GL gel filtration column to the chromatography system between the injection valve and the UV monitor. An active flow attachment process reduces the introduction of air bubbles onto the column. It is best to have a spring-loaded syringe filled with column storage solution attached to the column outlet line to create a reverse flow during the attachment procedure. Once the column's inlet line is connected, immediately remove the spring-loaded syringe to prevent pressure buildup. Attach the column outlet line to the UV monitor and stop the flow from pump A.
8. Equilibrate the Superdex 200 10/30 column with two column volumes of running buffer (one column volume = 24 ml) at a flow rate of 0.5 ml/min with a pressure limit cutoff set at 1 MPa. Monitor the UV trace to ensure that the buffer has exchanged and a baseline at 280 nm has been established.
9. Make protein samples for gel filtration runs. Using 1.5 ml tubes, make 120 µl protein solutions: Tube 1: 20 µM tubulin; Tube 2: 20 µM tubulin-binding protein; Tube 3: 20 µM tubulin + 20 µM tubulin-binding protein. This 1:1 tubulin: tubulin-binding protein stoichiometry can be adjusted in attempts to saturate

binding or to meet non-1:1 binding stoichiometries. Use running buffer to adjust the final volume of protein samples to 120 µl. If tubulin binding is GTP-dependent, the concentration of GTP in the 120 µl solution can be increased from 50 µM to 1 mM by adding 1.2 µl of a 100 mM GTP solution. Prepare protein samples 30 minutes prior to injection, allowing them to incubate at 4°C. (See Note 6).

10. Fit a 5 ml syringe with an injection needle and load 5 ml of running buffer. Set the chromatography injection valve to the load position. Flush the 50 µl loop with 4 ml of running buffer to clean and equilibrate the loop.
11. Fit a 1 ml syringe with an injection needle and load the 120 µl of protein sample. (See Note 7). Do not draw air into the syringe. Set the chromatography injection valve to the load position. Load the 120 µl protein solution into the 50 µl loop and leave the syringe mounted in the injection port. (See Note 8).
12. Run a Superdex 200 10/300 GL column method using a 0.5 ml/min flow rate on pump A and a pressure limit of 1 MPa. Inject the contents of the 50 µl loop using 0.5 ml of running buffer. Monitor absorbance at 280 NM. (See Note 9). Begin to collect eluate in 0.2 ml fractions 20 minutes post injection (once 10.5 ml have flowed over the column). Stop collecting fractions 50 minutes post injection (25.5 ml point). The total volume of the run should be 1.4 column volumes (33.6 ml).
13. Repeat steps 10 through 12 for all samples. The A_{280} chromatographic trace for each sample can be exported to a graphing program, plotted and overlaid for comparison.

14. Comparative analysis of sample fractions using SDS-PAGE: To collected fractions, add 50 µl of 5 x SDS gel loading buffer. Fractions can be stored at -20°C or used immediately for SDS-PAGE analysis. Choose a window of fractions across all runs that cover the range of peak elution. Heat the samples at 95°C for 5 minutes. Follow the procedure in section 3.4 for running and analyzing SDS-polyacrylamide gels.

Taxol-stabilized microtubule cosedimentation assay

1. Preparation of taxol-stabilized microtubules. Dilute tubulin to 2.2 mg/ml (20 µM) in BRB80 buffer. Add GTP and DTT to a final concentration of 1 mM each. Incubate at 4°C for 5 minutes then warm to 37°C. Introduce taxol stepwise as follows: add 1/100 volume of 20 µM taxol in DMSO. Mix gently and incubate at 37°C for 5 minutes. Add 1/100 volume of 0.2 mM taxol in DMSO. Mix gently and incubate at 37°C for 5 minutes. Add 1/100 volume of 2 mM taxol, mix and incubate at 37°C for 15 minutes. Taxol-stabilized microtubules are now formed and can be stored at room temperature. (See Note 10).
2. Exchange the microtubule binding protein under investigation into BRB80 buffer using an Amicon Ultra centrifugal filter as outlined in section 3.1.2. Centrifuge the protein at 100,000 x g at 25°C to clarify. Take the supernatant and determine the protein concentration following the method outlined in section 3.1.4.
3. Warm a Beckman TLA100 fixed angle rotor and a Beckman Optima TL ultracentrifuge to 25°C. An equivalent rotor (fixed angle or swinging bucket) or centrifuge may be substituted.

4. Using 1.5 ml tubes, create 120 µl samples, containing 10 µM taxol-stabilized microtubules (60 µl of product from step 3.2.1) and 10 µM microtubule binding protein. Other taxol-stabilized microtubule: microtubule binding protein ratios can be used promote microtubule saturation and/or determine an apparent affinity (9). Add taxol to maintain a final concentration of 20 µM and add 2 x BRB80 and water to reach a final volume of 120 µl in 1 x BRB80. Create control samples of taxol-stabilized microtubules alone and microtubule binding protein alone. Incubate samples at 25°C for 20 minutes.
5. For each sample, fill a 7 x 20 mm polycarbonate ultracentrifuge tube with 150 µl of the taxol-glycerol cushion solution and equilibrate at 25°C. (See Note 11)
6. Once the microtubule-microtubule binding protein incubation is complete, layer 100 µl of the protein sample above the 150 µl glycerol cushion. Save the remaining 20 µl of protein sample for SDS-PAGE analysis, designated as "load".
7. Insert the centrifuge tubes into the TLA100 rotor. (See Note 12). Centrifuge the samples at 100,000 x g for 30 minutes at 25°C.
8. Remove 50 µl off the top of the supernatant and save this for SDS-PAGE analysis, designated as "supernatant". Remove the remaining 50 µl of solution atop the glycerol cushion and discard. Wash the interface three times with 100 µl of 1 x BRB80 at 25°C.
9. Remove the 150 µl glycerol cushion, keeping the pipet tip on the opposite face of the tube from the pellet.
10. Resuspend the pellet in 100 µl of BRB80 supplemented with 20 µM taxol and save this sample, designated as "pellet".

11. To each sample (load, supernatant and pellet), add 0.25 volumes of 5 x SDS gel loading buffer. Heat the samples to 95°C for 5 minutes. The samples can now be analyzed by SDS-PAGE following the protocol outlined in section 3.4.

Dynamic microtubule cosedimentation assay

1. Follow steps 3.2.2 and 3.2.3, performing these steps at 37°C instead of 25°C.
2. Using 1.5 ml tubes, create 120 µl protein samples in 1 x BRB80 supplemented with 5% DMSO and 1 mM GTP. Protein samples include Tube 1: 20 µM tubulin; Tube 2: 20 µM microtubule binding protein; Tube 3: 20 µM tubulin and 20 µM microtubule binding protein. The concentration of microtubule binding protein can be varied in this assay. Incubate samples at 37°C for 20 minutes to initiate microtubule polymerization.
3. For each sample, fill a 7 x 20 mm polycarbonate ultracentrifuge tubes with 150 µl of the GTP-glycerol cushion solution. (See Note 11). Insert the centrifuge tubes into the 37°C TLA100 rotor. (See Note 12). Warm the rotor and tubes to 37°C.
4. Follow steps 3.2.6 – 3.2.9, performing these steps at 37°C instead of 25°C.
5. Resuspend the pellet in 100 µl of BRB80 supplemented with 5% DMSO and 1 mM GTP and save this sample, designated as "pellet".
6. Follow step 3.2.11.
7. The amount of tubulin in the pellet corresponds with the fraction of polymerized tubulin while the amount in the supernatant represents unpolymerized tubulin, representative of the critical concentration. The level of tubulin in the supernatant and pellet can be quantitated and analyzed to determine if a microtubule or

tubulin binding protein shifts tubulin towards a polymerized or depolymerized state.

SDS-polyacrylamide gel electrophoresis

1. Load a SDS polyacrylamide Tris-HCl gel (15% resolving gel or 10-20% linear gradient gel) onto a gel rig apparatus and fill reservoirs with Tris-glycine SDS running buffer. (See Notes 5 and 13).
2. Remove the comb from the wells and wash the wells with running buffer by pipetting up and down repeatedly in each well. Load equal volumes of protein samples into respective wells, including one well for molecular weight markers. Run the gel at 150 V until the dye front reaches the bottom of the resolving gel. For optimal separation of tubulin (55 kDa) and the tubulin binding protein, use the Pre-stained Molecular Weight Markers as a guide to stop the electrophoresis.
3. Analyze the gel by Coomassie staining, silver staining or Western blot. For Coomassie staining, remove the gel from its case, transfer to a clean container and incubate in Coomassie stain for one hour on a rotating platform. Remove the Coomassie stain and add distain solution. Add a Kimwipe to promote the destaining process.
4. Once destained sufficiently, the gel can be scanned and analyzed for tubulin binding. Quantitative measurements can be made using the Image J program (NIH) to measure band intensity.

Notes

1. Tubulin can be purified from bovine or porcine brain (Borisy et al., 1975). If investigations are anticipated to require gram quantities of tubulin over the course of a year, purifying tubulin can be a cost-effective measure.
2. The gel filtration running buffer can be modified to suit the solubility requirements of the tubulin-binding protein by altering the buffer, pH or salt composition and concentration.
3. A Superose 6 gel filtration column (GE Healthcare) or equivalent may substitute. Ensure that the individual components and complex are within the separation range of the column. Molecular weight standards should be run over the column to determine the column's resolution and to calibrate the column. The chromatography system can also be used in-line with a static light scattering unit to determine the mass of a complex (Slep and Vale, 2007).
4. 40% glycerol can be substituted with 40% sucrose.
5. SDS-PAGE gels can be readily created in the laboratory following standard procedures.
6. 120 µl of protein solution is used to ensure that the 50 µl injection loop is completely filled. This amount can be reduced if reagents are limiting.
7. A disposable 1 ml syringe may be used and is listed here due to common available. A smaller, Hamilton syringe is an alternative option.
8. If the syringe is removed from the injection port, sample can drain from the injection loop before being injected onto the column.

9. To specifically monitor a tubulin shift, tubulin can be doped 1:100 with rhodamine-labeled tubulin (Cytoskeleton, Inc.). A multi-wavelength monitor can be used to detect absorbance at 280 nm (total protein with 280 nm absorbance character) and 500 nm (rhodamine-labeled tubulin) simultaneously. If excess tubulin binding protein masks the location of tubulin, this method enables distinct determination of the tubulin elution profile. Flours can also be covalently attached to the tubulin binding protein or genetically engineered, such as an eGFP fusion, monitored at 460 nm.
10. If the microtubule binding protein is expected to recognize a feature at the end of the microtubule, shearing the taxol-stabilized microtubules by passing them through a 26- or 30-gauge needle can increase the number of microtubule ends. (Pasqualone and Huffaker, 1994).
11. An additional tube may need to be used to balance the rotor.
12. Mark the outermost segment of the centrifuge tube's rim with a lab marker to designate the side of the tube that will contain the pellet.
13. If multiple samples are analyzed, it may be advantageous to skip wells to avoid cross contamination during gel loading or to group the supernatant samples and the pellet samples independently with an empty well between them.

REFERENCES

1. Borisy, G.G., Marcum, J.M., Olmsted, J.B., Murphy, D.B., and Johnson, K.A. (1975). Purification of tubulin and associated high molecular weight proteins from porcine brain and characterization of microtubule assembly in vitro. Annals of the New York Academy of Sciences, *253*, 107-132.

2. Brouhard, G.J., Stear, J.H., Noetzel, T.L., Al-Bassam, J., Kinoshita, K., Harrison, S.C., Howard, J., and Hyman, A.A. (2008). XMAP215 is a processive microtubule polymerase. Cell, *132*, 79-88.

3. Budde, P.P., Desai, A. and Heald, R. (2006). Analysis of microtubule polymerization in vitro and during the cell cycle in Xenopus egg extracts. Methods, *38*, 29-34.

4. Desai, A. and Mitchison, T.J. (1997). Microtubule polymerization dynamics. Annual Review of Cell and Developmental Biology, *13*, 83-117.

5. Gill, S.C. and von Hippel, P.H. (1989). Calculation of protein extinction coefficients from amino acid sequence data. Analytical Biochemistry. *182*, 319-326.

6. Margolis, R.L. (1981). Role of GTP hydrolysis in microtubule treadmilling and assembly. Proceedings of the National Academy of Science of the United States of America, *78*, 1586-1590.

7. Moores, C.A., Hekmat-Nejad, M., Sakowics, R. and Milligan, R.A. (2002). A mechanism for microtubule depolymerization by KinI kinesins. Molecular Cell, *9* 903-909.

8. Pasqualone, D. and Huffaker, T.C. (1994). STU1, a suppressor of a beta-tubulin mutation, encodes a novel and essential component of the yeast mitotic spindle. The Journal of Cell Biology, *127*, 1973-1984.

9. Slep, K.C. and Vale, R.D. (2007). Structural basis of microtubule plus end tracking by XMAP215, CLIP-170, and EB1. Molecular Cell, *27*, 976-991.

10. Vitre, B., Coquelle, F.M., Heichette, C., Chretien, D., and Arnal, I. (2008). EB1 regulates microtubule dynamics and tubulin sheet closure in vitro. Nature Cell Biology, *10*, 415-421.

CHAPTER 3: THE XMAP215 FAMILY DRIVES MICROTUBULE POLYMERIZATION USING A STRUCTURALLY DIVERSE TOG ARRAY

Summary

XMAP215 family members are potent microtubule (MT) polymerases, with mutants displaying reduced MT growth rates and aberrant spindle morphologies. XMAP215 proteins contain arrayed TOG domains that bind tubulin. Whether these TOG domains are functionally equivalent and how they collectively operate to drive polymerization remains unknown. Here, we present crystal structures of TOG4 from *Drosophila* Msps and human ch-TOG. These TOG4 structures architecturally depart from the structures of TOG domains 1 and 2, revealing a conserved domain bend that predicts a novel engagement with α-tubulin. *In vitro* assays show differential tubulin-binding affinities across the TOG array, as well as differential effects on MT nucleation and polymerization. We used *Drosophila* S2 cells depleted of endogenous Msps to assess the importance of individual TOG domains. While a TOG1-4 array largely rescues MT polymerization rates, mutating tubulin-binding determinants in any single TOG domain dramatically reduces rescue activity. Our work highlights the structurally diverse, yet positionally conserved TOG array that drives MT polymerization.

Experimental Procedures

Multi-species alignment

Alignments were produced using CLUSTALW, and adjusted manually based on structural information and secondary structure prediction algorithms (JPred2). Proteins aligned to determine levels of cross-species conservation included ch-TOG (human), Msps (*D. melanogaster*), XMAP215 (*X. laevis*), Stu2 (*S. cerevisiae*), Dis1 (*S. pombe*), Alp14 (*S. pombe*), Mor1 (*A. thaliana*), CP224 (*D. discoideum*), TMBP200 (*N. tabacum*), CKAP5 (*G. gallus*), CKAP5 (*M. musculus*), CKAP5 (*B. taurus*), and CKAP5 (*P. troglodytes*).

Cloning and expression

Msps and ch-TOG bacterial expression constructs were generated by subcloning single or multiple TOG domains into pET28 (Novagen), generating a thrombin-cleavable N-terminal H_6 tagged protein. Fragments subcloned include Msps TOG1-2 (1-505), Msps TOG1-2 (1-516), Msps TOG3-4 (581-1080), Msps TOG4 (848-1087) and ch-TOG TOG4 (846-1081). Mutations were generated using single or multiple rounds of QuikChange mutagenesis (Agilent Technologies). Constructs were transformed into BL21 DE3 (pLysS) *E. coli* and grown at 37° C in 6 L Luria Broth under kanamycin selection (50 μg/L) to an optical density of 1.0 (600 nm). Protein expression was induced with 100 μM IPTG for 16 hours at 18° C. Cells were harvested by centrifugation at 2100 x g for 10 min, resuspended in 300 ml buffer A (25 mM Tris pH 8.0, 300 mM NaCl, 10 mM Imidazole, 0.1% β-ME) and stored at -20° C. SeMet-substituted Msps TOG4 and ch-TOG TOG4 were generated using B834 auxotrophic *E. coli* and minimal media containing L-SeMet (Leahy et al., 1994).

Protein purification

Msps and ch-TOG constructs were purified by sequential Ni^{2+}-NTA and ion exchange chromatography as follows. Cell pellets were thawed and lysed by sonication at 4° C. Phenylmethylsulfonyl fluoride (1 mM final) was added during lysis to prevent proteolytic degradation. Cell lysate was clarified by centrifugation at 23,000 x g for 45 min and the supernatant loaded onto a 10 ml Ni^{2+}-NTA column (Qiagen). The column was washed with 600 ml buffer A and protein eluted using a 250 ml linear gradient between buffer A and B (buffer B = buffer A supplemented with 290 mM imidazole). Protein containing fractions were pooled, $CaCl_2$ added to 1 mM and 0.1 mg bovine α-thrombin added to proteolytically remove the H_6-tag. Thrombin digest proceeded for 16 hours at 4° C. Digested protein was filtered over 0.5 ml Benzamadine sepharose (GE Healthcare), concentrated in a Millipore Ultrafree 10,000 MWCO concentrator, and exchanged into buffer C (25 mM HEPES pH 7.0, 0.1 % β-ME). Protein was loaded onto a 10 ml SP-sepharose fast flow column (GE Healthcare), washed with 200 ml buffer C and eluted over a 250 ml linear gradient between buffer C and D (buffer D = buffer C supplemented with 1 M NaCl). Protein fractions were pooled, concentrated and exchanged into 25 mM HEPES pH 7.0, in a Millipore Ultrafree 10,000 MWCO concentrator to 15 mg/ml or greater, frozen in liquid nitrogen and stored at -80° C. Purification of SeMet-substituted protein proceeded according to the above protocol, except buffers were supplemented with 5 mM L-methionine.

Crystallization

Msps and ch-TOG TOG4 domains were crystallized using the hanging drop vapor diffusion method. 2 µl of Msps TOG4 (native and SeMet-substituted protein) at 15 mg/ml was added to an equal volume of a mother liquor containing 21% PEG 4000, 100 mM Tris

pH 8.5, and 400 mM Li_2SO_4 and equilibrated against 1 ml of mother liquor at 20° C. Crystals were transferred to a cryoprotection solution containing mother liquor supplemented with 15% PEG 4000 and flash frozen in liquid nitrogen. 2 µl of ch-TOG TOG4 at 10 mg/ml was added to an equal volume of a mother liquor containing 28% PEG 4000, 100 mM Tris pH 7.5, and 125 mM $MgCl_2$, equilibrated against 0.5 ml of mother liquor at 20° C. SeMet-substituted ch-TOG TOG4 crystallization followed native parameters except optimal crystals formed using a 0.5 ml well solution of 27.5% PEG 4000, 100 mM Tris pH 7.5, and 70 mM $MgCl_2$.

Data collection, structure determination, and refinement

Isomorphous Msps TOG4 native and selenium SAD peak data sets were collected on single crystals to a resolution of 1.65 and 1.9 Å respectively. Diffraction data were collected at the Advanced Light Source 8.3.1. beamline at 100 K. Msps TOG4 crystals belong to the P1 space group with one molecule in the asymmetric unit. ch-TOG TOG4 native and selenium SAD peak data sets were collected on single crystals to resolutions of 1.9 and 2.5 Å respectively. Diffraction data were collected at the Advanced Photon Source beamlines 22-BM and 22-ID. chTOG native and SeMet-substituted crystals belong to the space groups $P2_12_12_1$ and $P4_32_12$ respectively, with two and one molecules in the asymmetric unit. Data were indexed, integrated and scaled using HKL2000 (Otwinowski et al., 1997). Selenium sites were identified and used to generate initial density modified electron density maps using PHENIX AutoSol (Adams, et al., 2010). Initial models were built using AutoBuild (PHENIX) followed by reiterative manual building in Coot and refinement using phenix.refine (PHENIX) (Adams et al., 2010; Emsley et al., 2010). Selenomethionine-substituted structures were refined against a MLHL target function. The native Msps TOG4

structure was extended to 1.65 Å resolution against a ML target function. ch-TOG TOG4 coordinates were used to solve the native ch-TOG TOG4 structure by the molecular replacement method (AutoMR, PHENIX) and the structure refined as above using a ML target function. The Free R used a random 10% of the data excluded from refinement. Information regarding data statistics, model building and refinement is presented in Table 1. Electrostatics were calculated using APBS (Baker et al., 2001). Pairwise alignments and rmsd values were calculated using the Dali pairwise alignment server (Hasegawa and Holm, 2009). The atomic coordinates will be deposited in the Protein Data Bank for Msps TOG4, ch-TOG SeMet TOG4, space group $P4_32_12$ and ch-TOG TOG4, space group $P2_12_12_1$.

Gel filtration

A Superdex 200 10/300 gel filtration column (GE Healthcare) was used to perform tubulin-binding gel filtration assays. The column was equilibrated in running buffer (20 mM PIPES pH 6.5, 200 mM KCl, 2mM $MgCl_2$, 0.1% β-ME, 50 μM GTP) at 4° C. 120 μl of TOG protein (40 μM) and tubulin (20 μM) was incubated for 25 minutes at 4° C in running buffer supplemented with 150 μM GTP and loaded onto the gel filtration column at a flow rate of 0.5 ml/min.

Light scattering tubulin polymerization assay

Tubulin polymerization was monitored using a SPEX Fluorolog-3 spectrofluorometer (Horiba Jobin Yvon) in T-format, high-voltage mode with the excitation and detection wavelengths set at 350 nm and the excitation and emission slits set at 0.5 and 0.75 nm respectively. The cuvette holder was maintained at 37° C. Clarified tubulin samples (20 μM final concentration) were prepared in the presence or absence of Msps TOG constructs (1 μM final concentration) in polymerization buffer (50 mM MES pH 6.6, 3.4 M glycerol, 5 mM

DTT, 1 mM EGTA, 5 mM $MgSO_4$, 1 mM GTP) and incubated at 4° C for 10 minutes prior to the polymerization assay. 300 µl samples were injected into a 4 mm path length quartz cuvette at room temperature, then immediately placed into the 37° C cuvette holder and scattering recorded at 350 nm in 1 second intervals over 1500 seconds. Spikes in scattering within the first 100 seconds were the result of samples equilibrating to 37 °C.

In vitro microscopic analysis of tubulin polymerization

Tubulin samples (20 µM) doped with 10% rhodamine labeled tubulin were prepared in the presence or absence of Msps34 (1 nM final concentration) in BRB80 (80mM PIPES, 1mM $MgCl_2$, 1mM EGTA, pH 6.8) supplemented with 10% DMSO and 1mM GTP. After incubating on ice for 20 minutes, samples placed at 37° C for 3 minutes then diluted 2-fold into polymerization buffer supplemented with 20 µM taxol. Samples were then flowed into acid washed, poly-lysine and dm1α coated flow chambers and incubated for 30 minutes. Samples were then washed with PBS and fixed with PBS supplemented with 4% para-formaldehyde for 10 minutes. Chambers were washed with PBS and Dako fluorescent mounting media was added. Images were taken using Eclipse Ti microscope with a 40x oil NA-1.0 objective, driven by NIS Elements software (Nikon). Images were processed with ImageJ (NIH) software**.**

Drosophila S2 cell expression constructs

Msps constructs containing TOGs 1-4 (residues 1-1080) were subcloned using Gateway pENTR DTOPO cloning system (Invitrogen) into a final zeocin selective pIZ backbone vector that contained a metallothionein promoter, Gateway (Invitrogen) LR recombination sites, and a COOH-terminal GFP tag. Msps 498-1079 was subcloned into a pMT A vector backbone containing a metallothionein promoter and a COOH-terminal tRFP

(Currie et al., 2011). Mutations were generated using single or multiple rounds of QuikChange mutagenesis (Agilent Technologies). EB1:EB1-tRFP was constructed by cloning approximately 1.5kb of genomic DNA containing the EB1 promoter 5' of EB1-GFP (Rogers et al., 2002). The Msps TOG1-5 GFP and Msps 498-1080 construct has been described previously (Currie et al., 2011).

Cell culture and transfection

S2 cells were grown in Sf-900 media and passed every 3-5 days. Transfections were performed using the Amaxa Nucleofector II transfection system (Lonza) according to the manufacturer's protocol. Constructs were treated with dsRNA for 7 days as previously described (Rogers and Rogers, 2008) and induced 12-18 hours prior to imaging with 80 μM copper sulfate.

RNAi production

For RNAi, the T7 promoter was attached to primer sequences specific to the coding region at the COOH-terminal region of Msps (residues 1752-1927) and dsRNA was generated using T7 RiboMAX *in vitro* transcription (Promega). Primer sequences used were: forward 5'-GCCGAAGTTTACAGACCTGC-3' and reverse 5'-TGTACTTGTGAAATGGGGCA-3'.

Fluorescence microscopy

S2 cells were seeded onto conconavalin-A coated glass bottom dishes (Matek) 30 minutes prior to imaging in Schneider's medium supplemented with 10% FBS. Time-lapse images were collected at room temperature using a 100x numerical aperture 1.45, Plan Apochromat objective using a VT-Hawk (Visitech) 2D array scanning confocal system with

an Orca-R2 CCD camera controlled using VisiTech Vox software. Images were acquired at 3-second frame intervals over 4 minutes.

EB1-tRFP comet tracking

EB1 comet velocities were obtained from time-lapse movies using the ImageJ (N.I.H.) plugin, Manual Tracking (Fabrice Cordelières, Institut Curie, Orsay, France). Single EB1 comets were tracked for their lifetime and the velocity was calculated using 30-second intervals. Mean 30-second velocities were plotted by box-and-whiskers plot (GraphPad, Prism). All TOG1-4-GFP constructs were induced with equivalent levels of copper sulfate. In order to measure EB1 comet rates in cells expressing Msps GFP constructs within a common expression range, the average GFP fluorescence intensity per area was calculated for each cell. Only cells with an average GFP fluorescence intensity per area that fell within a normalized range of 0.6-1.0 were analyzed, limiting the relative concentration of Msps constructs in cells examined to a range spanning 1.7-fold above the minimal concentration scored. Statistical significance was determined using an unpaired T test to calculate two-tailed p-values.

Circular dichroism

Circular dichroism (CD) spectra of individual *Drosophila* TOG domains were collected at room temperature using a Chirascan-plus CD spectrometer (Applied Photophysics, Leatherhead, UK). The TOG domains (TOG1, TOG2, TOG3, TOG4 and TOG5) were diluted to 0.1 mg/ml in 10mM sodium phosphate buffer (pH 7.5) and 50mM sodium fluoride. Spectra were taken using a 1mm path-length cuvette from 260 to 185 nm with a step size of 0.5 nm and a 1.25s time per point. A baseline CD spectrum was recorded and subtracted from each spectrum. Spectra were smoothed using Chirascan-plus software.

Melts were obtained by monitoring CD at 208 and 220 nm in 1°*C* step size from 20°C to 94°C. Melting temperatures of the various proteins were obtained by calculating the first derivative of the melt curves.

Microtubule cosedimentation

Taxol stabilized microtubules were prepared by diluting tubuling to 2.2 mg/mL (20 μM) in BRB80 (80mM PIPES, 1mM $MgCl_2$, 1mM EGTA, pH 6.8) supplemented with 1mM GTP and 1mM DTT. Taxol was added stepwise as follows: 1/100 volume of 20 μM taxol in DMSO was added and samples were incubated at 37 °C for 5 minutes. 1/100 volume of 200 μM taxol in DMSO was added and samples were incubated at 37 °C for 5 minutes. 1/100 volume of 2 mM taxol in DMSO was added and samples were incubated at 37 °C for 15 minutes. Msps constructs were exchanged into BRB80 and 10 μM protein was mixed with 10 μM taxol-stabilized microtubules. The sample was incubated for 20 minutes at 25 °C, layered onto a taxol-glycerol chision, and centrifuged at 100,000 xg for 30 minutes at 25 °C. SDS-PAGE was used to visualize protein in the supernatant and the pellet.

Results

TOG domains in the XMAP215 array display position-dependent conservation

TOG domains in the XMAP215 family are arranged in a pentameric array in higher eukaryotes including human and *Drosophila*, and a dimeric array in yeast (Figure 3-1A). To investigate the similarity of TOG domains in the XMAP215 family array we performed an alignment across 13 diverse species. We mapped residues that were 80% identical (green) and 80% similar (yellow) for each specific TOG domain in the array (i.e. residues conserved across TOG1, residues conserved across TOG2, etc.). Figure 3-1B displays the conservation,

mapped onto three species: human ch-TOG, *Drosophila* Msps, and *S. cerevisiae* Stu2, with all TOG domains from these species aligned. While each specific TOG domain in the array shows a high degree of cross-species conservation, most of this cross-species conservation is not maintained across the different TOG domains within a species. TOG domains comprise 2007). We note greater conservation across the array in HR A and B than in HRs C-F, six HRs (A-F) that form a solenoid-like structure (Al-Bassam et al., 2007; Slep and Vale, suggesting that TOG domains may have divergent structures and or functions in their C-terminal region. To quantitate the differences between TOG domains within and across species, we analyzed and compared human ch-TOG, *Drosophila* Msps, and *S. cerevisiae* Stu2. We first calculated the identity between TOG domains within a species based on the alignment presented in Figure 3-1B (Figure 3-S1 A-C). Consistent with what we observed in our sequence alignment, identity ranged from a low of 11.7% (Msps TOG3 vs. TOG5) to a high of 21.8% (TOG2 vs. TOG4 for both Msps and ch-TOG). We next compared identity across species (Figure 3-1C, 3-S1D, E). When ch-TOG and Msps TOG domains were compared, non-equivalent TOG domains had identities that ranged from 10.4% to 19.7% (Figure 3-1C). Surprisingly, TOG domains at equivalent positions retained much higher sequence identity, spanning 40.1% (TOG3) to 56.5% (TOG1). This reveals that TOG domains have retained positional conservation across species more than pan-array conservation within a species. Similar trends are evident when Msps and ch-TOG are compared with Stu2. Stu2 TOG1 and TOG2 are most identical to Msps and ch-TOG TOG1 and TOG2 respectively (20.7 – 26.4% identity) while Msps and ch-TOG TOG3-5 show significantly lower identity to Stu2 TOG1 or TOG2 (9.2 – 15.8%). These analyses indicate

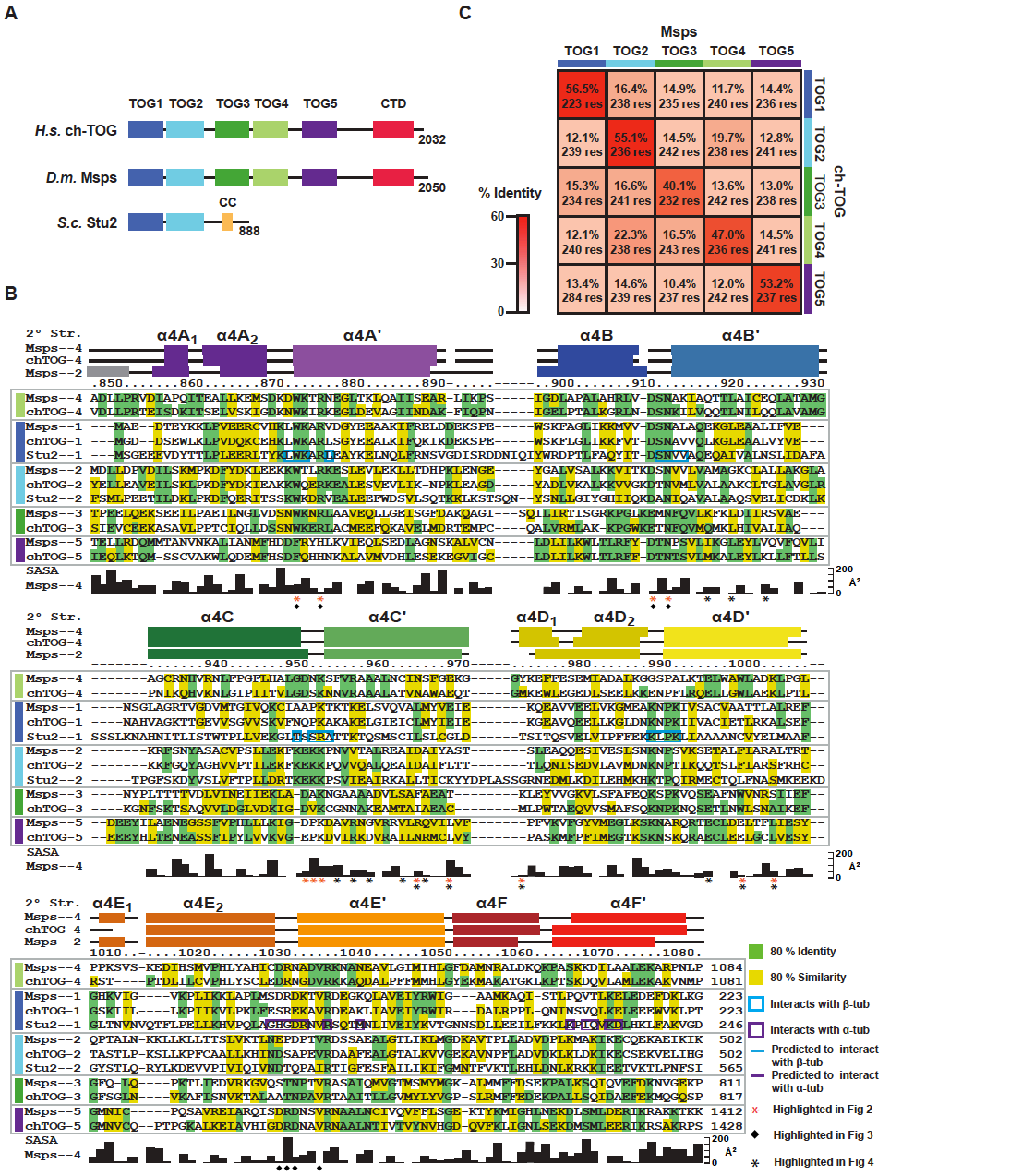

Figure 3-1. TOG domains with unique and universally conserved determinants comprise the XMAP215 family TOG array. (A) Domain architecture of XMAP215 family members ch-TOG, Msps, and Stu2 (CTD: C-terminal Domain; CC: Coiled Coil). (B) Sequence alignment of TOG domains from Msps, ch-TOG, and Stu2. Class-specific TOG conservation has been mapped based on a multi-species alignment: residues with 80% identity (highlighted green) and 80% similarity (highlighted yellow) are indicated for each individual TOG class (TOG1, TOG2, … TOG5). Residue numbers are for Msps TOG4. Msps TOG4 solvent accessible surface area (SASA) is plotted. Stu2 TOG1 residues that interact with α- and β-tubulin are boxed in blue and purple respectively. (C) Identity matrix, comparing sequence identity between Msps and ch-TOG TOG domains.

that TOG domains within an array have position-specific conservation. We asked whether this correlated with position-specific TOG structure and polarized TOG array activity.

Msps TOG4 comprises six HEAT repeats and forms an oblong structure with conserved intra-HEAT loops

XMAP215 family TOG domain structures determined to date include Stu2 TOG1, Stu2 TOG2, Msps TOG2, and Zyg-9 TOG3 (Ayaz et al., 2012; Slep and Vale, 2007; Al-Bassam et al., 2007). These XMAP215 family TOG structures show a similar TOG domain architecture in the arrangement of HRs and the conformation of the intra-HEAT loops that form the tubulin-binding surface (Figure 3-S2). Circular dichroism (CD) analysis revealed all *Drosophila* TOG domain (1-5) are α-helical and have varying thermostability (Figure 3-S3) however, whether all TOG domains in the array have a similar domain architecture remains outstanding. We thus examined whether TOG4 conforms to the architecture of XMAP215 family TOG domain structures determined to date. We obtained native and selenomethionine (SeMet)-substituted isomorphous TOG4 crystals from which native and a single wavelength anomalous dispersion (SAD) data sets were collected respectively. The Msps TOG4 structure was refined to 1.65 Å resolution with R and R_{free} values of 15.7 and 18.7 respectively. Crystallographic and refinement information is presented in Table 1.

Like other TOG domains, the Msps TOG4 structure is helical, composed of six HRs that form an oblong structure of dimensions 15 x 30 x 55 Å (Figure 3-2A). HRs are defined by an antiparallel pair of helices in which the first helix undergoes a bend near its N-terminus. HRs are labeled A-F with paired helices denoted X and X' (Slep and Vale, 2007).

If a helix is split, we delineate it with subscripts: X_1 and X_2. The number that precedes the HR indicates the specific TOG domain, i.e. TOG4. As observed in other TOG domains, the TOG4 HRs are structurally divided into two triads: HR A-C and HR D-F. Within a triad, the HRs pack linearly against one another with a slight twist, common in HR-containing proteins (Andrade et al., 2001). Between TOG4 HR C and D, there is an offset afforded by $\alpha4D_1$, that effectively positions α4D' alongside α4C (Figure 3-2A, lower panel). While the HR A-C triad has a right-handed twist, the HR D-F triad has a right-handed twist between repeats D and E, but a dramatic change to a left-handed twist between HR E and F. Msps TOG4 has conserved, intra-HEAT determinants in the first HR triad that parallel those used by Stu2 TOG1 to bind β-tubulin. Mapping TOG4-specific conservation onto the Msps TOG4 structure using the contours in Figure 3-1B maps the highest degree of invariance and similarity to the intra-HEAT loops (Figure 3-2B, upper panel). This surface has a net positive charge (Figure 3-2B, lower panel) that would complement the negatively charged tubulin surface on the MT exterior. Previous work mutating residues on this face of TOG1 and TOG2 abrogated the ability of the TOG domains to bind tubulin (Al-Bassam et al., 2007; Slep and Vale, 2007; Ayaz et al., 2012). In the recent Stu2 TOG1-αβ-tubulin complex structure, the TOG1 intra-HEAT loop face engages αβ-tubulin heterodimer: HR A-D binds β-tubulin and HR E-F binds α-tubulin (Ayaz et al., 2012). Similar tubulin-binding determinants are found on the TOG4 intra-HEAT surface, including a conserved, surface-exposed tryptophan (W874) in the intra-HEAT A loop and a lysine residue (K954) in the intra-HEAT C loop (Figure 3-2C, D). The intra-HEAT A loop tryptophan (W874) is conserved across all Msps TOG domains except TOG5, where a phenylalanine is positioned.

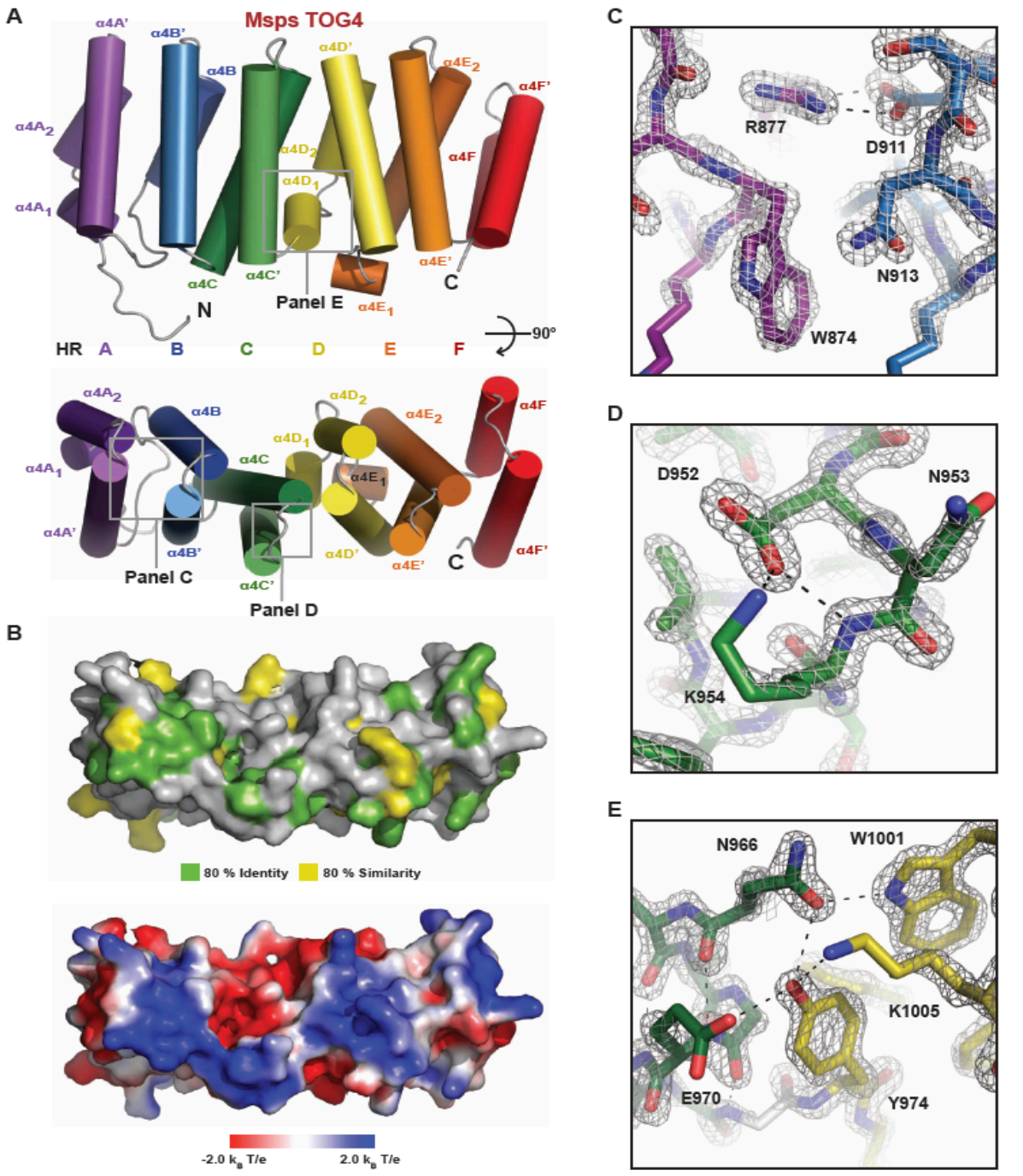

Figure 3-2. Structure of Msps TOG4. (A) Cartoon representation of the Msps TOG4 domain. TOG4 consists of six HRs, A-F. (B) Msps TOG4 in surface representation (oriented as in A, lower panel) mapping TOG4-specific conservation (above) as in Figure 3-1B and electrostatics (below). (C-E) $2F_o$-F_c electron density map (2σ) illustrating the HR A loop W874 residue and the R877-D911 salt bridge (C), the HR C loop D952-K954 interaction (D), and the buried HR C-D interaction network (E).

W874 is stabilized by a conserved salt bridge formed between aspartate D911 and arginine R877 (Figure 3-2C). In the intra-HEAT C loop, K954 is stabilized by a hydrogen bond between its backbone amide and side chain amine with the aspartate D952 side chain carboxyl (Figure 3-2D). The highest degree of surface-exposed intra-HEAT conservation maps to the HR A-C triad, consistent with the idea that these TOG4 HR A-C triad determinants engage β-tubulin as observed in the Stu2-TOG1-αβ-tubulin structure. At the interface of the two HR triads, Msps TOG4 uses a set of TOG4-specific conserved determinants to form a buried hydrogen-bond network involving HR C N966 and E970 and HR D Y974, W1001, and K1005 (Figure 3-2E). HR C and HR D are bridged by the $\alpha 4D_1$ helix that directs Msps Y974 (ch-TOG M974) into the domain's core. Surprisingly, the presence of $\alpha 4D_1$ and its bulky side chains wedge the two HR triads apart into an architecture not observed in XMAP215 family TOG domains determined to date, as we describe in detail below.

Human ch-TOG TOG4 is structurally identical to Drosophila Msps TOG4

Before comparing and contrasting structural differences between TOG domains within a species' array, we asked whether the structure of TOG4 was conserved across species and chose human ch-TOG TOG4 as a comparative target. We determined the structure of human ch-TOG TOG4 in two space groups (Figure 3-3A-C). The structure of SeMet-substituted TOG4 was determined to 2.5 Å resolution (space group $P4_32_12$; one TOG4 molecule in the asymmetric unit) and refined to R and R_{free} values of 20.8 and 27.6 respectively. A native structure was also determined to 1.9 Å resolution (space group

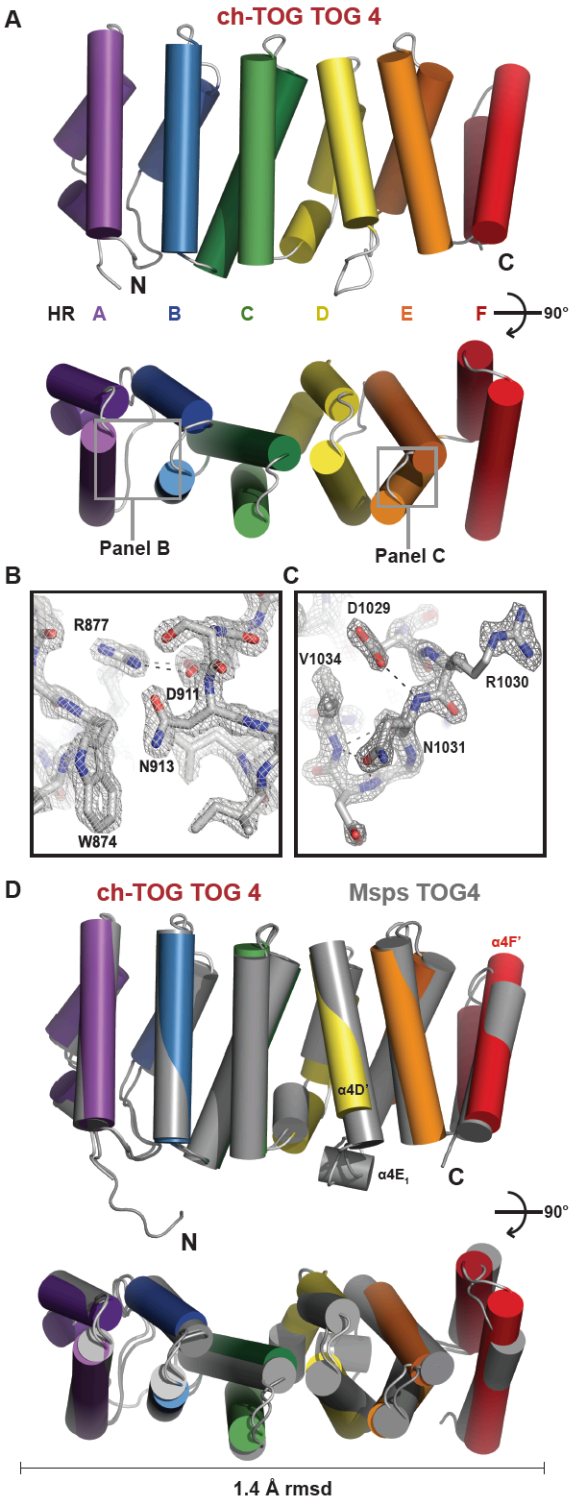

Figure 3-3. Structure of ch-TOG TOG4. (A) Cartoon representation of ch-TOG TOG4. (B-C) $2F_o$-F_c electron density map (2σ) of the ch-TOG TOG4 structure showing conserved determinants in the HR A (B) and HR E (C) loops. (D) Pairwise alignment of ch-TOG TOG4 (color) and Msps TOG4 (gray) showing structural conservation with a 1.4 Å rmsd over 226 Cα atoms.

$P2_12_12_1$; two TOG4 molecules in the asymmetric unit) and refined to R and R_{free} values of 17.5 and 19.6 respectively. Crystallographic details are presented in Table 1.

The ch-TOG TOG4 structure aligns well to the Msps TOG4 structure with a Cα rmsd of 1.4 Å across 226 residues, indicative of high structural conservation (Figure 3-3D). The ch-TOG TOG4 structures we determined in different space groups showed nearly identical conformations with low pairwise Cα rmsd values ranging from 0.7 to 0.8 Å (Figure 3-S3). This suggests that TOG4 is structurally static both within and across species. ch-TOG TOG4 and Msps TOG4 HR A-F structurally align with minor differences in the terminal region of HR D, the absence of $\alpha4E_1$ in ch-TOG, and an extension of ch-TOG's α4F' helix. Many of the TOG4 intra-HEAT loops residues are conserved between *Drosophila* and human and utilize similar flanking residues to buttress their rotamer arrangement. In the ch-TOG TOG4 structure, the conserved HR A loop tryptophan, W874, is solvent exposed and stabilized by a R877-D911 salt bridge as observed in Msps TOG4 (Figure 3-3B). Likewise, the conserved HR E loop aspartate, D1029, is similarly stabilized by a hydrogen bond with the asparagine N1031 backbone amide (Figure 3-3C).

TOG4 is structurally distinct

XMAP215 family TOG structures determined to date (yeast TOG1 and TOG2, *Drosophila* TOG2, and *C. elegans* TOG3) are structurally similar (Figure 3-S2). We next asked how TOG4 compares to these structures by focusing on the intra-species comparison of *Drosophila* Msps TOG2 and TOG4 (Figure 3-4A). Surprisingly, Msps TOG2 and Msps TOG4 align quite poorly with an rmsd of 4.5 Å across 226 Cα atoms (Figure 3-S2A). The individual HR triads align better; the HR A-C triads align with an rmsd of 2.0 Å and the HR

D-F triads align with an rmsd of 2.8 Å (Figure 3-4B-C; Table 2). Because the HR A-C triads align reasonably well and contain the highly conserved β-tubulin binding determinants (including the HR A loop tryptophan), we aligned Msps TOG2 and TOG4 over this conserved, functional reference region to see how the C-terminal HR triads were comparatively positioned. In this alignment, TOG4, like TOG2, retains a relatively flat surface across its tubulin-binding face. However, the TOG4 HR D-F triad, while maintained in this plane, is dramatically reoriented ~45° relative to TOG2's HR D-F triad, effectively positioning HR F 15 Å away from its TOG2 counterpart (Figure 3-4D-E, see red arrow in D). The differential positioning of the HR D-F triad is mirrored by a lower degree of conservation between the TOG2 and TOG4 HR D-F intra-HEAT loop sequences (Figure 3-1B). This contrasts with the sequence conservation in the HR A-C triad intra-HEAT loops that exists across all TOG domains in the array. Together, these differences suggest that if the TOG4 HR D-F triad engages tubulin, we anticipate that its binding mode will be distinct from the tubulin-binding mode of TOG1 and TOG2. Two regions likely underlie the conformational differences between TOG4 and TOG2. The first site occurs between helices αB' and αC' (Figure 3-4F). The TOG2 α2B' and α2C' helices pack in close proximity via TOG2-specific conserved alanine and glycine residues including A338, G341, and A345 in α2B' and A380, A384, and A387 in α2C'. In contrast, the TOG4 α4B'-α4C' interface contains large side chains including Q918 and L921 in α4B' and F956 in α4C'. In TOG4, this results in a 4 Å displacement of the α4C' N-terminal region relative to TOG2 α2C' (Figure 3-4F, right panel, red arrow). The second site occurs between HR C and HR D at the HR triad junction (Figure 3-4G). A major difference between TOG2 and TOG4 at this junction is the

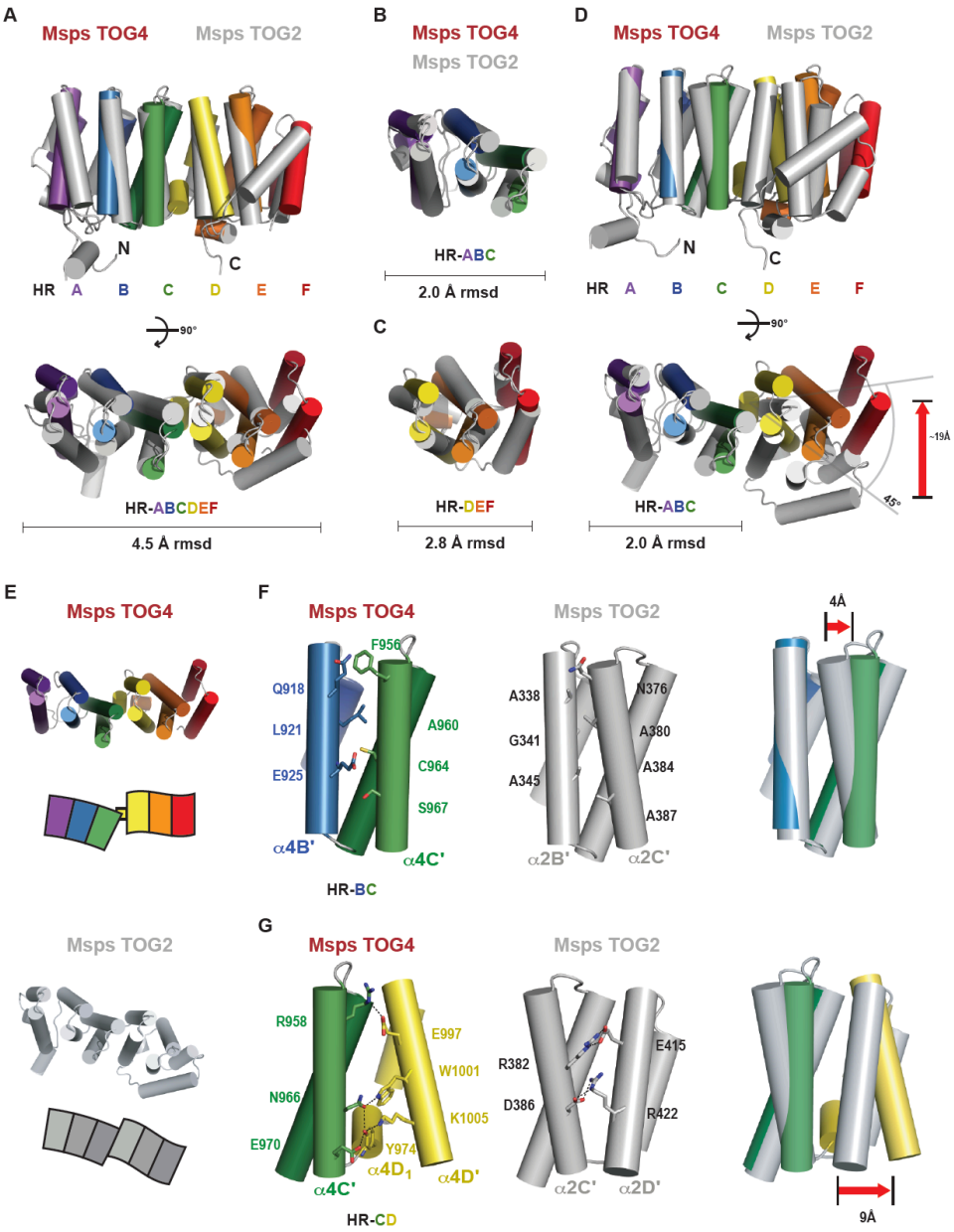

Figure 3-4. Msps TOG4 is structurally distinct from Msps TOG2. (A) Pairwise alignment of Msps TOG4 (color) and Msps TOG2 (gray) across the full domain yields a 4.5 Å rmsd. (B-C) Pairwise alignment of Msps TOG4 and Msps TOG2 across the first HR triad (B, 2.0 Å rmsd) and the second HR triad (C, 2.8 Å rmsd). (D) Superpositioning of Msps TOG4 and Msps TOG2 based on the first HR triad alignment shown in B, highlighting the 45° difference in the orientation of each domain's second HR triad, and the 19 Å differential placement of HR F. (E) Comparative views of Msps TOG4 and Msps TOG2 structures oriented as in D; models shown below. (F) The Msps TOG4 α4B'-α4C' interface contains bulky, conserved residues whereas the Msps TOG2 α2B' and α2C' interface has conserved residues with no or small side chains. (G) Msps TOG4 contains the $\alpha4D_1$ helical insert that forms an extensive interaction network at the base of HR C and HR D, absent in Msps TOG2.

presence of the TOG4-specific α4D$_1$ helix that bridges HR C and HR D and comparatively expands the interface between the triads. As discussed, Msps α4D$_1$ Y974 expands the core, forming a buried hydrogen bond network with N966 and E970 from α4C' as well as K1005 from α4D'. Msps α4D' also places the TOG4-specific conserved residue W1001 between HR C and HR D where it forms a hydrogen bond with the N966 side chain (also observed in ch-TOG TOG4). In contrast, TOG2 lacks a helical insert between HR C and HR D. As a result, the C-terminal regions of TOG2 α2C' and α2D' come in close proximity, stabilized by a D386-R422 salt bridge. Effectively, bulky side chains a α4D$_1$ helical insert displace the TOG4 HR D C-terminal region 9 Å relative to TOG2's HR D (Figure 3-4G, right panel, red arrow). These two sites underlie a major structural perturbation of the TOG architecture that positions TOG4 HR F 19 Å from the homologous position of TOG2 HR F. Thus, the position-specific conservation of TOG domains in the array (Figure 3-S1) mirrors position-specific structure: we find that the spatial arrangement of HRs in *Drosophila* Msps TOG2 and yeast Stu2 TOG2 is conserved, just as the spatial arrangement of HRs in *Drosophila* Msps TOG4 and human ch-TOG TOG4 is conserved. However, the spatial arrangement of HRs in TOG4 is distinct from that in TOG2. This indicates that TOG domains in the XMAP215 family have conserved, position-specific architectures within the array.

The TOG4 structure suggests differential tubulin-binding modes along the TOG array

To investigate how TOG4 might interact with tubulin, we superimposed Msps TOG4 onto the structure of the Stu2 TOG1-αβ-tubulin complex (Ayaz *et al.*, 2012). While Msps TOG4 and Stu2 TOG1 align poorly with an rmsd of 4.2 Å across 202 Cα residues (Table 2), the HR A-C triad intra-HEAT loops used to engage β-tubulin retain a high degree

of identity between Msps TOG4 and Stu2 TOG1 (33 %). We therefore docked Msps TOG4 onto the Stu2 TOG1-tubulin complex by structurally aligning the TOG4 and TOG1 HR A-C triads, which align reasonably well with an rmsd of 2.5 Å over this region (Figure 3-5A). This HR A-C triad alignment enabled us to generate a model of Msps TOG4 bound to tubulin (Figure 3-5B). When Stu2 TOG1 and Msps TOG4 are aligned over the HR A-C triads, the TOG4 HR D-F triad shows a dramatically different architecture than Stu2 TOG1 HR D-F, culminating in a 17 Å differential positioning of HR F, similar to the architectural change evident in the TOG2 - TOG4 comparison presented above (Figures 3-4D, 5A, red arrows). Our model is consistent with the idea that Msps TOG4 preferentially binds curved tubulin. In the Stu2 TOG1-αβ-tubulin structure, TOG1 binds curved tubulin, a quaternary conformation observed in non-polymerized tubulin (Rice et al., 2008; Pecqueur et al., 2012). This contrasts with the straight tubulin conformation, determined from zinc-induced tubulin sheets thought to represent the structure of tubulin in MT protofilaments (Nogales et al., 1998; Lowe et al., 2001). When the straight tubulin structure is docked onto the Stu2 TOG1-αβ-tubulin complex by structurally aligning β-tubulin, a gap is evident between TOG1 HR E-F and α-tubulin (Figure 3-5B, red arrow). Similarly, in our TOG4-αβ-tubulin model, TOG4's HRs fully engage αβ-tubulin in the curved conformation, but not in the straight conformation (Figure 3-5C, red arrow), suggesting that tubulin maintains a curved conformation when bound to TOG1 or TOG4.

Stu2 TOG1 binds αβ-tubulin using intra-HEAT loop residues; HR A-D bind β-tubulin and HR E-F bind α-tubulin (Figure 3-1B, see Stu2 TOG1 α- and β-tubulin binding residues boxed in blue and purple respectively). Since we aligned Stu2 TOG1 and Msps TOG4 over

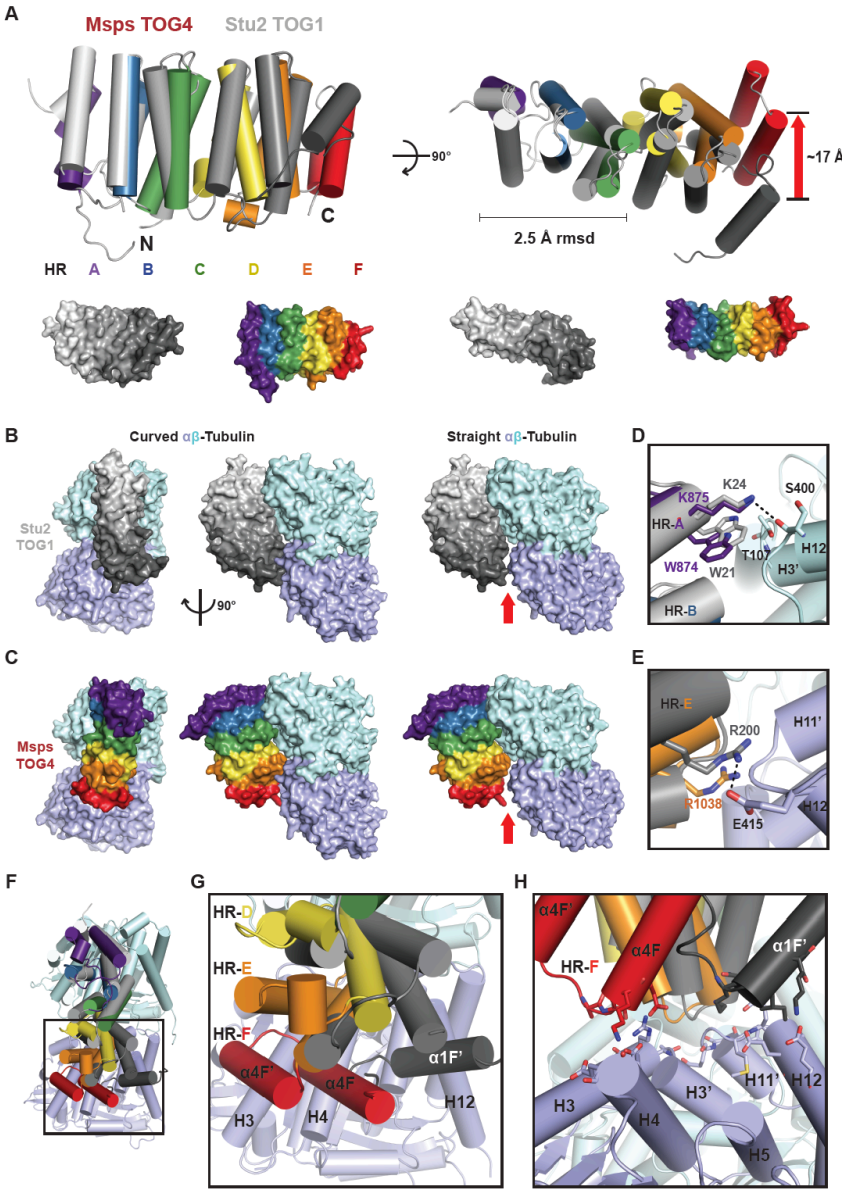

Figure 3-5. TOG4 is predicted to form TOG4-specific contacts with tubulin. (A) Msps TOG4 (color) and Stu2 TOG1 (gray) aligned pairwise over the first HR triad (HR A-C) with an 2.5 Å rmsd over HR A-C, highlighting the differential arrangement of each domain's second HR triad and the 17 Å shift in HR F (red arrow). Lower images show identical orientations in surface representation. (B) Stu2 TOG1 bound to curved αβ-tubulin (left; Ayaz et al., 2011) versus straight tubulin (modeled at right). (C) Msps TOG4 was docked onto the Stu2 TOG1-αβ-tubulin structure and model presented in B by aligning the first HR triads as in A. (D) Msps TOG4 conserved HR A residues W874 and K875 can interact with β-tubulin residues T107 and S400 respectively as observed in the Stu2 TOG1-αβ-tubulin structure. (E) Msps TOG4 conserved HR E residue R1038 is within 5 Å of α-tubulin E415, and is likely to reposition and form a salt bridge as observed with Stu2 TOG1 R200. (F) Major differences between the Stu2 TOG1-αβ-tubulin and Msps TOG4-αβ-tubulin model are observed in HR F's interaction with α-tubulin. (G-H) Zoom view of the region boxed in F (G) and shown after a 90° rotation about the x-axis (H).

the first HR triad, we observe, as expected, that HR A-C intra-HEAT loop residues conserved between Stu2 TOG1 and Msps TOG4 are equivalently positioned to interact with β-tubulin. Key interactions with β-tubulin involve Stu2 TOG1 HR A residues W21 and K24 that engage β-tubulin residues T107 and S400 respectively. Our Msps TOG4 model suggests a similar mode of interaction; HR A residues W874 and K875 are positioned to interact with β-tubulin residues T107 and S400 (Figure 3-5D). We also see conserved interactions that extend into the second HR triad. Stu2 TOG1 HR E residue R200 forms a salt bridge with α-tubulin residue E415. While Msps HR E is positioned different than Stu2 TOG1 HR E, the Msps TOG4 HR E R1038 side chain is positioned within range to form a homologous salt bridge with α-tubulin E415 (Figure 3-5E).

While the TOG4 N-terminal HRs position intra-HEAT loop determinants in conformations that would facilitate TOG-tubulin interactions homologous to those observed in the Stu2 TOG1-αβ-tubulin structure, major differences are evident in the position of the HR F intra-HEAT loop (Figure 3-5C, F-H). Stu2 TOG1 HR F is positioned to interact with the α-tubulin H12 helix. In contrast, Msps TOG4 HR F is positioned to interact with the α-tubulin H3 and H4 helices, ~17 Å away from the H12 helix. Collectively, this model suggests that Msps TOG4 binds the αβ-tubulin heterodimer in a unique fashion, with some TOG-tubulin interaction determinants common to the Stu2 TOG1-tublin interaction, and others distinct to TOG4. These findings suggest that different TOG domains in the array make specific, non-equivalent interactions with tubulin.

Msps TOG1-2 and TOG3-4 constructs show dramatically different tubulin-binding and MT polymerization activities

To investigate the tubulin-binding activity of different TOG domains in the array, we analyzed the ability of paired TOG domains to bind tubulin using a gel filtration shift assay (Campbell and Slep, 2011). Previous work analyzing the ability of Msps TOG1 and TOG2 to bind and shift tubulin over gel filtration found that a detectable shift could be obtained with a TOG1-2 construct but not with either TOG domain individually or in trans (Slep and Vale, 2007). We first analyzed the ability of a Msps TOG1-2 construct (40 μM) to bind tubulin (20 μM) and reproduced the previously reported binding result, observing earlier peak elution, indicative of relatively stable complex formation (Figure 3-6A, see green arrow). We then analyzed the ability of TOG3-4 to bind tubulin. TOG3-4 itself produced a bimodal elution profile due to a degradation product that eluted later and contained individual TOG3 and TOG4 domains (Figure 3-S7C). We increased the total amount of protein load so that the amount of TOG3-4 was approximately 40 μM. Interestingly, no detectable peak shift was evident when TOG3-4 was incubated and run with tubulin (Figure 3-6B). Additionally, neither construct cosediments with taxol stabilized MTs (Figure 3-S7). Previous cell data suggests TOG3-4 could contribute to MT lattice binding. A construct extending from the end of TOG2 to the end of TOG4 (linker-TOG34) was previously shown to decorate the MT lattice in *Drosophila* S2cells. To test the contribution of TOG3-4 to this interaction, we created single and double tryptophan to glutamic acid mutations and assayed for lattice association. Mutating the TOG domains resulted in a decrease in MT interaction (Figure 3-S8). This, along with the gel filtration data, indicates that the TOG domains in the TOG1-2 and TOG3-4 constructs have significantly different tubulin/MT-binding properties and that if

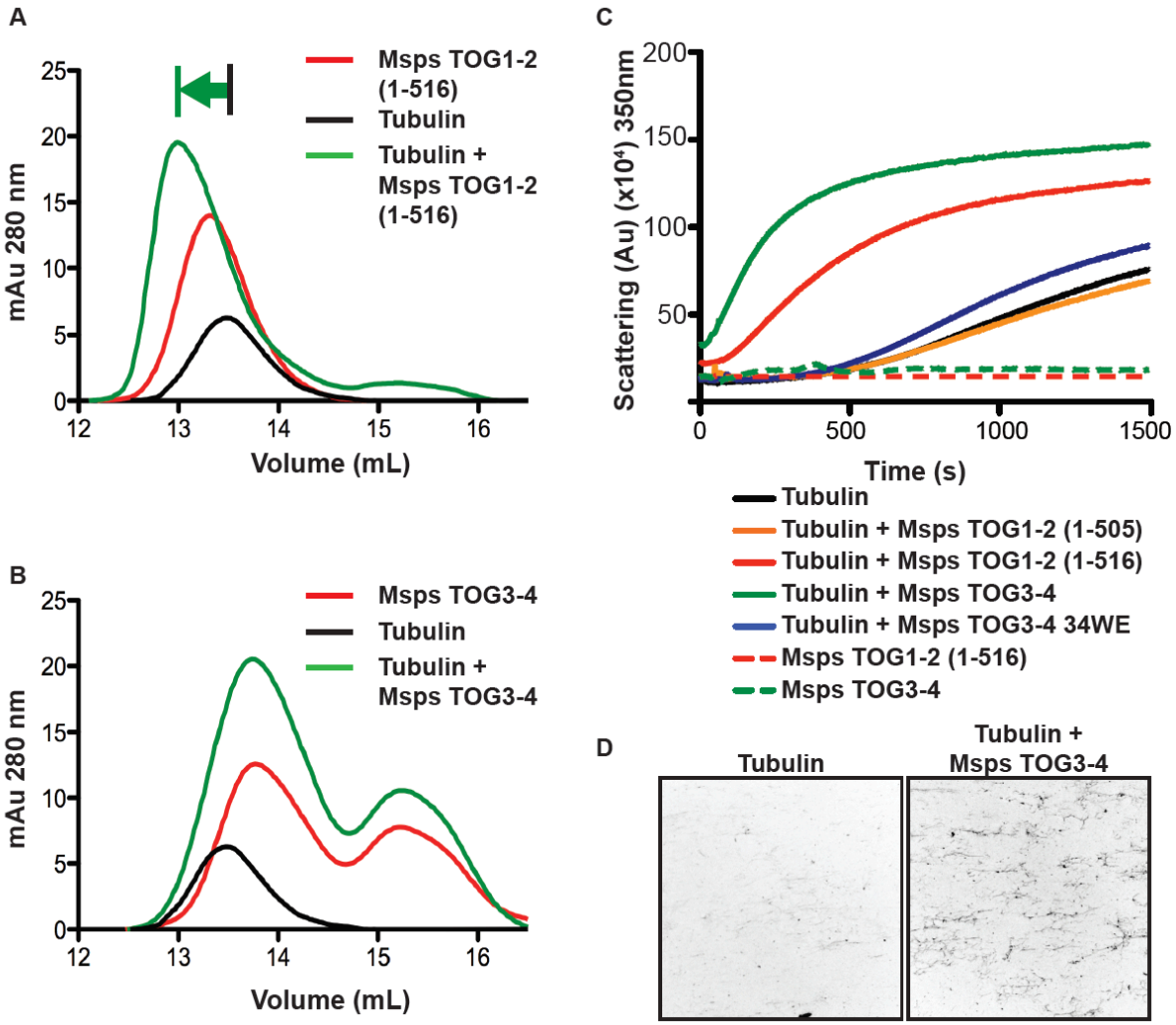

Figure 3-6. Paired Msps TOG domains show differential tubulin binding and MT polymerization activities *in vitro*. (A) TOG1-2 (40 μM) binds and shifts tubulin (20 μM) to an earlier elution peak over gel filtration. (B) TOG3-4 (40 μM) fails to shift tubulin (20 μM) over gel filtration. (C) Light scattering curves of tubulin (15 μM) polymerized at 37° C alone or in the presence of Msps TOG1-2 or TOG3-4 constructs (1 μM). TOG constructs alone showed no scattering activity. (D) Images of *in vitro* microtubule polymerization in the absence (left) and presence (right) of 1nM Msps34. Tubulin was doped with 10% rhodamine labeled tubulin.

TOG3 and TOG4 each bind free tubulin, their tubulin-binding affinities do not facilitate the stable interaction observed between TOG1-2 and tubulin over gel filtration.

We next analyzed how Msps TOG1-2 and TOG3-4 individually affected MT polymerization *in vitro* using a 90° light scattering assay. Tubulin alone (15 μM) showed standard polymerization behavior with polymerization-dependent scattering apparent after a ~400 second lag time (Figure 3-6C). Tubulin in the presence of TOG1-2 (residues 1-505, 1 μM) did not alter tubulin polymerization behavior as previously observed (Slep and Vale, 2007). In contrast, a TOG1-2 construct that contained an 11 amino acid C-terminal extension (residues 1-516, 1 μM) promoted MT polymerization after only a ~100 second lag time and showed faster bulk polymerization kinetics than observed with tubulin alone. The linker region bridging TOG2 and TOG3 has been shown to promote MT lattice association in cell culture, and we hypothesize that a series of basic residues in this C-terminal extension work in concert with the TOG domains to drive MT polymerization. We next investigated how a TOG3-4 construct (with no N- or C-terminal extension, 1 μM) affected MT polymerization behavior. Surprisingly, TOG3-4 drove polymerization even faster than the TOG1-2 (1-516) construct, with only a ~50 second lag time followed by a growth rate slightly faster than the TOG1-2 (1-516)-induced polymerization rate (Figure 3-6C, D). TOG pairs alone showed no light scattering activity over time. We next analyzed the bulk tubulin polymerization activity of a TOG3-4 construct in which the conserved HR A loop tryptophan in both TOG3 and TOG4 was mutated to glutamate, a mutation shown to ablate tubulin binding in other TOG domains (Slep and Vale, 2007) but not affect TOG structure (by CD analysis: Leano et al., 2013). We found that the TOG3-4 double mutant did not dramatically alter tubulin polymerization kinetics from what we observed with the tubulin alone control. Together,

these data suggest that TOG3 and TOG4 use conserved tubulin-binding intra-HEAT loop determinants to drive microtubule nucleation and polymerization. While TOG1-2 (1-505) is not sufficient to drive MT nucleation and polymerization but requires a C-terminal extension (1-516), TOG3-4 has potent MT nucleation and polymerization activity mediated by its TOG domains' tubulin-binding determinants.

Msps-dependent MT polymerization activity requires a fully functional TOG array

The differences in TOG domain structure and tubulin interaction properties suggest that individual TOG domains may differentially contribute to a collective, array-dependent MT polymerization mechanism. To analyze how the constituent TOG domains in the array contribute to MT polymerization we performed in cell MT polymerization rescue assays on a minimal Msps construct (Figure 3-7A)(Currie et al., 2011). We treated *Drosophila* S2 cells with dsRNA targeting the *msps* coding region (Msps C-terminal residues 1752-1928). Western blot analysis confirmed RNAi-mediated Msps depletion (Figure 7B). Msps-depleted cells and control dsRNA-treated cells were transfected with an *EB1*:*EB1-tRFP* construct and time lapse images were acquired. EB1-tRFP comet velocities were measured as a read-out for MT polymerization rates (Figure 3-7C). In control dsRNA-treated cells transfected with a *GFP* control, the mean EB1 comet velocity was 12.2 μm/min (Figure 3-7C,D). In contrast, cells treated with *msps* dsRNA had a significantly reduced mean EB1 comet velocity of 2.1μm/min (Figure 3-7C,E; $p<0.0001$), consistent with a previous report (Currie et al., 2011). We next attempted to rescue MT polymerization rates in the *msps* dsRNA-treated cells using an *msps* construct containing the first four TOG domains (TOG1-4) (Figure 3-7C,F). In cells transfected with the *msps TOG1-4-GFP* construct, EB1-tRFP mean comet velocity increased

to 6.1 μm/min, largely rescuing MT polymerization rates, as previously observed (Currie et al., 2011; $p<0.0001$). A *msps TOG1-5-GFP* construct showed similar rescue activity, with a mean comet velocity of 6.7 μm/min (Figure 3-7C,G; $p<0.0001$). Expression of *msps-GFP* constructs was verified by western blot (Figure 3-S4) and only cells whose' GFP intensity fell within a specified range were scored (see Materials and Methods).

To determine whether changes in EB1 comet velocities were due to decreased MT polymerization rates or MT sliding, we analyzed EB1 comet length. EB1 binds the MT lattice with highest affinity when tubulin subunits are in a GTP-hydrolytic state mimicked by a GTPγS-bound MT lattice (Maurer et al., 2011; Maurer et al., 2012). The on-axis length of tubulin in this transient state should scale linearly with the MT growth rate. We analyzed averaged intensity line-scans of EB1-tRFP MT plus end comets in control dsRNA-treated cells transfected with *GFP*, *msps* dsRNA-treated cells transfected with *GFP*, and *msps* dsRNA-treated cells transfected with *msps TOG1-4-GFP* (Figure 3-S5A). The EB1 comet lengths measured in these cells scaled linearly with EB1 comet velocity, indicating that EB1 comet velocity correlated with MT polymerization rates under these different treatments (Figure 3-S5B).

We then used this system to explore the role of individual TOG domains within the *msps TOG1-4* construct, to correlate cellular observations with our structural observations and *in vitro* results. To probe the role of TOG domains in the TOG1-4 array, we systematically mutated the HR A loop tryptophan to glutamate in each of the four TOG domains (Figure 3-7I-L), a mutation previously shown to ablate TOG-tubulin interactions (Slep and Vale, 2007; Leano et al., 2013). When *TOG1-4-GFP* constructs containing

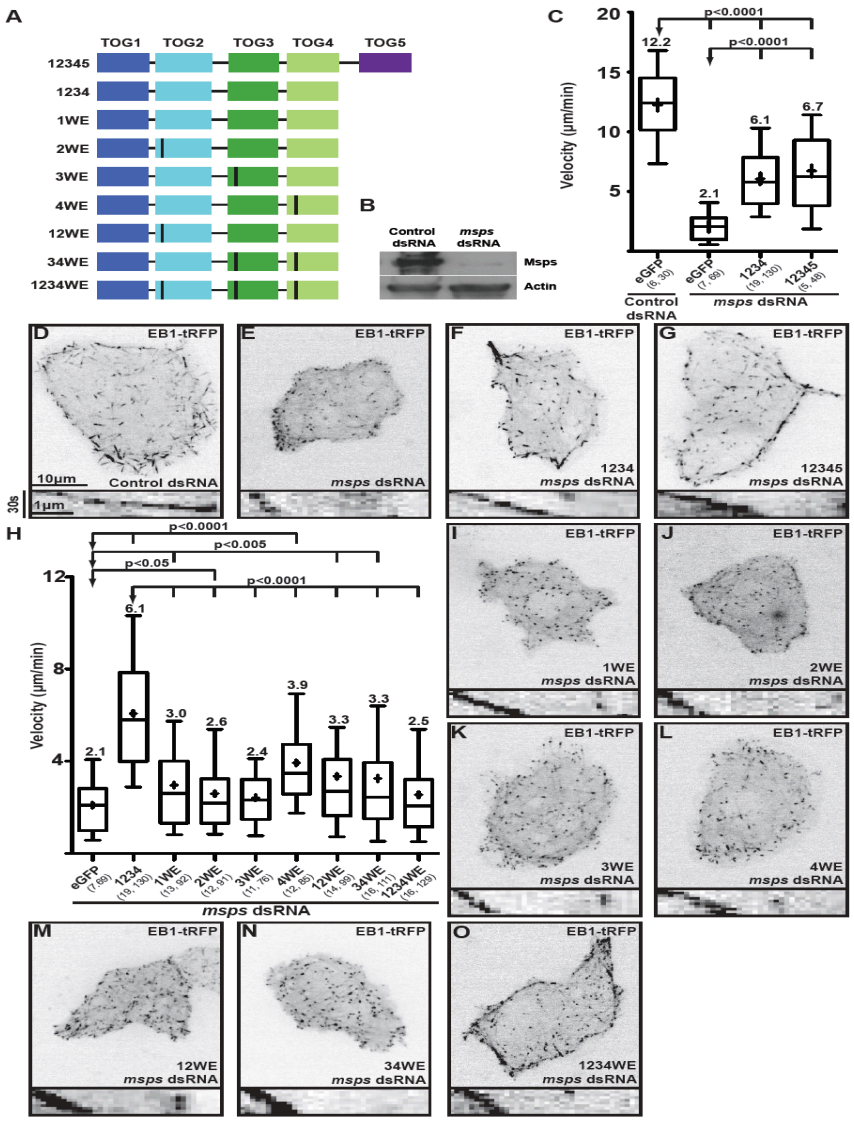

Figure 7. Msps requires a functional TOG array to rescue MT polymerization in cells. (A) Msps GFP constructs analyzed; vertical lines indicate an HR A loop W→E mutation. (B) Western blot showing RNAi-mediated Msps depletion in *Drosophila* S2 cells (SK dsRNA control; antibodies: anti-Msps, anti-actin loading control). (C) Distribution of EB1 comet velocities from Msps rescue experiments. (D) Projection image (30 sec) of a S2 cell expressing EB1-tRFP treated with control dsRNA (above) and a kymograph of a representative EB1 comet from this cell (below). (E-G) EB1 comet velocity is reduced when Msps is depleted (E) but can be largely rescued with Msps TOG1-4 (F) or Msps TOG1-5 (G). (H) Distribution of EB1 comet velocities in Msps dsRNA-treated cells, transfected with Msps TOG1-4 mutant rescue constructs. Mutating the conserved HR A loop tryptophan individually (I-L), in pairs (M-N), or across all four TOG domains (O) fails to rescue EB1 comet velocities. Scale bar in projection images: 10 μm, in kymographs: 30 seconds and 1 μm. Box and whisker plots in C and H confer the following information: whiskers: 10th and 90th percentile; boxes: 25th and 75th percentile; line: median; cross: mean. Numbers in parentheses indicate the number of cells analyzed and the total number of EB1 comets tracked. Two-tailed P-values were calculated using an unpaired T test.

individual mutations in one of the four TOG domains were transfected into *msps* dsRNA-treated cells, rescued mean EB1 comet velocities were substantially reduced, with rates of 3.0, 2.6, 2.4 and 3.9 μm/min for constructs with TOG domains 1 (1WE), 2 (2WE), 3 (3WE),and 4 (4WE) mutated respectively (Figure 3-7H-L; $p<0.0001$). When pairs of TOG domains were mutated (either the TOG1-2 pair (12WE), or the TOG3-4 pair (34WE)), mean EB1 comet velocities were similarly reduced at 3.3 μm/min (Figure 3-7H,M-N; $p<0.0001$). Mutations in all four TOG domains also disrupted rescue of MT polymerization rates, with a mean EB1 comet velocity of 2.5 μm/min (Figure 3-7H,O; $p<0.0001$). These data suggest that each of the first four TOG domains of the *TOG1-4* construct is important for Msps' ability to promote microtubule polymerization.

Discussion

Higher eukaryotic XMAP215 family members contain a pentameric TOG domain array, but how the TOG array promotes MT polymerization remains to be determined. Recent work established the binding polarity of Stu2 TOG1 on tubulin, revealing that the TOG1 N-terminal four HRs engage β-tubulin and the two C-terminal HRs engage α-tubulin (Ayaz et al., 2012). Because all TOG domains in the array have conserved tubulin-binding determinants in the first HR triad, a simplistic model would suggest that each TOG domain binds a tubulin heterodimer. Whether the TOG array binds multiple tubulin heterodimers is debated. If they do, how the multivalent molecule's TOG domains are arranged to interact with the MT lattice and promote tubulin incorporation remains to be determined.

To better understand the TOG array mechanism, it is important to characterize the structural and functional properties of each domain within the polarized array. We analyzed

the TOG domains in the XMAP215 family TOG array and noted TOG class-specific conservation. Our structures of *Drosophila* Msps TOG4 and human ch-TOG TOG4 revealed that TOG4 is structurally conserved across species, but its architecture differs from structures determined to date of Stu2 TOG1, Stu2 TOG2, Msps TOG2, and Zyg-9 TOG3 (Al-Bassam et al., 2007; Slep and Vale, 2007; Ayaz et al., 2012). While TOG1, TOG2 and TOG3 are similar, TOG4's second HR triad is positioned quite differently, and its arrangement predicts a TOG4-specific interaction with α-tubulin. This indicates that the XMAP215 TOG array is structurally polarized, with position-dependent features conserved across species. Why TOG domains in the array would have different tubulin-binding modes may involve the recognition of different tubulin structural states and/or differential interactions with other tubulin/MT-binding proteins.

Consistent with these structural differences, our *in vitro* tubulin binding assays indicate that TOG domains have different affinities for free tubulin. Previous work analyzing Msps TOG1 and TOG2 found that while the individual TOG domains do not show detectable tubulin-binding over gel filtration, a TOG1-2 construct does bind tubulin. This finding suggests that a multivalent TOG array enhances the TOG-tubulin interaction, potentially by promoting cooperative lateral or longitudinal tubulin-tubulin contacts (Slep and Vale, 2007). While TOG1-2 binds tubulin over gel filtration, TOG3-4 does not display detectable tubulin-binding activity. However, previous work suggests TOG3 and TOG4 do potentiate tubulin binding in the context of the TOG array. A full-length XMAP215 construct showed tubulin-binding activity over gel filtration (Widlund et al., 2011). When the tubulin-binding determinants in TOG1 and TOG2 or TOG3 and TOG4 were mutated, the full-length XMAP215 construct still retained some, albeit reduced, tubulin-binding activity. When all

five TOG domains were mutated, tubulin-binding activity was nearly abrogated. This suggests that TOG domains have different tubulin-binding activity but utilize common tubulin-binding determinants in a multivalent array to bind tubulin. Thus, we predict that TOG3 and TOG4 have weak tubulin-binding affinities that preclude detection of tubulin binding by a TOG3-4 construct as assayed over gel filtration, but that these affinities are tuned to work cooperatively in the context of a larger TOG array. We hypothesize that these affinities are positionally tuned along the array to recognize free tubulin and/or MT lattice features with association and dissociation rates commensurate with the incorporation of 25 tubulin heterodimers into a protofilament per second (calculated based on a MT growth rate of 12 μm/min in *Drosophila* S2 cells). The existence of transient interactions between Msps TOG3-4 and tubulin is suggested by our *in vitro* tubulin polymerization assay in which TOG3-4 induced rapid MT nucleation and polymerization. While TOG1-2 and TOG3-4 both induced MT nucleation, TOG3-4-induced nucleation occurred more rapidly, within the first 50 seconds of the experiment. The greater nucleation activity of the TOG3-4 pair and the higher affinity of the TOG1-2 pair for free tubulin may have implications for the polarity of the TOG array at the polymerizing plus end. The Stu2 TOG1-αβ-tubulin complex shows that TOG1 is polarized on the tubulin heterodimer, with its N- and C-termini oriented towards the MT plus and minus end respectively (Ayaz et al., 2012). In a simplistic model, XMAP215 members may position TOG1 at the polymerizing plus end with TOG domains 2-5 arranged sequentially, just distal to the MT tip (Figure 3-S6). This orientation would position the C-terminal SLAIN2/Sentin-binding elements just behind the polymerizing MT plus end, which would correlate with the localization of EB1, which binds the lattice just distal to the

polymerizing MT plus end and recruits the SLAIN2/Sentin-XMAP215 complex (van der Vaart et al., 2011; Li et al., 2011; Maurer et al., 2012; Nakamura et al., 2012).

An XMAP215 mechanism involving a polarized TOG array bound to a polymerizing MT plus end likely engages differential TOG function. These differential TOG functions may range from MT lattice binding activity and nucleation, to the binding of free tubulin and potentiating its stable incorporation into the MT lattice by templating and/or lowering the tubulin heterodimer's off-rate of at the MT plus end. Our in cell MT polymerization rescue experiments indicate that TOG domains work in an array, with each domain mobilizing similar tubulin-binding determinants to promote MT growth. TOG1-4 largely rescued MT polymerization activity, increasing it 2.9-fold above the 2.1 μm/min observed when Msps was depleted. Mutating the predicted tubulin-binding determinants in any single TOG domain in the TOG1-4 construct substantially diminished the rescue activity. The most dramatic effect was evident when TOG1, TOG2, or TOG3 was mutated. In contrast, the TOG4 mutant was able to partially restore polymerization with a 1.9-fold enhancement in the MT growth rate. This suggests that three contiguous N-terminal wild-type TOG domains function with greater efficiency than three wild-type TOG domains interspersed with a mutant TOG domain. This result highlights the importance of a functional, continuous, TOG array, that polymerization activity is polarized from the N-terminal TOG domains, and that larger, contiguous functional TOG arrays enhance MT polymerization rates (TOG1-5 > TOG1-4 > TOG1-4 4WE). Evolutionary support for the idea that polymerization activity is polarized from the N-terminal TOG domains comes from XMAP215 family members that do not have a pentameric TOG array, including *S. cerevisiae* Stu2 and *C. elegans* Zyg-9. Stu2 has two TOG domains that are respectively most similar in sequence to TOG1 and TOG2

from XMAP215 pentameric array members (Figure 3-S1D-E). Zyg-9 has three TOG domains, the first two showing greatest sequence similarity to TOG1 from XMAP215 pentameric array members, and the third showing greatest sequence similarity to TOG5. This underscores the evolutionary pressure to maintain a functionally polarized TOG array.

Our work highlights key features of the XMAP215 TOG array that further our mechanistic understanding of this critical MT regulator. First, TOG domains function in an array to promote MT polymerization. Second, TOG domains in the array have different structures but are positionally conserved. Third, TOG domains in the array have different affinities for tubulin heterodimers and different MT nucleation activities. Collectively, this suggests that TOG domains, in general, mobilize an array-based mechanism to regulate MT dynamics and that differential TOG architecture in the array is mechanistically positioned to perform different regulatory actions on MTs (Figure 3-S9). Recent work examining the structure and function of a cryptic TOG domain in the CLASP family revealed that CLASP comprises a TOG array (Leano et al., 2013). This work showed that CLASP's second TOG domain adopts a unique bent architecture across its tubulin-binding face and that this domain is critical for CLASP's activity. While the XMAP215 TOG array promotes MT polymerization, the CLASP TOG array promotes MT pause in interphase and MT polymerization during mitosis. Collectively, a TOG array paradigm is emerging for these two key MT regulators, where structurally distinct TOG domains in specific arrangements can differentially modulate MT dynamics. Structural insight into how architecturally distinct TOG domain arrays interact with multiple tubulin heterodimers, the role of the linker regions that bridge the TOG domains, and the concerted effect their binding partners play on MT dynamics awaits further investigation.

REFERENCES

1. Adams, P.D., Afonine, P.V., Bunkoczi, G., Chen, V.B., Davis, I.W., Echols, N., Headd, J.J., Hung, L.W., Kapral, G.J., Grosse-Kunstleve, R.W*., et al.* (2010). PHENIX: a comprehensive Python-based system for macromolecular structure solution. Acta Crystallogr D Biol Crystallogr *66*, 213-221.

2. Al-Bassam, J., Larsen, N.A., Hyman, A.A., and Harrison, S.C. (2007). Crystal structure of a TOG domain: conserved features of XMAP215/Dis1-family TOG domains and implications for tubulin binding. Structure *15*, 355-362.

3. Andrade, M.A., Petosa, C., O'Donoghue, S.I., Muller, C.W., and Bork, P. (2001). Comparison of ARM and HEAT protein repeats. J Mol Biol *309*, 1-18.

4. Ayaz, P., Ye, X., Huddleston, P., Brautigam, C.A., and Rice, L.M. (2012). A TOG:alphabeta-tubulin complex structure reveals conformation-based mechanisms for a microtubule polymerase. Science *337*, 857-860.

5. Baker, N.A., Sept, D., Joseph, S., Holst, M.J., and McCammon, J.A. (2001). Electrostatics of nanosystems: application to microtubules and the ribosome. Proc Natl Acad Sci U S A *98*, 10037-10041.

6. Campbell, J.N., and Slep, K.C. (2011). αβ-Tubulin and Microtubule binding assays. Methods in Molecular Biology, *777*, 87-97.

7. Currie, J.D., Stewman, S., Schimizzi, G., Slep, K.C., Ma, A., and Rogers, S.L. (2011). The microtubule lattice and plus-end association of Drosophila Mini spindles is spatially regulated to fine-tune microtubule dynamics. Mol Biol Cell *22*, 4343-4361.

8. Emsley, P., Lohkamp, B., Scott, W.G., and Cowtan, K. (2010). Features and development of Coot. Acta Crystallogr D Biol Crystallogr *66*, 486-501.

9. Hasegawa, H., and Holm, L. (2009). Advances and pitfalls of protein structural alignment. Curr Opin Struc Biol *19*, 341-348.

10. Leahy, D.J., Erickson, H.P., Aukhil, I., Joshi, P., and Hendrickson, W.A. (1994). Crystallization of a fragment of human fibronectin: introduction of methionine by site-directed mutagenesis to allow phasing via selenomethionine. Proteins *19*, 48-54.

11. Leano, J.B., Rogers, S.L., and Slep, K.C. (2013). A Cryptic TOG Domain with a Distinct Architecture Underlies CLASP-Dependent Bipolar Spindle Formation. Structure.

12. Li, W., Miki, T., Watanabe, T., Kakeno, M., Sugiyama, I., Kaibuchi, K., and Goshima, G. (2011). EB1 promotes microtubule dynamics by recruiting Sentin in Drosophila cells. J Cell Biol *193*, 973-983.

13. Lowe, J., Li, H., Downing, K.H., and Nogales, E. (2001). Refined structure of alpha beta-tubulin at 3.5 A resolution. J Mol Biol *313*, 1045-1057.

14. Maurer, S.P., Fourniol, F.J., Bohner, G., Moores, C.A., and Surrey, T. (2012). EBs recognize a nucleotide-dependent structural cap at growing microtubule ends. Cell *149*, 371-382.

15. Nakamura, S., Grigoriev, I., Nogi, T., Hamaji, T., Cassimeris, L., and Mimori-Kiyosue, Y. (2012). Dissecting the nanoscale distributions and functions of microtubule-end-binding proteins EB1 and ch-TOG in interphase HeLa cells. PLoS One *7*, e51442.

16. Nogales, E., Wolf, S.G., and Downing, K.H. (1998). Structure of the alpha beta tubulin dimer by electron crystallography. Nature *391*, 199-203.

17. Otwinowski, Z., and Minor, W. (1997). Processing of X-ray diffraction data collected in oscillation mode. In Methods in Enzymology, C.W. Carter and R.M. Sweet, eds. (Charlottesville: University of Virginia), pp. 307-326.

18. Pecqueur, L., Duellberg, C., Dreier, B., Jiang, Q.Y., Wang, C.G., Pluckthun, A., Surrey, T., Gigant, B., and Knossow, M. (2012). A designed ankyrin repeat protein selected to bind to tubulin caps the microtubule plus end. P Natl Acad Sci USA *109*, 12011-12016.

19. Rice, L.M., Montabana, E.A., and Agard, D.A. (2008). The lattice as allosteric effector: Structural studies of alpha beta- and gamma-tubulin clarify the role of GTP in microtubule assembly. P Natl Acad Sci USA *105*, 5378-5383.

20. Rogers, S.L., and Rogers, G.C. (2008). Culture of Drosophila S2 cells and their use for RNAi-mediated loss-of-function studies and immunofluorescence microscopy. Nat Protoc *3*, 606-611.

21. Slep, K.C., and Vale, R.D. (2007). Structural basis of microtubule plus end tracking by XMAP215, CLIP-170, and EB1. Mol Cell *27*, 976-991.

22. van der Vaart, B., Manatschal, C., Grigoriev, I., Olieric, V., Gouveia, S.M., Bjelic, S., Demmers, J., Vorobjev, I., Hoogenraad, C.C., Steinmetz, M.O.*, et al.* (2011). SLAIN2 links microtubule plus end-tracking proteins and controls microtubule growth in interphase. J Cell Biol *193*, 1083-1099.

23. Widlund, P.O., Stear, J.H., Pozniakovsky, A., Zanic, M., Reber, S., Brouhard, G.J., Hyman, A.A., and Howard, J. (2011). XMAP215 polymerase activity is built by combining multiple tubulin-binding TOG domains and a basic lattice-binding region. Proceedings of the National Academy of Science of the United States of America, *108*, 2741-2746.

TABLES

Table 3-1. Crystallographic data, phasing, and refinement statistics

Structure	**Msps TOG 4**		**ch-TOG TOG 4**	
Crystal	**Native**	**SeMet**	**Native**	**SeMet**
Space Group	P1	P1	$P2_12_12_1$	$P4_32_12$
Unit Cell				
***a, b, c* (Å)**	31.8, 32.6, 59.8	31.7, 32.4, 60.1	64.4, 74.3, 93.7	79.1, 79.1, 68.5
α, β, γ (°)	100.1, 95.2, 110.0	100.1, 95.1, 109.7	90, 90, 90	90, 90, 90
Wavelength (Å)	1.12714	0.97957	1.00000	0.97926
d_{min} (Å)	1.65 (1.71-1.65)	1.90 (1.97-1.90)	1.90 (1.97-1.90)	2.5 (2.59-2.50)
No. observations: measured / unique	45402 (3809) / 25054 (2355)	64094 (5383) / 33239 (3229)	255235 (22145) / 35954 (3515)	106775 (9490) / 14453 (1438)
Redundancy	1.9 (1.6)	2.0 (1.7)	7.1 (6.3)	7.4 (6.6)
Completeness (%)	95.3 (88.9)	96.6 (93.8)	100.0 (100.0)	99.9 (99.7)
I/σ	33.0 (5.7)	29.5 (14.7)	22.9 (4.7)	19.9 (3.3)
R_{sym} (%)[a]	2.1 (11.7)	2.2 (4.8)	8.2 (42.8)	9.5 (49.7)
Resolution (Å) at which anomalous completeness exceeds 85% for I/σI > 5, > 3, > 2		2.0, 1.9, 1.9		3.4, 3.1, 2.9
SAD phasing: overall log-likelihood gain / figure of merit		160751 / 0.741 (0.726)		79522 / 0.36 (0.20)
Figure of merit[b] Centrics / Acentrics		0 (0) / 0.75 (0.75)		0.12 (0.11) / 0.42 (0.22)
Figure of merit[b] after density modification Centrics / Acentrics		0 (0) / 0.83 (0.74)		0.61 (0.24) / 0.66 (0.35)
Figure of merit[b]	0.89 (0.85)		0.87 (0.84)	0.81 (0.83)
Refinement (Å)	29.9-1.65 (1.69-1.65)		48.7-1.90 (1.95- 1.90)	28.0-2.50 (2.65-2.50)
R value[c]	15.7 (21.0)		17.5 (21.0)	20.8 (20.8)
R_{free}[d]	18.7 (30.2)		21.5 (28.5)	27.6 (29.4)
Rmsd bond lengths (Å)	0.006		0.007	0.008
Rmsd bond angles (°)	1.00		1.07	1.20
Mean B (min/max) ($Å^2$)	18.2 (4.6/74.6)		21.4 (5.7/78.6)	37.9 (17.9/131.9)
No. protein atoms/ solvent atoms	1805/401 (2 SO_4)		3541/360	1790/48

Values in parentheses are for the highest resolution shells unless otherwise denoted.

[a] $R_{sym}=\Sigma_h\Sigma_i|I_i(h)-\langle I(h)\rangle|/\Sigma_h\Sigma_i I_i(h)$ where $I_i(h)$ is the integrated intensity of the *i*th reflection with the Miller Index *h* and $\langle I(h)\rangle$ is the average over Friedel and symmetry equivalents.

[b] Figure of merit is the weighted mean of the cosine of the deviation from α_{best}.

[c] R value = $\Sigma(|F_{obs}|-k|F_{calc}|)/\Sigma|F_{obs}|$.

[d] R_{free} is calculated using a 10% subset of the data that is removed randomly from the original data and excluded from refinement.

Table 3-2. Pairwise alignment of TOG domains

Protein 1	Protein 2	rmsd	# Res. aligned	% Identity
Msps TOG4	chTOG TOG4 Native Protomer A	1.4	226	45
Msps TOG4	chTOG TOG4 Native Protomer B	1.3	223	46
chTOG TOG4 Native Protomer A	chTOG TOG4 Native Protomer B	0.5	224	100
chTOG TOG4 Native Protomer A	chTOG TOG4 SeMet	0.8	227	97
chTOG TOG4 Native Protomer B	chTOG TOG4 SeMet	0.7	224	97
Msps TOG2	**Msps TOG4**	**rmsd**	**# Res. aligned**	**% Identity**
HR-A	HR-A	1.5	33	18
HR-B	HR-B	1.2	33	27
HR-C	HR-C	1.4	38	18
HR-D	HR-D	1.7	32	25
HR-E	HR-E	2.0	41	15
HR-F	HR-F	2.6	28	18
HR-AB	HR-AB	1.8	74	20
HR-BC	HR-BC	1.7	73	22
HR-CD	HR-CD	1.9	72	21
HR-DE	HR-DE	2.2	76	18
HR-EF	HR-EF	2.5	67	15
HR-ABC	HR-ABC	2.0	113	19
HR-BCD	HR-BCD	2.3	107	22
HR-CDE	HR-CDE	2.4	116	19
HR-DEF	HR-DEF	2.8	104	18
HR-ABCD	HR-ABCD	2.7	148	20
HR-ABCDE	HR-ABCDE	3.4	197	21
HR-ABCDEF	HR-ABCDEF	4.5	226	20
Stu2 TOG1	**Msps TOG4**	**rmsd**	**# Res. aligned**	**% Identity**
HR-ABC	HR-ABC	2.5	102	19
HR-DEF	HR-DEF	2.8	95	12
HR-ABCDEF	HR-ABCDEF	4.2	202	15

SUPPLEMENTAL FIGURES

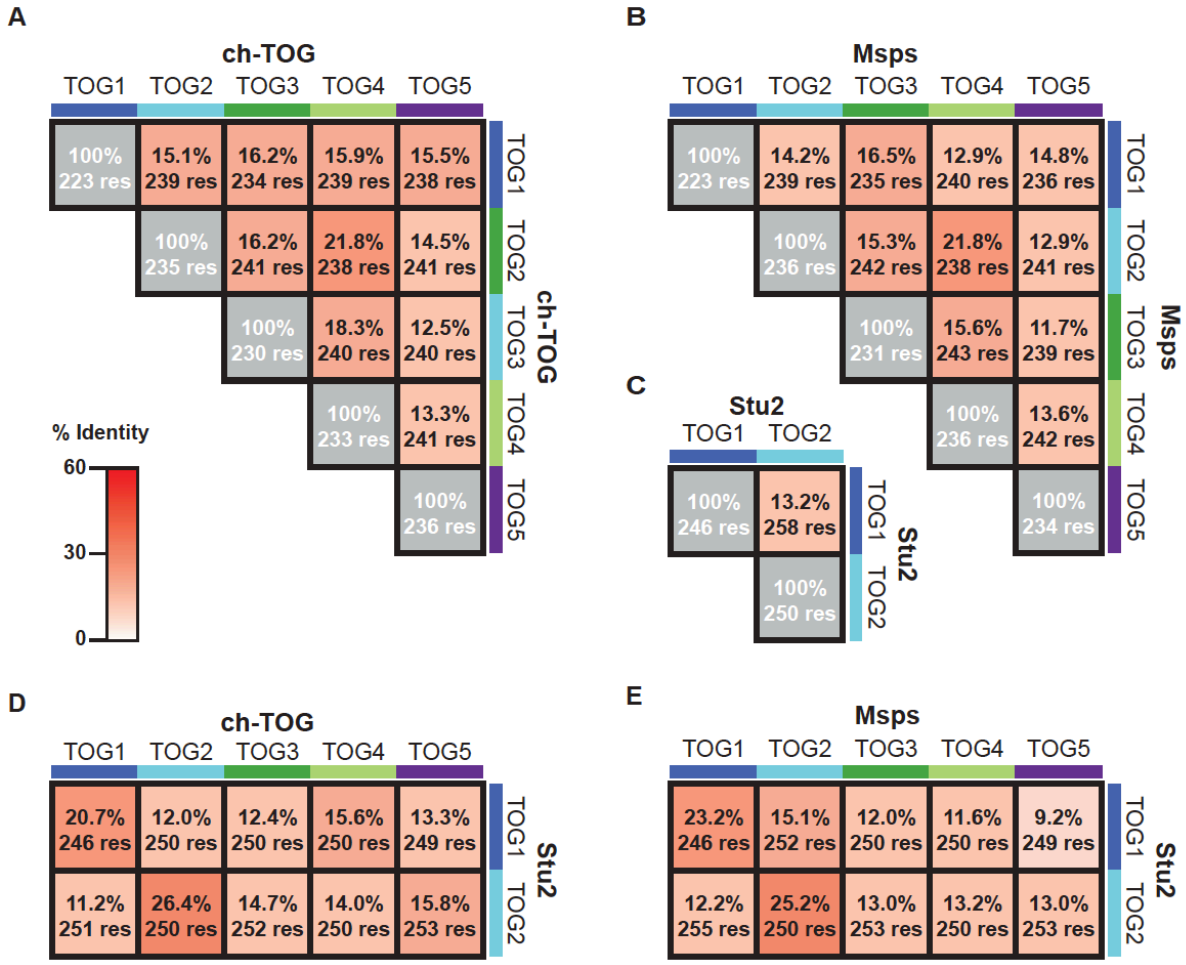

Figure 3-S1. TOG domains show positional conservation in the array. (A-E) Identity matrices, comparing TOG domains within a protein (A, ch-TOG; B, Msps; C, Stu2) or across species (D, ch-TOG vs. Stu2; E, Msps vs. Stu2). Percent identity, based on the alignment presented in Figure 1C, is indicated in each cell with the corresponding number of aligned residues listed below. Percent identity is contoured from 0% (white) to 60% (red). 100% identity is shown in gray.

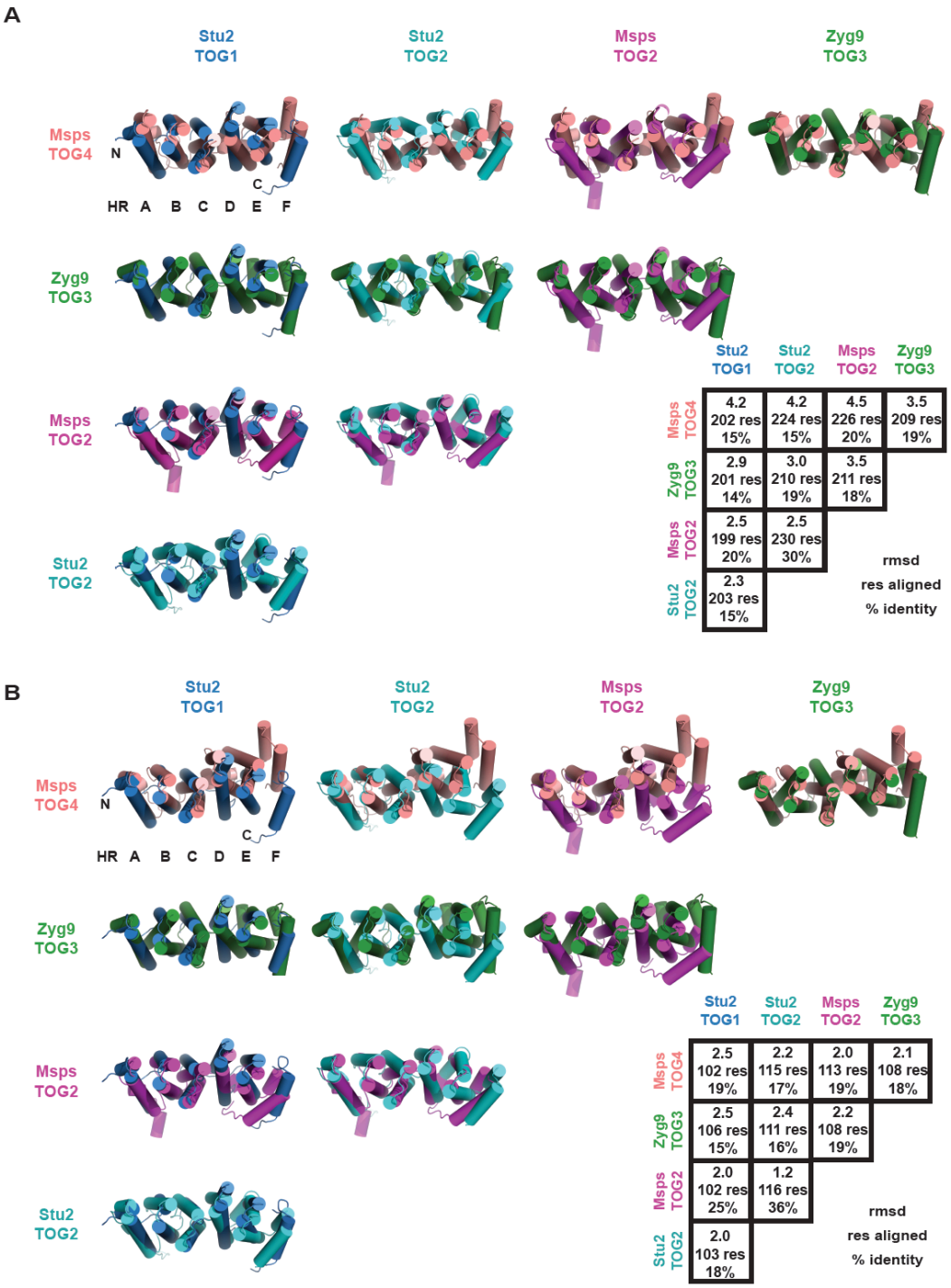

Figure 3-S2. The TOG4 structure is architecturally distinct from other XMAP215 TOG structures. Pairwise structural alignment matrix of XMAP215 family TOG domains: Stu2 TOG1 (dark blue), Stu2 TOG2 (cyan), Msps TOG2 (purple), Zyg-9 TOG3 (green), and Msps TOG4 (pink). Domains are shown in cartoon representation. Matrices in the lower right indicate the rmsd values (top) for the number of Cα atoms aligned (center), and the percent identity across the aligned region (bottom). (A) Pairwise structural alignment performed across HR A-F. (B) Pairwise structural alignment performed across HR A-C.

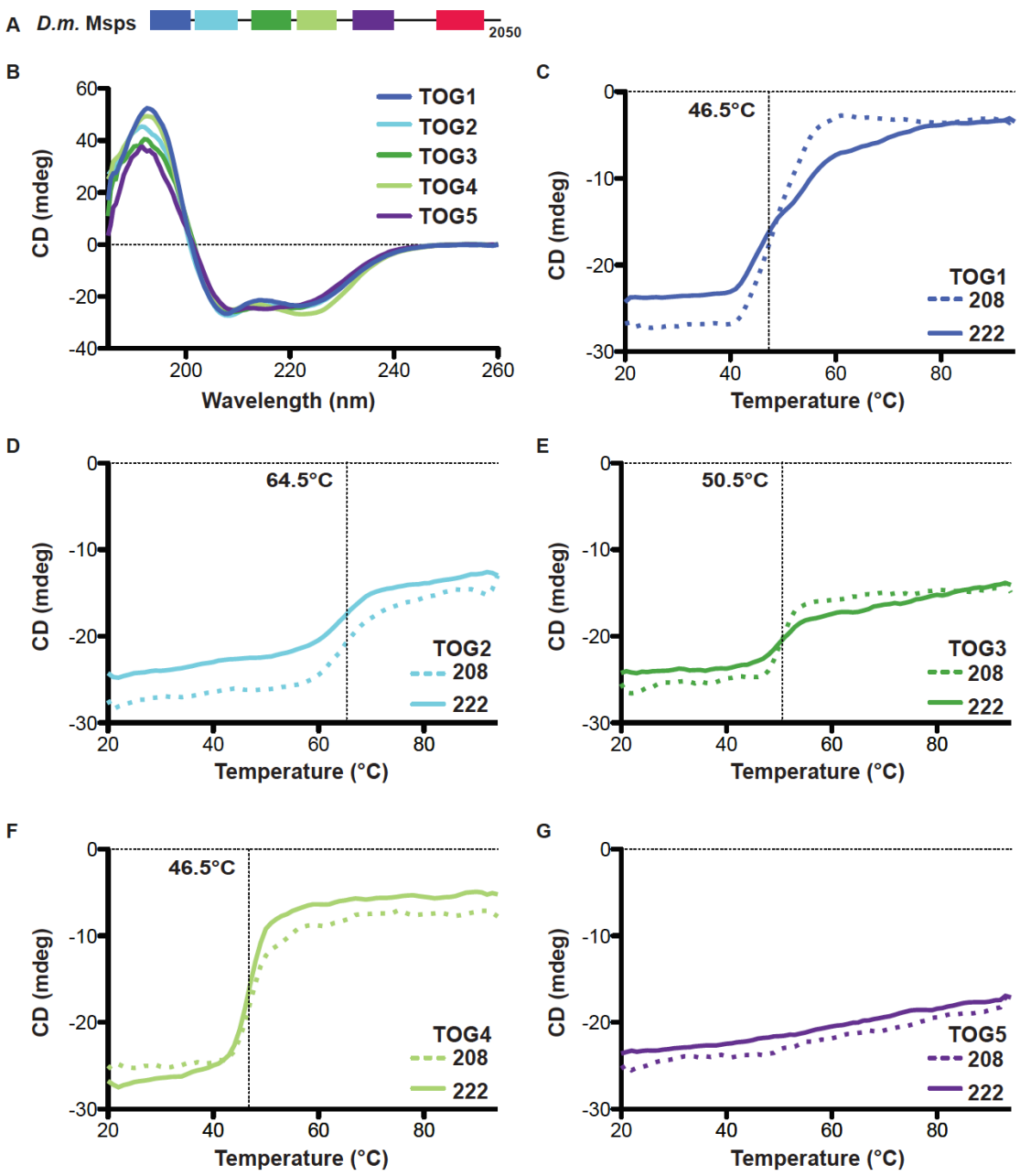

FIGURE 3-S3. Individual Msps TOG domains are α-helical and have varying thermostability. (A) Domain architecture of *Drosophila* Msps. (B) CD spectra of Msps TOG1 (blue), TOG2 (cyan), TOG3 (green), TOG4 (light green), and TOG5 (purple) at 23°C, pH 7.5 (0.1 mg/ml). Spectra show minima at 208 and 222 nm, indicative of similar α-helical structure in each of the TOG domains. (C-G) CD melts of Msps TOG1 (C), TOG2 (D), TOG3 (E), TOG4 (F), and TOG5 (G). CD signal was monitored at 208 nm (dashed trace) and 222 nm (solid trace) in 1°C step size from 20°C to 94°C. The inflection points were 46.5°C, 64.5°C, 50.5°C, and 46.5°C for TOG1, TOG2, TOG3, and TOG4, respectively. TOG5 had no inflection point suggesting it is unstable.

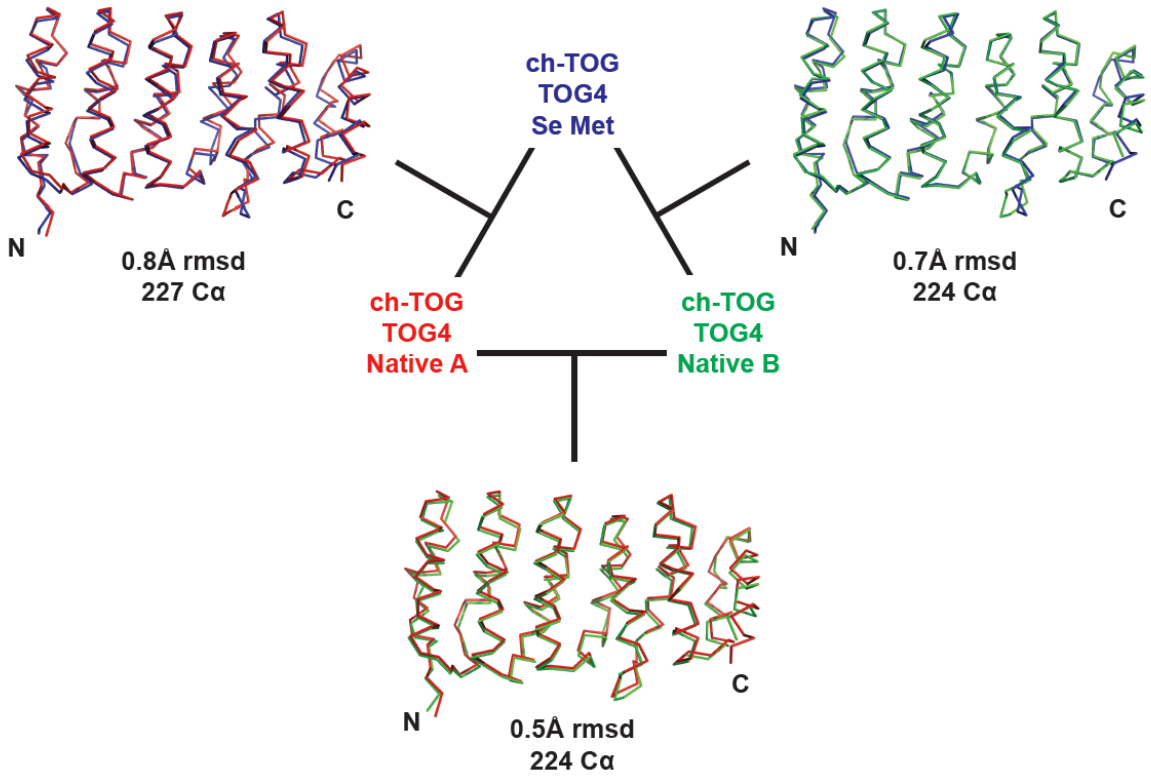

Figure 3-S4. TOG4 protomer structures are similar within and across space groups. Pairwise structural alignment of human ch-TOG TOG4 determined in two different crystal forms (ch-TOG TOG4 SeMet, $P4_32_12$ (blue); ch-TOG TOG4 native, $P2_12_12_1$ protomer A (red), ch-TOG TOG4 native, $P2_12_12_1$ protomer B (green). Cα rmsd values are indicated below each alignment with the corresponding number of Cα atoms aligned.

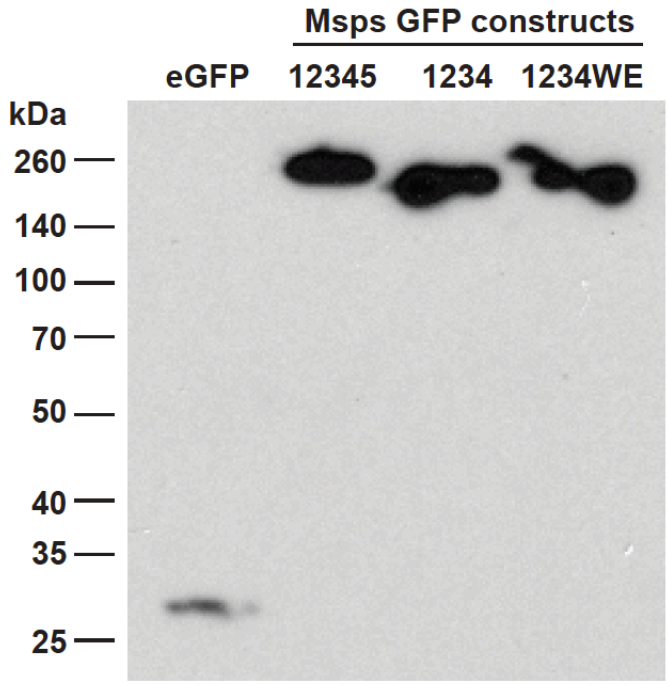

Figure 3-S5. Msps constructs express at the correct molecular weight. Western blot analysis of extracts from *Drosophila* S2 cells transfected with GFP control, Msps TOG1-5-GFP (12345), Msps TOG1-4-GFP (1234), or Msps TOG1-4-GFP with each TOG domain's HR A loop tryptophan mutated to glutamate (1234WE), and probed with anti-GFP antibody. All constructs expressed and ran at their expected molecular weight.

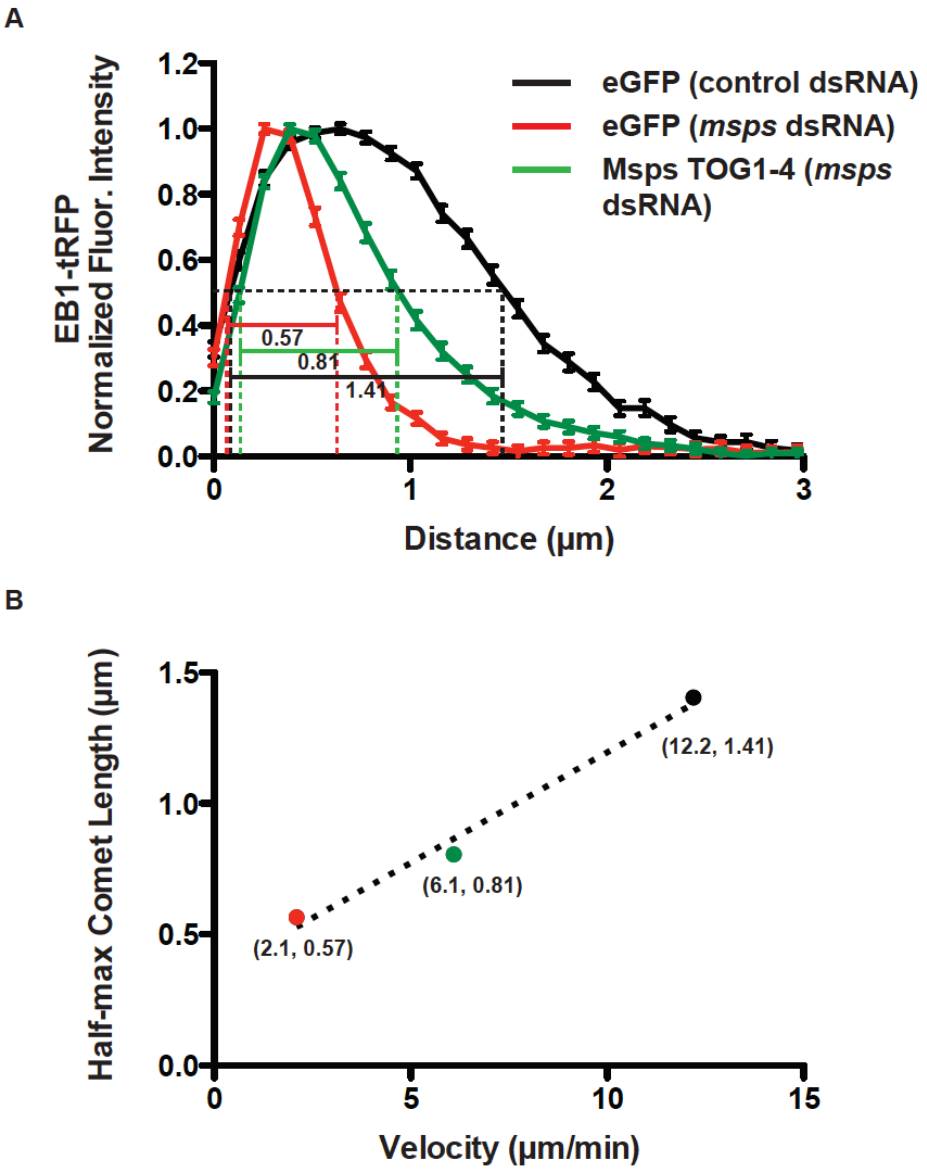

Figure 3-S6. EB1 comet length scales with the MT polymerization rate. (A) Fluorescence line scans along MT plus ends measuring the relative EB1-tRFP signal intensity. Shown are averaged line scans from S2 cells 1) treated with control dsRNA and transfected with a GFP control vector (black trace), 2) treated with *msps* dsRNA and transfected with a GFP control vector (red trace), and 3) treated with *msps* dsRNA and transfected with Msps TOG1-4-GFP (green trace). Distance (µm) is measured from the MT plus end towards the minus end. The length of half-maximal intensity comet length is indicated for each trace (µm). (B) The length of half-maximal EB1-tRFP comet intensity (y-axis) is plotted relative to the average velocity of these comets (x-axis). EB1 half-maximal comet length scales linearly with MT plus end velocity, indicating that MT sliding is not disproportionately affecting the various analyses.

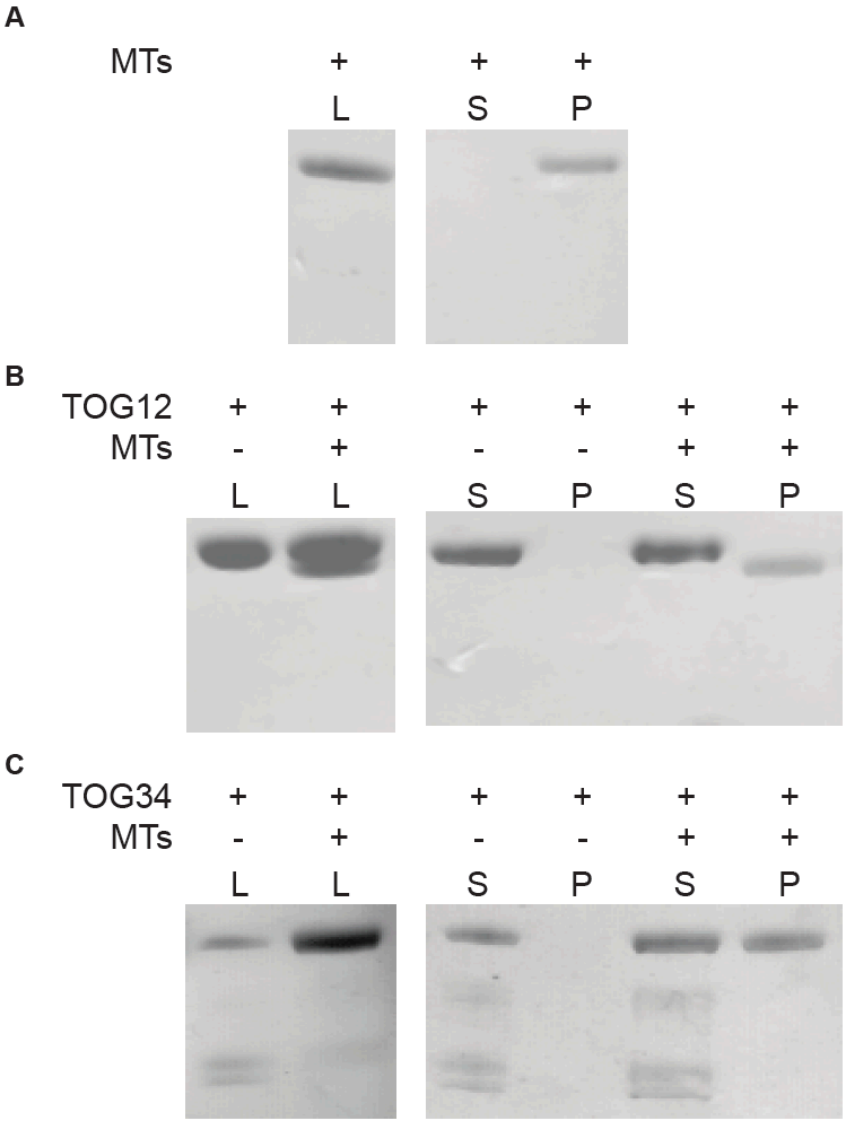

Figure 3-S7. Msps TOG1-2 and TOG3-4 do not bind to taxol stabilized MTs. Cosedimentation assays done in the presence or absence of MTs show TOG12 and TOG34 do no interact with taxol MTs. Load samples for MT control (A) TOG12 (B) and TOG34 (C) are shown in the left panel while supernatant and pellet are shown in the right panel.

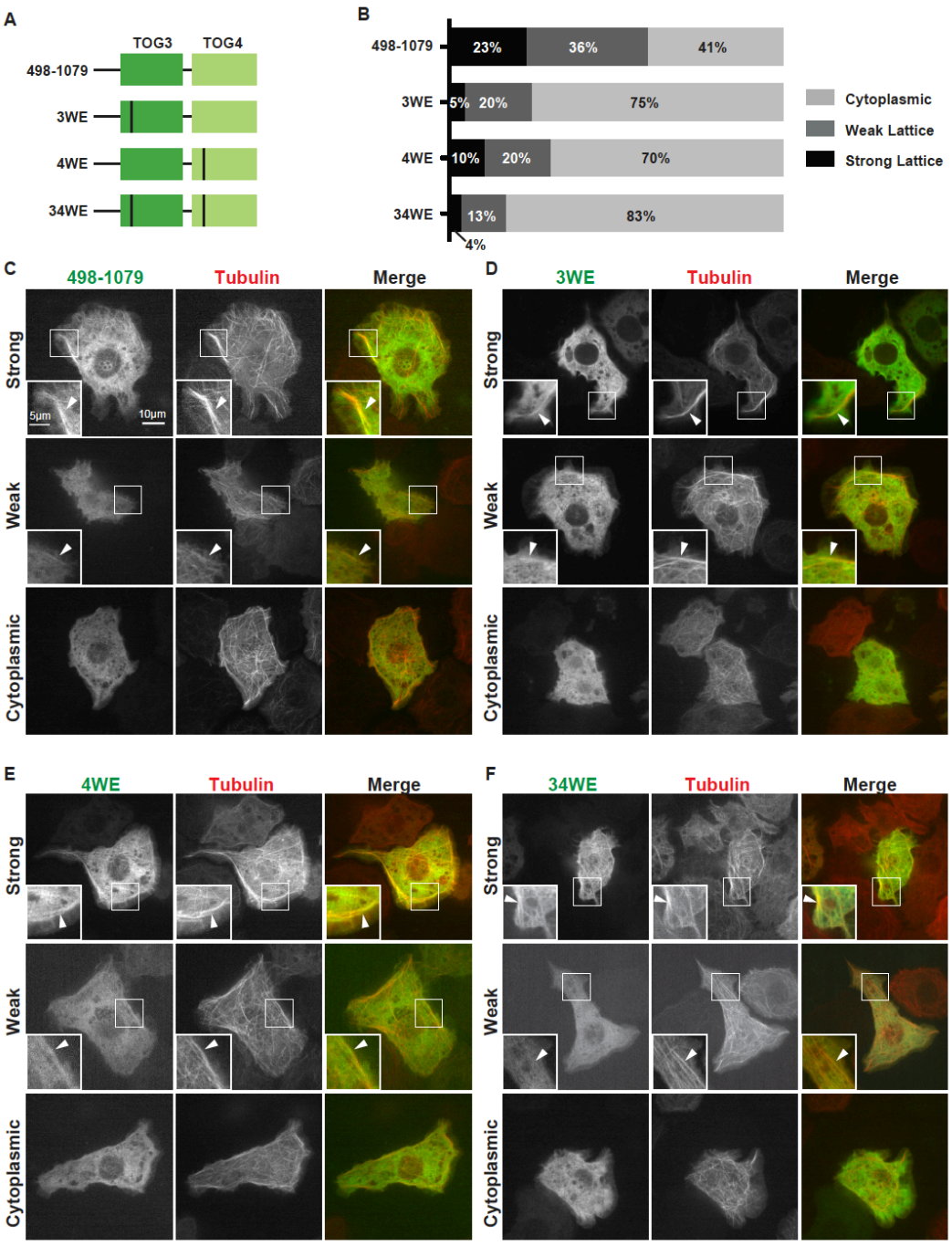

FIGURE 3-S8. TOG3 and TOG4 contribute to Msps MT lattice binding. (A) Msps tRFP constructs analyzed; vertical line represents a HRA loop W→E mutation. (B) Distribution of Msps 498-1079 tRFP lattice binding in *Drosophila* S2 cells transfected α-tubulin GFP. Msps localization was binned into three categories: strong lattice binding (black), weak lattice binding (dark gray) and cytoplasmic (light gray). Error bars represent standard deviation. Representative images from each category are displayed (C-F). Mutating individual (D-E) or paired (F) conserved HR A loop tryptophans resulted in a increase in cytoplasmic localization. Scale bars in images: 10μm, and in insets: 5μm. Statistical significance was determined using an unpaired T test to calculate two-tailed p-values for the cytoplasmic bin.

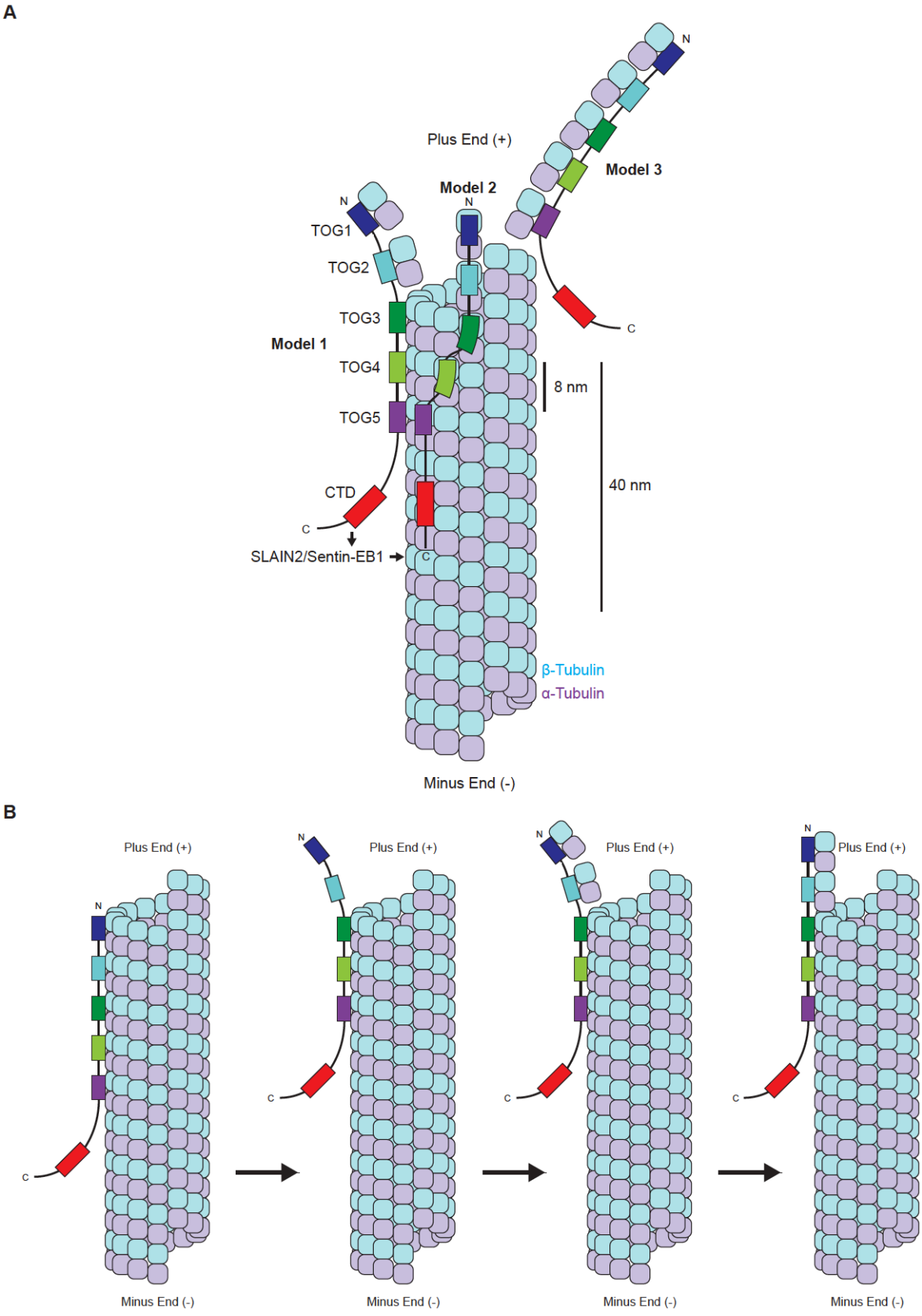
A
Plus End (+)
Model 3
Model 2
Model 1
TOG1
TOG2
TOG3
TOG4
TOG5
CTD
SLAIN2/Sentin-EB1
8 nm
40 nm
β-Tubulin
α-Tubulin
Minus End (-)
B
Plus End (+)
Minus End (-)

Figure 3-S9. Models of XMAP215 family proteins at the microtubule plus end. (A) Three simplistic models are presented showing a XMAP215 family member with a pentameric TOG array interacting with and adding tubulin heterodimers to the MT plus end. The MT plus end is shown as a B-lattice, though data suggests that the polymerizing MT plus end may be an open sheet. The TOG domains are colored as in Figure 3-1A. Given that a conserved tryptophan in the HR A loop of each of the first four TOG domains when mutated to glutamate reduces rescue activity, it is likely that this tryptophan is used by each TOG domain to interact with a tubulin heterodimer as observed in the Stu2 TOG1-αβ-tubulin structure (Ayaz et al., 2011). Each TOG domain is shown interacting with a tubulin heterodimer in the lattice with the polarity observed in the Stu2 TOG1-αβ-tubulin structure: the TOG domain's N- and C-termini directed towards the MT plus and minus end respectively. Model 1 shows the XMAP215 family member processes along the MT plus end resulting in TOGs 1-2 free to bind free tubulin and TOGs 3-4 interacting with the very distal MT plus-end. This model presented is simplistic, and has the full array bound to sequential tubulin subunits along a single protofilament, but whether all TOG domains bind the same protofilament (Model 2), whether they are arranged from the plus end to the minus end, and what the lateral and longitudinal spacing of each TOG domain on the lattice is remains to be determined. Model 3 illustrates a templating model where all five TOG domains bind tubulin and incorporate multiple heterodimers into the lattice at once. (B) Model of tubulin heterodimer incorporation based on Model 1. This model is similar to previously proposed models (Widlund et al., 2011) and includes diffusion to the plus-end, followed by complex formation with free tubulin, and incorporation into the lattice. Each model, as presented, would position the XMAP215 C-terminal domain (CTD) distal to the MT plus end where it would interact with EB1 via SLAIN2/Sentin. Relative scales are shown at right.

CHAPTER 4: A STRUCTURE/FUNCTION ANALYSIS OF THE *DROSOPHILA* TACC FAMLY MEMBER DTACC

Summary

TACC family proteins have proven important structural components of the mitotic spindle apparatus. Disruption of TACC function causes disorganized and unstable spindle microtubules leading to multiple biological consequences including chromosome instability, developmental problems, and cancer (reviewed in Thakur et al., 2013). The mechanism in which TACC functions at the centrosome is still poorly understood. Our study aims to further the field of centrosome biology by understanding how TACC is interacting with its binding partners, specifically XMAP215 family members. Here we have identified a minimal domain of the *Drosophila* TACC family member, DTACC, that confers TACC dimerization, localizes to spindle poles in mitosis and tracks along the MT plus-end potentially through an interaction with the XMAP215 family member Msps in interphase. Mutational analysis has identified specific residues important for Msps binding and centrosome localization within the minimal domain of DTACC. Further analysis is ongoing in the lab to probe the effects of the potent mutations on both DTACC dimerization and the Msps-DTACC interaction. We also hop to identify centrosomal binding factors that interact with TACC, and to structural characterize the DTACC-Msps interaction.

Experimental Procedures

Multiple species alignment

Alignments were produced using ClustalW. Proteins aligned were DTACC (*D. melanogaster*), hTACC3 (human), rTACC3 (*O. cuniculus*), mTACC3 (*M. musculus*), Maskin (*X. laevis*), zTACC3 (*D. rerio*), TACC (*D. discoidium*), and TAC-1 (*C. elegans*).

Drosophila S2 cell expression constructs

DTACC constructs were subcloned using the Gateway pENTR D-TOPO cloning system (Invitrogen) in a final zeocin selective pIZ backbone destination vector with a metallothionine promoter and a C-terminal GFP tag. The following constructs were constructed: 1-1063, 1064-1176, 1064-1255, 1064-1308, 1094-1308, 1123-1308, 1162-1308, 1177-1308, 1209-1255, 1209-1308, and 1256-1308. Mutations were generated using QuikChange (Agilent technologies). α-tubulin-mCherry was made by subcloning α-tubulin into a final pIZ backbone vector with a metallothionine promoter and a COOH-terminal mCherry tag.

Cell culture, transfections, and RNAi

Drosophila S2 cells were grown in Sf-900 media and passed every 3-5 days. S2 cells were treated with dsRNA for 5 days (Rogers and Rogers, 2008) and transfected using the Amaxa Nucleofector II transfection system (Lonza) according to the manufacturers protocol. Cells were induced with 100μM $CuSO_4$ for 12-18 hours. Primers for dsRNA were designed by attaching the T7 promotor sequence to primer sequences targeting the 3' UTR sequence (5'-ACTCATCTCGCGATTGTCCGGAATGTAATTT-3' and reverse 5'-GTATTATGCATAAATTAATTTTTTCGTGTATTT-3') or the N-terminal coding sequence (base pairs 1144-1674; 5'-TCAAAACCAGAGAATAATTTTGTGCAC-3' and reverse 5'-

ATCCACATCCATGTTATCAAGCTCC-3') of DTACC. dsRNA was generated using the T7 RiboMAX *in vitro* transcription system. DTACC knockdown was confirmed by western blot.

Fluorescence microscopy

Drosophila S2 cells were plated onto concanavalin A coated glass bottom dishes in Schneider's media supplemented with 10% FBS and incubated for 30 minutes prior to imaging. Time-lapse images were collected at 25°C with a 100x 1.45 NA aperture, Plan Apochromat objective using a VT-Hawk (Visitech) 2D array scanning confocal system with an Orca-R2 CCD camera controlled using VisiTech Vox software. Images were collected at a 3 second per frame interval over 4 minutes.

Cloning, expression, and purification

DTACC constructs were generated by subcloning into pET28 (Novagen), which contains a thrombin-cleavable, N-terminal 6xHis tag. DTACC fragments included 1064-1304, 1064-1176, and 1177-1304. Constructs were transformed into BL21 DE3 (pLysS) *E. coli* cells and grown in Luria Broth at 37°C to an optical density of 0.8 (600 nm). Protein expression was induced with 100 μM IPTG at 18°C for 18 hours. Cells were harvested by centrifugation at 3,500 rpm for 10 minutes at 4°C and resuspended in Buffer A (25 mM Tris pH 8.0, 300 mM NaCl, 10 mM Imidazole, 0.1% β-ME). Cells were lysed via sonication in the presence of phenylmethylsulfonyl fluoride to prevent proteolytic degradation. Lysate was cleared by centrifugation at 15,000rpm for 45 min at 4°C. Supernatant was loaded onto a Ni^{2+}-NTA column (Qiagen), washed with 300 ml of Buffer A, and eluted using a 250 ml linear salt gradient (0-300 mM imidazole). Fractions containing protein were pooled and 0.1mg of bovine α-thrombin was added to remove the 6xHis tag. Protein was incubated for

18 hours at 4°C then passed over a 0.5 ml Benzamidine sepharose (GE Healthcare). Protein was exchanged into Buffer S (constructs 1064-1304 and 1064-1176; 25mM Tris pH 8.0, 0.1% β-ME) or Buffer Q (1176-1304; 25mM HEPES pH 7.0, 0.1% β-ME) using a Millipore Ultrafree 10K MWCO concentrator. Sample was loaded onto a SP-sepharose or Q-sepharose, respectively and eluted using a 250 ml linear salt gradient (0-1M NaCl). Fractions containing protein were pooled, exchanged into storage buffer (25mM HEPES pH 7.0, 0.1% β-ME), frozen in liquid nitrogen, and stored at -80°C.

SEC-MALS

100 µl of 145 µM DTACC 1064-1308, 1064-1176, or 1177-1304 was injected onto a Superdex 200 10/300 GL gel filtration column (GE Healthcare) in 25mM HEPES pH 7.5, 300 mM NaCl, 0.2 g/L NaN_3 coupled with a Wyatt DAWN HELIOS II light scattering instrument with a Wyatt Optilab T-rEX refractometer. Molecular weights were calculated using light scattering and refractive index data with the Wyatt Astra V software package (Wyatt Technology Corp) (REF). For binding experiments with Msps, proteins were mixed with a 2:1 Msps:TACC ratio and allowed to incubated for 10 min on ice before injection onto the gel filtration column.

Results

TACC family proteins contain a conserved 200 amino acid TACC domain

The defining feature of the TACC family of proteins is the presence of a conserved 200 amino acid TACC domain (Figure 4-1A). To investigate the conservation of this TACC domain, we performed a multi-species alignment across eight diverse species. We mapped residues that displayed 80% sequences identity (green) and 80% sequence similarity (yellow)

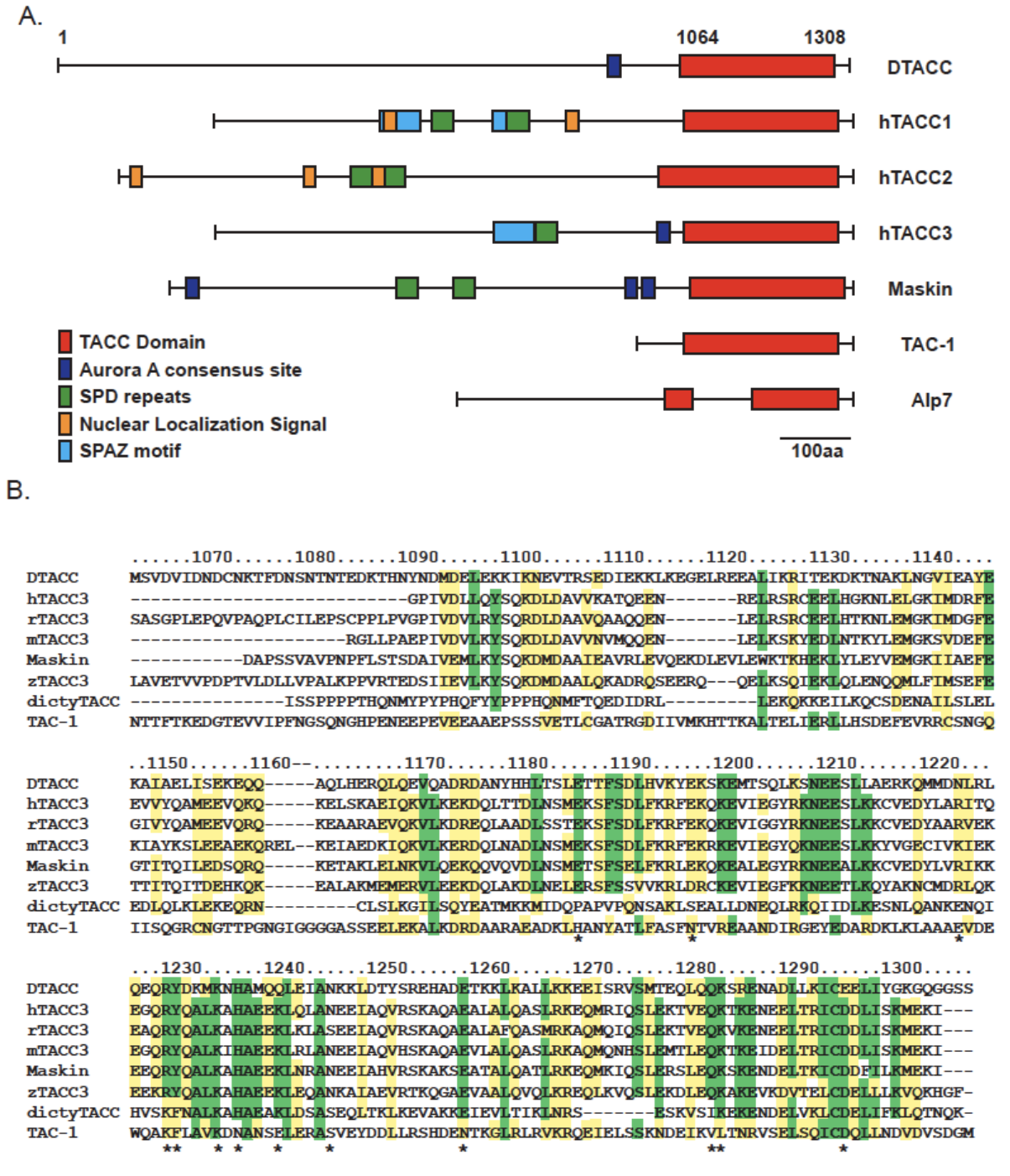

Figure 4-1. TACC family proteins contain conserve 200 amino acid TACC domains. (A) Domain architecture of *Drosophila* TACC family member, DTACC. (B) Sequence alignment of TACC domains from DTACC (*D. melanogaster*), hTACC3 (human), rTACC3 (*O. cuniculus*), mTACC3 (*M. musculus*), Maskin (*X. laevis*), zTACC3 (*D. rerio*), TACC (*D. discoidium*), and TAC-1 (*C. elegans*). Residue numbers are for *Drosophila* DTACC. Conservation has been mapped: 75% identity is highlighted in green and 75% similarity is highlighted in yellow. Stars indicate mutations made in Figure 4-5.

for the 200 amino acid TACC domain onto the eight species including DTACC (*D. melanogaster*), hTACC3 (human), rTACC3 (*O. cuniculus*), mTACC3 (*M. musculus*), Maskin (*X. laevis*), zTACC3 (*D. rerio*), dictyTACC (*D. discoidium*), and TAC-1 (*C. elegans*) (Figure 4-1B). While the conservation across the entire TACC domain is high, we note increased conservation in the latter 100 amino acids of the TACC domain (DTACC residues 1177-1308) suggesting functional conservation within this region.

The Drosophila TACC domain confers localization to the MT plus-end and centrosomes

While the TACC domain exhibits a high degree of conservation across species, the N-terminal regions are more divergent in both sequence and function. Previous studies have identified various functional domains in the N-terminal region in many of the TACC family members including SPD repeats, SPAZ motifs, nuclear localization sequences, and Aurora A consensus sites. DTACC contains an Aurora A phosphorylation site N-terminal of the TACC domain however, little else is known about the N-terminal 1000 amino acids (Figure 4-1A, Peset and Vernos, 2008). The Raff laboratory has shown two distinct localization patterns for DTACC: the centrosome and to the plus-end of MTs via an interaction with the microtubule polymerase Msps (Gergely et al., 2000a; Lee et al., 2001). To investigate which regions of DTACC are responsible for the observed localization patterns, we performed in cell localization assays with truncated DTACC constructs; an N-terminal construct (residues 1-1063) and the TACC domain (residues 1064-1308) (Figure 4-2A). *Drosophila* S2 cells were treated over seven days with RNAi targeting the 3'UTR for the N-terminal construct or base pairs 1144-1674 for the TACC domain. RNAi depletion of endogenous DTACC was

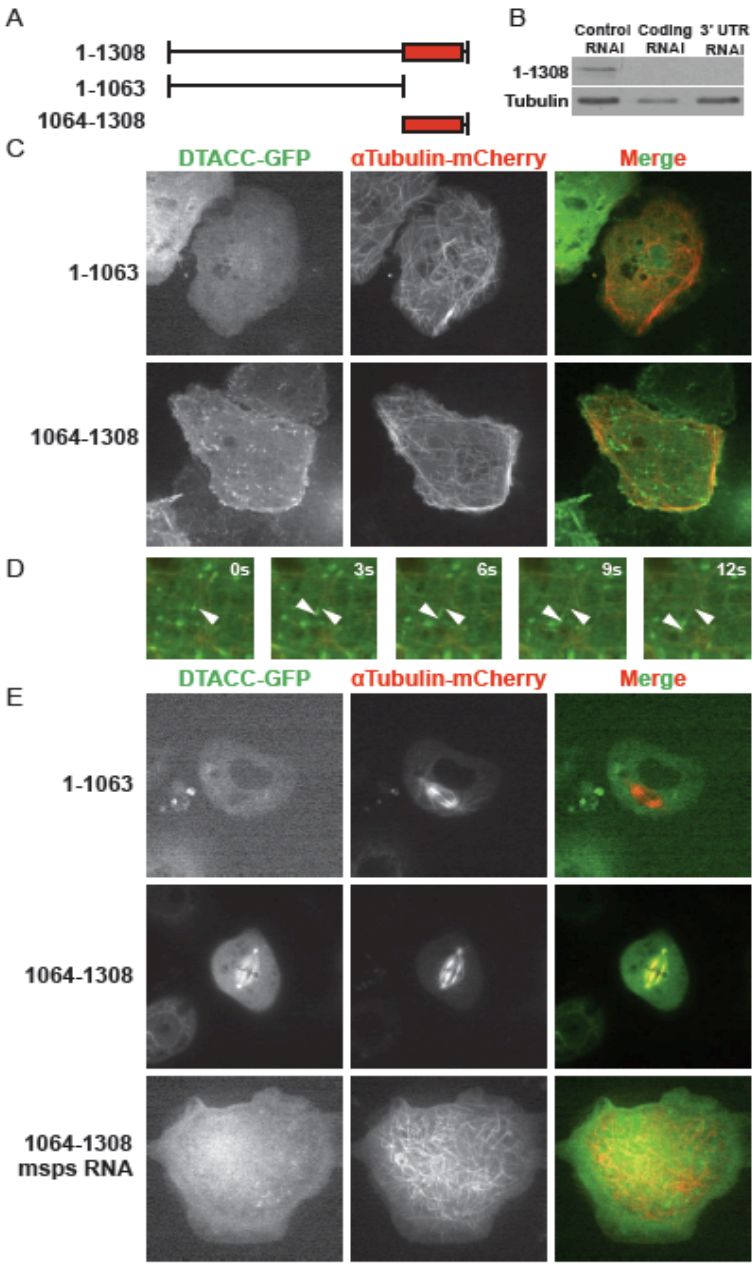

Figure 4-2. The conserved C-terminal 200 amino acid TACC domain tracks along MT plus-ends and confers localization to centrosomes. (A) DTACC truncation constructs analyzed. (B). Western blot of *Drosophila* S2 cells treated with RNA targeting DTACC coding and 3'UTR sequences for 3 days (C) Interphase localization pattern for DTACC truncation constructs in (A). S2 cells were transfected with GFP-tagged DTACC constructs (left, displayed in green) and α-tubulin-mCherry (middle, displayed in red) and DTACC expression induced for 18 hours. DTACC 1-1063 (top) was cytoplasmic while DTACC 1064-1308 (bottom) localized to the MT plus-ends (arrows). (D) Time-lapse images illustrating DTACC 1064-1308 (arrows) tracking along two MT plus-ends. (E) Mitotic localization of DTACC truncation constructs. DTACC 1-1063 (top) was cytoplasmic while DTACC 1064-1308 robustly decorated the spindle and localized to centrosomes (middle). Plus end localization was lost when cells were treated with *msps* RNA (bottom).

confirmed by Western blot analysis (Figure 4-2B). Truncation constructs labeled with a C-terminal GFP were co-transfected in S2 cells with α-tubulin-mCherry and assayed for localization during interphase and mitosis. The N–terminal 1-1063 construct showed no distinct localization patterns, exhibiting disperse cytoplasmic localization in both interphase and mitotic cells (Figure 4-2C, D, top). The TACC domain robustly localized to MT plus-ends during interphase (Figure 4-2C) and tracked along growing microtubules (Figure 4-2D). The TACC domain also exhibited strong localization to spindle poles, spindle MTs, and kinetochores during mitosis (Figure 4-2E). These data show that the TACC domain is necessary for DTACC localization patterns noted in cells.

Though DTACC has been shown to localize to MT plus ends, there is no direct interaction between DTACC and MTs. Previous work in the field suggests the tip-tracking interaction could be facilitated by DTACC's interaction with the XMAP215 family homolog in *Drosophila,* Minispindles (Msps) (Lee et al., 2001). The XMAP215 family promotes microtubule polymerization and processes along the growing MT plus-ends. To test whether the observed DTACC plus-end localization is a result of interaction with Msps we performed similar assays with the TACC domain in Msps RNA treated S2 cells. In a Msps knock-down background, DTACC is no longer at the MT plus-end, but displays cytoplasmic localization during interphase (Figure 4-2D). This observation suggests that plus-end binding is due to an interaction with Msps and can be used to analyze the DTACC-Msps interaction.

DTACC residues 1177-1308 are a minimal domain that localizes to the MT plus-end and centrosomes

Secondary structure predictions suggest the TACC domain is folded in a coiled-coil with one predicted break. To analyze if the entire coiled-coil in necessary for plus-end

tracking or centrosome localization, we systematically truncated the TACC domain and assayed for localization in both interphase and mitosis. Truncations were based on both secondary structure predictions and breaks in conservation across the domain. We performed in cell localization assays as described above on the TACC domain truncation constructs (Figure 4-3A). Interphase localization revealed a minimal plus-end tracking domain consisting of residues 1177-1308 (Figure 4-3B). Truncating the domain N-terminally any further results in a loss of plus-end binding, suggesting that the entire region from 1177-1308 is necessary for interacting with Msps. The construct spanning 1177-1308 also localizes to centrosomes in mitosis however is less robust on the spindle MTs and kinetochores (Figure 4-3C) and a smaller construct (1209-1308) proved to contain the minimal residues necessary for centrosomal localization.

The TACC domain exists as a dimer in solution

Previous studies have reported that TACC forms a higher order oligomer (Gergely et al., 2000b, Thakur et al., 2013). To test the oligomerization state of the *Drosophila* TACC domain in solution, we performed size-exclusion chromatography coupled with multi-angle light scattering (SEC-MALS) on the entire TACC domain and two truncation constructs; the minimal domain (residues 1177-1304) and the preceding N-terminal residues (residues 1064-1176) (Figure 4-4A). The elution profile and molar mass for each construct at 145μM was obtained and analyzed in 25mM HEPES pH 7.5, 300 mM NaCl, 0.2 g/L NaN_3 (Figure 4-4B). The TACC domain (1064-1304) elution profile contained four distinct peaks with molar masses of 15.6 kDa, 24.5 kDa, 59.4 kDa, and 54.8 kDa. The expected molar mass of a 1064-

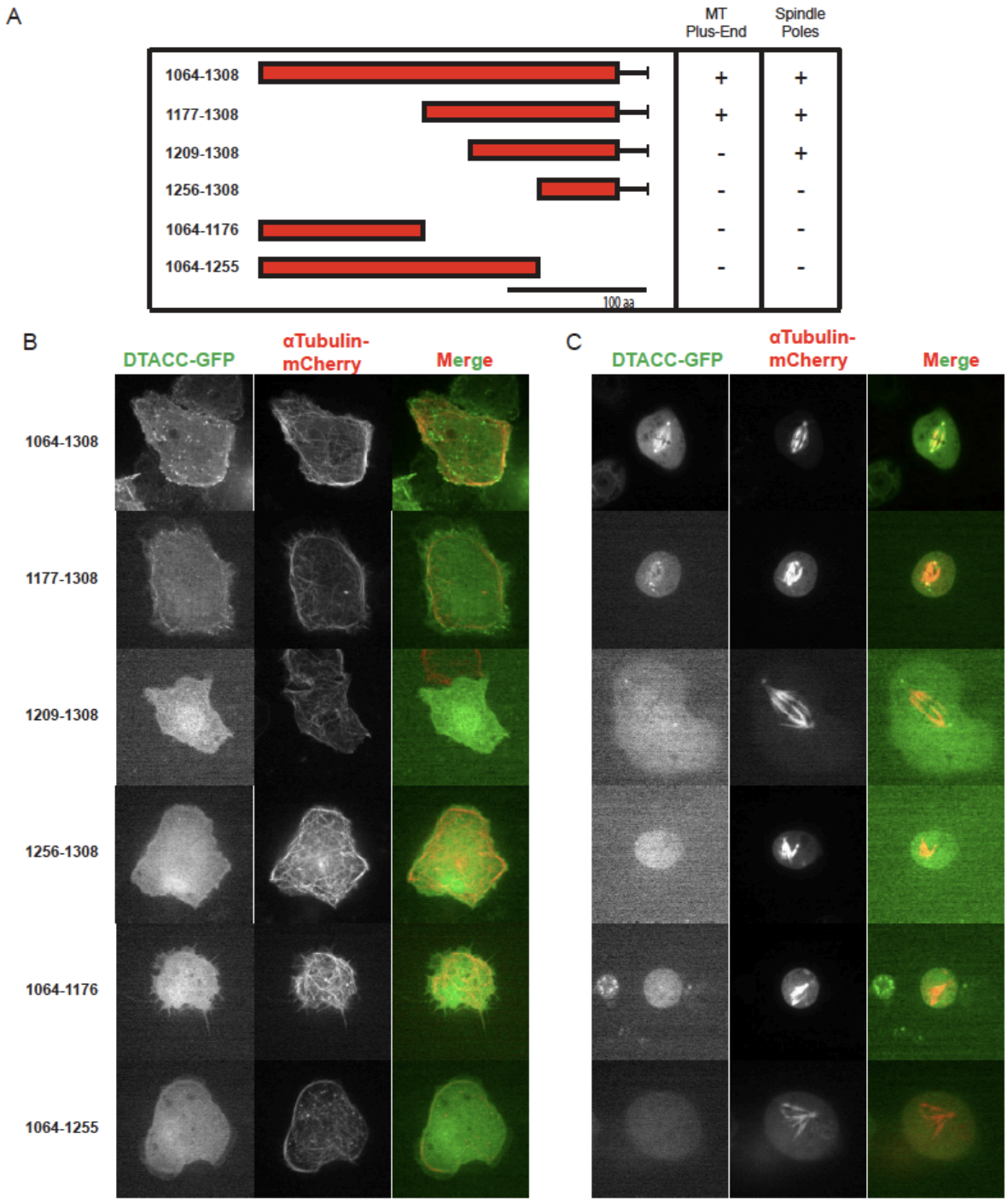

Figure 4-3. Structure/function analysis reveals minimal DTACC regions that confer MT plus-ends localization and centrosome localization. (A) TACC domain truncations analyzed. (B) Interphase localization of truncation constructs listed in (A). S2 cells were transiently transfected with GFP-tagged truncation (left) construct and α-tubulin-mCherry (middle) and scored for localization to microtubule plus ends. (C) Mitotic localization of TACC domain truncation constructs listed in (A). Mitotic cells were scored for localization to spindle poles.

1304 monomer is 28 kDa. Therefore, 1064-1308 is primarily a dimer under the conditions analyzed with 78% of the protein mass in the 59.4 kDa peak and 11% in the 54.8 kDa peak. This discrepancy in molar mass could be due to a variation in protein fold of the domain resulting in one more compact conformation or due to a degradation product that is smaller than the full-length protein. A peak equivalent to a monomeric form of 1064-1304 (24.5 kDa) was also observed however contained only a small pool (5.6%) of the total protein mass. A fourth smaller peak exhibited a calculated molar mass of 15.6 kDa, which is smaller than the expected molar mass of this construct (28kDa). This peak was only accountable for 4.8% of the protein mass injected and is potentially a contaminating protein or a degradation product. The 1064-1176 elution profile contained one distinct peak with 100% of the protein mass with a molecular weight of 14.5 kDa. The expected molecular mass of 1064-1176 is 15 kDa, indicating this fragments is a monomer under the conditions analyzed. The minimal domain, residues 1177-1304 also exhibited an elution profile with a single peak containing 100% of the protein mass. The calculated molar mass was 26.8 kDa and, with an expected molar mass of 17 kDa, our data indicates DTACC 1177-1304 is a dimer under these conditions analyzed. Together, these data show the minimal plus-end and centrosome localization domain also facilitates dimerization of DTACC.

Mutational analysis reveals distinct Msps binding and centrosome localization regions

To dissect the residues responsible for binding to Msps and localization to the centrosomes, we performed a mutational analysis of the minimal domain that localizes to both the MT plus-end and centrosome; residues 1177-1304. Mutations were designed based

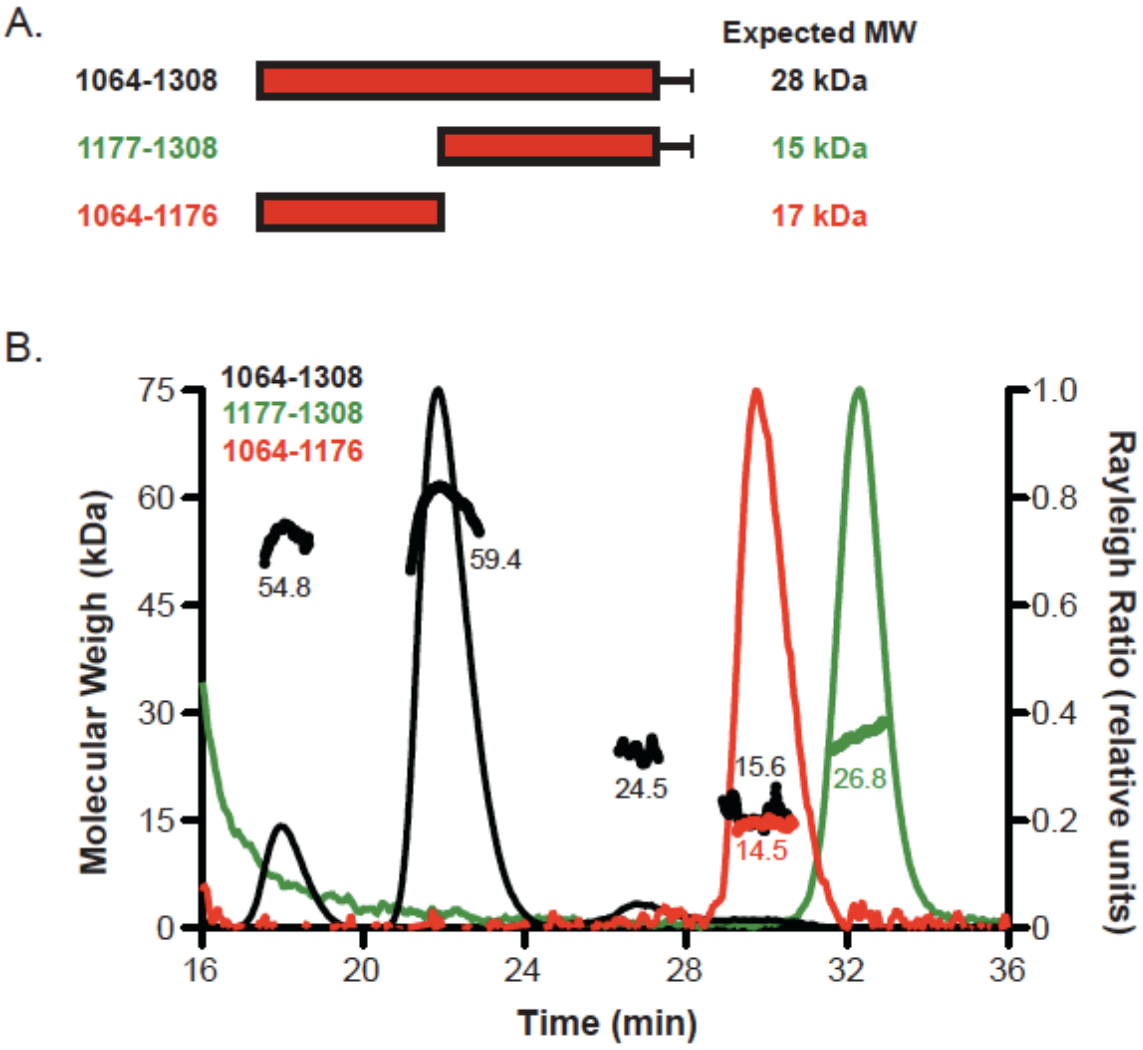

Figure 4-4. The DTACC minimal domain promotes TACC domain dimerization. (A) DTACC constructs analyzed by SEC-MALs. Constructs include the TACC domain (residues 1064-1304, black), the minimal domain that confers TACC localization patterns (1177-1304, green) and the N-terminal portion of the TACC domain (1064-1304, red). Expected molecular weights are shown (right). (B) SEC-MALs analysis. 100 µl of 145 µm DTACC construct were analyzed at pH 7.5. Each peak shows the molecular weight of the protein and the fraction of the total injected mass present in the peak.

on the predicted heptad repeat and targeted hypothetically exposed, conserved, charged residues (Figure 4-1B, asterisks). Of the 14 mutations tested, only three had no effect on the tip-tracking localization of the 1177-1304 (E1186K, E1197K, N1223E, Figure 4-5A, C). The majority of the charge reversal mutations resulted in a loss of plus-end localization (Figure 4-5A, C). These data suggest that DTACC interacts with Msps via a large binding interface that spans more than 60 amino acids. Introducing any charge reversal along this binding interface between residues 1230 and 1296 results in a loss of tip-tracking activity. Interestingly, two mutations (E1259K and E1296K) did not have clear localization, with 27% and 38% of cells still containing plus-end tracking localization. This differential localization could be due to the very C-terminal positioning of the mutations within the coiled-coil. If the Msps interaction encompasses the entire region of 1177-1304, mutations at the edge of this binding interface may be less penetrant than mutations in the core of the binding surface, thus accounting for the disparate localization observed with the E1259K and E1296K mutants.

We also assayed for the ability of these mutant constructs to localize to centrosomes in mitosis (Figure 4-5B, C). Unlike interphase localization, most mutations had not effect on centrosome localization. We found three mutations that interrupt centrosome localizations that mapped to a region of high conservation in the TACC domain (Figure 4-5D). Residue 1230R showed weak (30% of cells) to no (70% of cells) centrosome localization when mutated to a glutamic acid. Weak localization was defined by the presence of faint signal from the GFP-labeled TACC mutant construct on at least one spindle pole. The second mutation that resulted in loss of centrosome localization was 1231YA. To test if this was due to the loss of phosphorylation, we mutated the tyrosine to a non-phosphorylatable phenylalanine (Figure 4-5C). This construct was still able to localize to the centrosome,

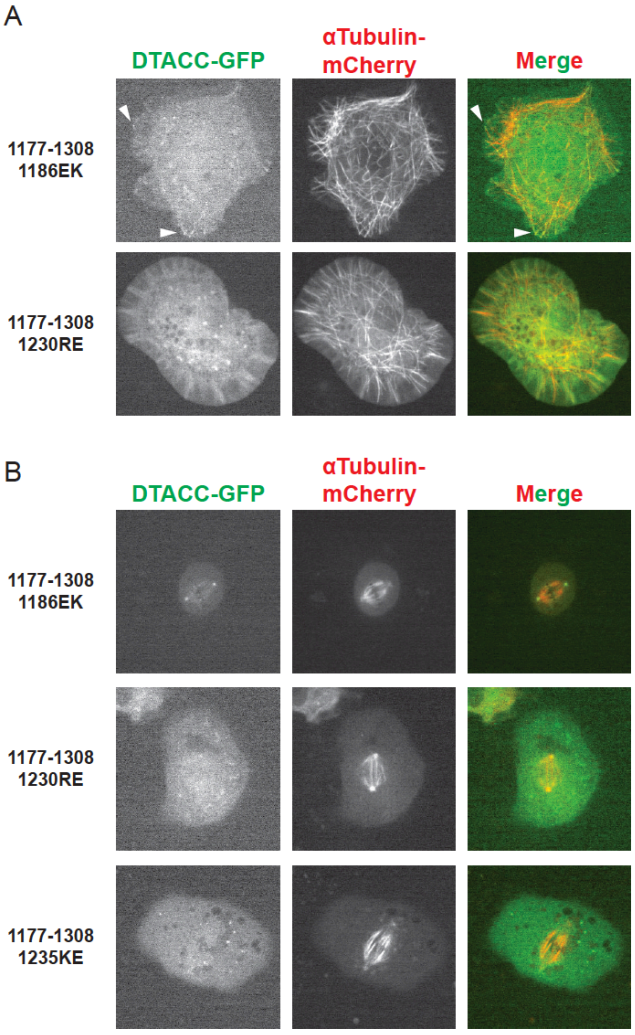

C

Mutation	MT Plus-End	Spindle Poles
E1186K	+	+
E1197K	+	+
N1223E	+	+
R1230E	-	- / weak +
Y1231A	-	-
Y1231F	-	+
K1235E	-	-
K1235A	-	+
H1237E	-	+
Q1241E	-	+
N1246E	-	+
E1259K	+/-	+
QK1283/4AE	-	+
E1296K	+/-	+

D

```
                .1230......1240
DTACC           QRYDKMKNHAMQQLE
hTACC3          QRYQALKAHAEEKLQ
rTACC3          QRYQALKAHAEEKLK
mTACC3          QRYQALKIHAEEKLR
Maskin          QRYQALKAHAEEKLN
zTACC3          KRYQALKAHAEEKLE
TACC(Dicty)     SKFNALKAHAEAKLD
TAC-1           AKFLAVKDNANSELE
                 **    *
```

Figure 4-5. Mutational analysis of DTACC 1177-1304 reveals residues important for Msps binding and/or centrosome localization. (A) Representative interphase localization images from the mutational analysis of DTACC minimal domain. Three mutations had no effect on the ability of residues 1177-1308 to plus-end track along growing microtubules (E1186K, top). However, 11 mutations resulted in a decrease of loss of plus-end binding (R1230E, bottom). (B) Representative mitotic images from the mutational analysis of DTACC minimal domain. 11 mutations had no affect on localization to centrosomes (E1186K, top), while three mutations resulted in a loss of localization at the spindle poles (1230RE, bottom). (C) Summary of DTACC minimal domain mutational analysis. Interestingly, two mutations (E1259K and E1296K) did not have clear localization, with 27% and 38% of cells still containing plus-end tracking localization indicated by the +/- notation. (D) Sequence conservation of region important for spindle pole localization. Asterisks indicate mutations resulting in loss of centrosome localization.

suggesting the tyrosine uses hydrophobic determinants to interact with a centrosomal target and does not require phosphorylation of this residue. The K1235E mutation also disrupted centrosome localization. Mutating the lysine to alanine (K1235A) had no affect on localization to the centrosome. Overall, these data implicate a highly conserved region within DTACC residues 1229 and 1241 that promotes centrosome localization.

Discussion

TACC family proteins have proven important structural components of the mitotic spindle apparatus. Disruption of TACC function causes disorganized and unstable spindle microtubules leading to multiple biological consequences including developmental problems and cancer (reviewed in Thakur et al., 2013). The mechanism in which TACC functions at the centrosome is still poorly understood. Our study aims to further the field of centrosome biology by understanding how TACC is interacting with its binding partners, specifically the XMAP215 family.

TACC family proteins are defined by the presence of a 200 amino acid conserved domain at the C-terminus predicted to be a coiled coil by secondary structure analysis (Figure 4-1). The N-termini of TACC family homologs are divergent and contain a range of domains (SPD repeats, Ser-Pro Azu-1 motifs, nuclear localization signals, and Aurora A phosphorylation sites) that contribute to non-mitotic functions (reviewed in Peset and Vernos, 2008). The *Drosophila* homolog, DTACC, has no reported conserved functional domains in the variable N-terminal region. This observation led us to test the localization of the N-terminal region for any distinct localization pattern (Figure 4-2C, E, top). The N-terminal region was cytoplasmic with no observed localization patterns in interphase or

mitosis. This does not rule out function in the N-terminal region as this domain could contribute to the regulation of TACC domain localization. Recent studies on the human homolog TACC3 and its binding partner ch-TOG showed an intra-molecular interaction between the central repeat region in the variable N-terminal domain and the second subdomain of the TACC domain (CC2, residues 530-630; Thakur et al., 2013). This data suggests an intra-molecular interaction prior to binding by other factors such as ch-TOG (Thakur et al., 2013). Sequence analysis of the N-terminal region of DTACC reveal a set of two repeats (residues 406-505 and 746-847). These repeat sequences contain approximately 32% identity and are highly charged with multiple glutamic and aspartic acid residues present. It would be interesting to examine whether this intra-molecular interaction is a conserved function of TACC proteins by testing the interaction of the repeats with the TACC domain in *Drosophila.*

Similar to previously published data, the *Drosophila* TACC domain alone can robustly localize to centrosomes (Figure 4-2D, bottom; Gergely et al., 2000; Peset et al., 2005). Faint plus-end localization was previously observed on astral microtubules during mitosis (Lee et al., 2001) however, little is known about TACC's localization in interphase due to cell-cycle dependent expression patterns. We observe DTACC's TACC domain localized robustly to MT plus-ends (Figure 4-2C, bottom) and tracking along growing MT plus ends (Figure 4-2D). While endogenous DTACC expression is specific to mitosis and is involved in Msps centrosome recruitment (Bellanger and Gonczy, 2003; Srayko et al., 2003; Sato et al., 2004; Conte et al., 2003; O'Brien et al., 2005; Kinoshita et al., 2005; Peset et al., 2005; Lee et al., 2001) we hypothesize that over-expression during interphase redirects DTACC's TACC domain constructs to growing MT plus-ends where Msps localizes. This

suggests two things: 1) that DTACC binding a centrosome factor or post-translationally modified factor specific to mitosis, and 2) that the DTACC-Msps interaction does not involve Msps residues that bind Sentin since Msps has sentin dependent MT plus-end localization. We tested this hypothesis by depleting S2 cells of Msps using RNAi and observed loss of the TACC domain at the MT plus-ends, confirming that TACC MT plus-end localization is downstream to Msps (Figure 4-2F). Current efforts in the lab aim to confirm the Msps-DTACC interaction observe in the cellular assays directly using biochemical analysis with purified components.

To analyze if the entire TACC domain coiled-coil is necessary for plus-end tracking or centrosome localization we systematically truncated the TACC domain and assayed for localization in both interphase and mitosis. We identified a minimal domain of the TACC domain that confers both plus-end and centrosome localization (Figure 4-3). Similar to the human homolog, TACC3, we notice a break point in the conservation (Figure 4-1B) and secondary structure prediction of DTACC's TACC domain. Compared to TACC3, DTACC residues 1064-1176 would correspond to CC1 and 1177-1304 to CC2 (Thakur et al., 2013). However, two reports on TACC3 suggest that the Msps binding domain is in the first half of the TACC domain (CC1 in Thakur et al., 2013; residues 654-713 in Hood et al., 2013). Our data conflicts with these reports; the N-terminal subdomain (1064-1176) of DTACC is cytoplasmic while the C-terminal subdomain (1177-1304) can track MT plus-ends implicating an interaction with Msps. This could either be a divergent interaction between DTACC and Msps unique to the *Drosophila* homolog or an interaction facilitated by an unidentified protein *in vivo*. To test whether this interaction is valid, we are currently using SEC-MALS with purified components to test for complex formation. Preliminary

experiments were performed using the TACC domain (residues 1064-1304) or the minimal Msps interaction domain (residues 1177-1304) and the putative TOG6 domain from Msps (residues 1596-1940) showed no interaction (Figure 4-S1). However, recent data from the Piekorz lab show the region of ch-TOG responsible for DTACC binding is a fragment C-terminal of the TOG6 domain that is not fully included in our Msps construct. We are designing Msps constructs that include this fragment and will test for interaction with both the whole TACC domain and the minimal tip-tracking domain 1177-1304.

The *Drosophila* TACC domain is a dimer in solution as shown by SEC-MALS (Figure 4-4). These data are in line with previously published work that TACC forms higher order oligomers (Gergely et al., 2000b; Thakur et al., 2013). The minimal tip-tracking domain confers dimerization while the subsequent N-terminal subdomain is monomeric in solution. The N-terminal subdomain could still dimerize in the context of the full-length TACC domain and the data would indicate the potential presence of a trigger sequence in the 1177-1304 construct. Triggers sequences are 13 residue consensus sequences (xxLExc-hxcxccx where x is any residue, c is a charged residue, and h is a hydrophobic residue) that can independently form a helical fold. When present this consensus sequence facilitates the formation of coiled-coils and, in some cases such as GCN4 and cortexillin I, are absolutely necessary for correct folding (Kammerer et al., 1998). No apparent trigger sequence has been identified in DTACC however there is potential for a divergent consensus sequence that is not easily recognized. Residues 1064-1176 could require the presence of this trigger sequence to form the predicted coiled-coil. In the context of the entire TACC domain, dimerization of 1177-1304 could induce dimerization of the first half of the domain, allowing for a more stable dimer and/or the correct positioning of factor binding interfaces.

Our mutational analysis of the minimal domain in DTACC shows a large region that spans upwards of 60 amino acids that is necessary for tip-tracking localization (Figure 4-5). There are three hypotheses as to what is causing loss of plus-end localization, the first being a loss of Msps binding interaction. The alternative hypotheses are 1) that the mutations disrupt the dimerization of the TACC domain, which could be necessary for factor binding or 2) the mutations cause misfolding or unstable proteins. To test these hypotheses, we are currently designing, cloning, and purifying mutated TACC constructs. Once purified, we will test these constructs for stability using Circular Dichroism (CD) and dimerization using SEC-MALS. Once we determine the region of Msps bound by DTACC, we will test DTACC mutant constructs for loss of complex formation using SEC-MALS. We were able to identify a highly conserve region in the TACC domain (residues 1230-1240) that facilitate factor binding to localize DTACC to the centrosome. Further analysis to identify the binding factor(s) is necessary to completely understand how DTACC is localized to the centrosome.

REFERENCES

1. Bellanger, J. M., and Gonczy, P. (2003). TAC-1 and ZYG-9 form a complex that promotes microtubule assembly in C. elegans embryos. Current Biology, 13(17), 1488-1498.

2. Conte, N., Delaval, B., Ginestier, C., Ferrand, A., Isnardon, D., Larroque, C., Prigent, C., Seraphin, B., Jacquemier, J., and Birnbaum, D. (2003). TACC1-chTOG-aurora A protein complex in breast cancer. Oncogene, *22*(50), 8102-8116.

3. Gergely, F., Kidd, D., Jeffers, K., Wakefield, J. G., and Raff, J. W. (2000a). DTACC: A novel centrosomal protein required for normal spindle function in the early drosophila embryo. The EMBO Journal, *19*(2), 241-252.

4. Gergely, F., Karlsson, C., Still, I., Cowell, J., Killmartin, J., and Raff, J.W. (2000b). The TACC domain identifies a family of centrosomal proteins that can interact with microtubules. Proceedings of the National Academy of Science of the United States of America, *97*(26), 14352-14357.

5. Kammerer, R.A., Schulthess, T., Landwehr, R., Lustig, A., Engel, J., Aebi, U., and Steinmetz, M.O. (1998). An autonomous folding unit mediates the assembly of two-stranded coiled coils. Proceedings of the National Academy of Science of the United States of America, *95*, 13419-13424.

6. Kinoshita, K., Noetzel, T. L., Pelletier, L., Mechtler, K., Drechsel, D. N., Schwager, A., Lee, M., Raff, J.W., and Hyman, A. A. (2005). Aurora A phosphorylation of TACC3/maskin is required for centrosome-dependent microtubule assembly in mitosis. The Journal of Cell Biology, *170*(7), 1047-1055.

7. Lee, M. J., Gergely, F., Jeffers, K., Peak-Chew, S. Y., and Raff, J. W. (2001). Msps/XMAP215 interacts with the centrosomal protein D-TACC to regulate microtubule behaviour. Nature Cell Biology, *3*(7), 643-649.

8. O'Brien, L. L., Albee, A. J., Liu, L., Tao, W., Dobrzyn, P., Lizarraga, S. B., and Wiese, C. (2005). The xenopus TACC homologue, maskin, functions in mitotic spindle assembly. Molecular Biology of the Cell, *16*(6), 2836-2847.

9. Peset, I., Seiler, J., Sardon, T., Bejarano, L. A., Rybina, S., and Vernos, I. (2005). Function and regulation of maskin, a TACC family protein, in microtubule growth during mitosis. The Journal of Cell Biology, *170*(7), 1057-1066.

10. Peset, I., and Vernos, I. (2008). The TACC proteins: TACC-ling microtubule dynamics and centrosome function. Trends in Cell Biology, *18*(8), 379-388.

11. Sato, M., Vardy, L., Angel Garcia, M., Koonrugsa, N., and Toda, T. (2004). Interdependency of fission yeast Alp14/TOG and coiled coil protein Alp7 in

microtubule localization and bipolar spindle formation. Molecular Biology of the Cell, *15*(4), 1609-1622.

12. Srayko, M., Quintin, S., Schwager, A., and Hyman, A. A. (2003). Caenorhabditis elegans TAC-1 and ZYG-9 form a complex that is essential for long astral and spindle microtubules. Current Biology*, 13*(17), 1506-1511.

13. Thakur, H. C., Singh, M., Nagel-Steger, L., Kremer, J., Prumbaum, D., Fansa, E. K., Ezzahoini, H., Nouri, K., Gremer, L., Abts, A., Schmitt, L., Raunser, S., Ahmadian, M.R., and Piekorz, R. P. (2014). The centrosomal adaptor TACC3 and the microtubule polymerase chTOG interact via defined C-terminal subdomains in an aurora-A kinase-independent manner. The Journal of Biological Chemistry, *289*(1), 74-88.

14. Thakur, H. C., Singh, M., Nagel-Steger, L., Prumbaum, D., Fansa, E. K., Gremer, L., Ezzohoini, H., Abts, A., Schmitt, L., Raunser, S., Ahmandian, M.R., and Piekorz, R. P. (2013). Role of centrosomal adaptor proteins of the TACC family in the regulation of microtubule dynamics during mitotic cell division. Biological Chemistry, *394*(11), 1411-1423.

SUPPLEMENTAL FIGURES

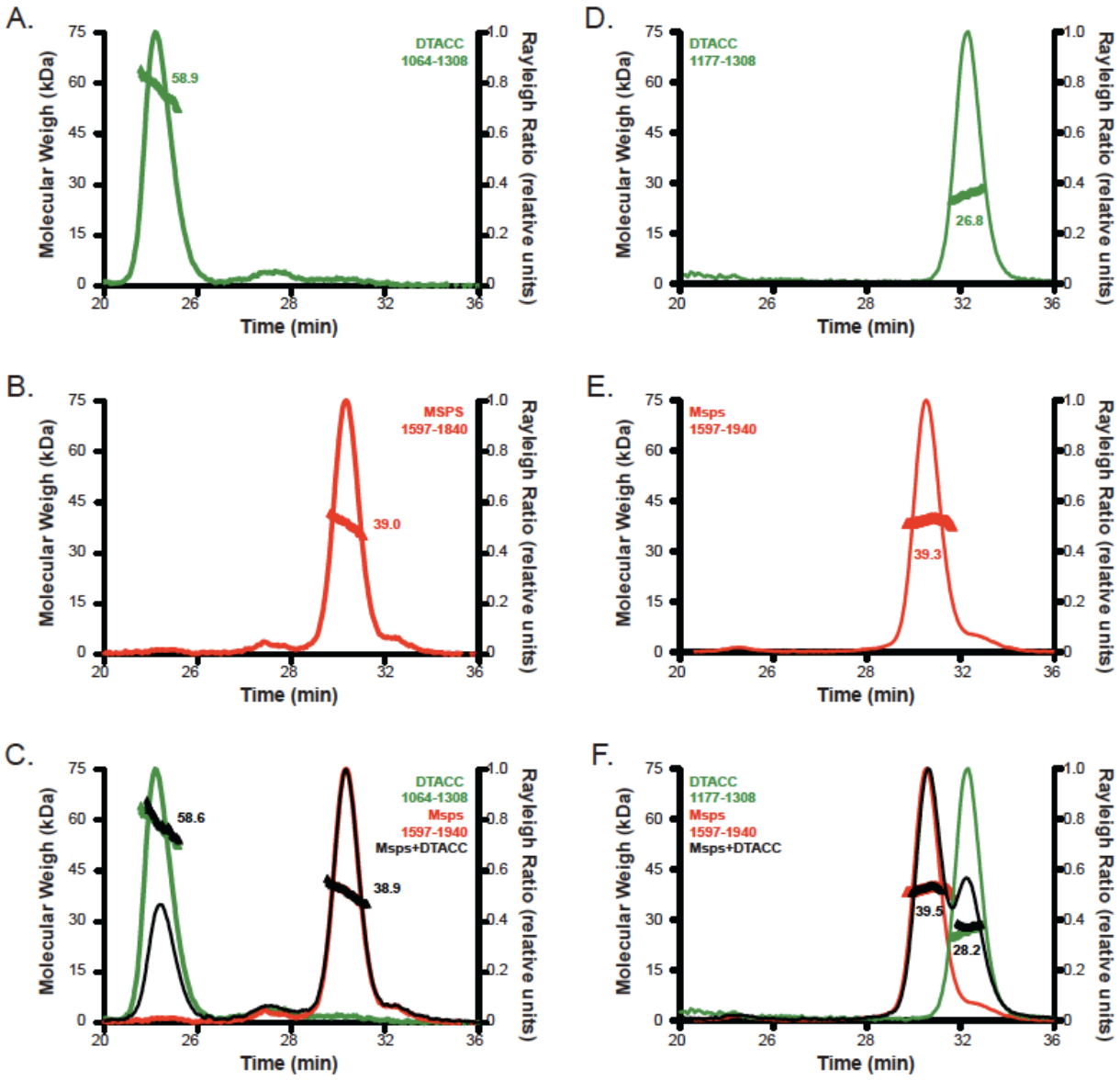

Figure 4-S1. The TACC domain does not interact with Msps through the putative TOG6 domain. SEC-MALS analysis. 100 µl of 145 µM *Drosophila* TACC domain (A), minimal domain 1177-1304 (B), and Msps putative TOG6 (residues 1594-1940) were analyzed at pH 7.5. Each peak shows the molecular weight of the protein. When incubated for complex formation, neither 1064-1304 nor 1177-1304 could interact with TOG6 indicated by no shift observed in the combined elution profiles.

CHAPTER 5: DISCUSSION AND FUTURE WORK

XMAP215 contains arrayed TOG domains that promote MT polymerization using a structurally distinct TOG array

XMAP215 family members are potent microtubule (MT) polymerases, with mutants displaying reduced MT growth rates and aberrant spindle morphologies. (Gard and Kirschner, 1987; Vasquez et al., 1994; Cullen et al., 1999; Tournebize et al., 2000; Kosco et al., 2001; Kawamura and Wasteneys, 2008; Kronja et al., 2009; Cassimeris et al., 2009; Zanic et al., 2013). TOG domain arrays, a defining feature of this protein family, have proven responsible for binding tubulin and promoting MT polymerization. However, there are many outstanding questions concerning mechanism in which this occurs. Do TOG domains functionally equivalently? How do they collectively operate to drive polymerization? Do TOG domain arrays bind multiple tubulin heterodimers? If so, how is the multivalent molecule's TOG array arranged to interact with the MT lattice and promote tubulin incorporation? To better understand the XMAP215 mechanism and to begin to address these questions we characterized structural and functional properties of individual and paired TOG domains within the *Drosophila* homolog, Msps.

Here, we determined the crystal structure of TOG4 from *Drosophila* Msps. This TOG4 structure architecturally departs from the structures of TOG domains solved to date of Stu2 TOG1, Stu2 TOG2, Msps TOG2, and Zyg-9 TOG3 (Al-Bassam et al., 2007; Slep and Vale, 2007; Ayaz et al., 2012), revealing a domain that predicts a novel engagement with α-

tubulin. We also present the structure of human ch-TOG TOG4, the first human TOG structure reported to date. This structure revealed that the differences observed in Msps TOG4 were conserved across species. This differential domain architecture indicates that the XMAP215 TOG array is structurally polarized, with position-dependent features conserved across species. Why TOG domains in the array would have different tubulin-binding modes may involve the recognition of different tubulin or MT structural states, differential tubulin binding affinities, and/or differential interactions with other tubulin/MT-binding proteins. To further support this hypothesis, structural analysis of the remaining TOG domains in the array (3 and 5) is needed. We hypothesize, based on our biochemical work, cellular analysis, and the conserved predicted tubulin binding determinants in TOG3's second HEAT repeat triad that TOG3 will exhibit a structure distinct from previously solved TOG domains and could be similar to our structure of TOG4. Attempts at crystallizing these domains are on going and will contribute greatly to our understanding of the polarized array. To date, we have no information on how TOG domains interact with one another or how architecturally distinct TOG domain arrays interact with tubulin heterodimers. Attempts to crystallize TOG1-2 constructs alone and in complex with multiple tubulin heterodimers are vital experiments to fully understand this protein's MT polymerization mechanism. Tubulin, however, has proven difficult to work with at a structural level due to its intrinsic ability to self-associate (Desai and Mitchison, 1997; Howard and Hyman, 2003). To address this caveat we are attempting to co-crystallize complexes with a *D*esigned *A*nkryin *R*epeat *P*rote*in* (DARPin) that has been used to crystallize tubulin in previous studies. DARPin binds β-tubulin outside of the TOG binding region and prevents longitudinal interactions of tubulin heterodimers (Pecquer et al., 2012).

In agreement with our observed structural differences, our *in vitro* assays show differential tubulin/MT-binding affinities across the TOG array, as well as differential effects on MT nucleation and polymerization. Previous work analyzing Msps TOG1 and TOG2 found that individual TOG domains show no detectable tubulin-binding over gel filtration, however a TOG1-2 construct does bind tubulin. This finding suggests that a multivalent TOG array enhances the TOG-tubulin interaction, potentially by promoting cooperative lateral or longitudinal tubulin-tubulin contacts (Slep and Vale, 2007). Surprisingly TOG3-4 exhibited no detectable binding by gel filtration. However, previous work suggests TOG3 and TOG4 do potentiate tubulin binding in the context of the TOG array (Widlund et al., 2011) and we showed that TOGs 3-4 contribute to MT lattice binding in cells. Together this data suggests a differential tubulin affinity that is tuned in the context of the full length molecule to recognized non-polymerized tubulin and/or MT lattice structures, process along the MT, and efficiently incorporate tubulin heterodimers into a polymerizing MT. Our *in vitro* polymerization assay supports the hypothesis of tuned affinities: TOG3-4 can rapidly induce MT polymerization *in vitro* while the higher affinity TOG1-2 requires a 11 amino acid linker extension that could potentiate a MT lattice association to work in concert with the TOG domains to drive MT polymerization. The structure of Stu1 TOG1 shows a polarized interaction with tubulin where the N-terminal TOG domain is positions towards the plus end (Ayaz et al., 2012) Together with our data, this suggests a polarized TOG arrangement the N-terminal TOG domains towards the plus end and C-terminal TOG domains just distal to the MT tip (Figure 3-S6). Future experiments that examine the role and contribution of the linker regions that bridge TOG domains in the MT polymerization mechanism will provide critical insight. Previous studies have shown that these inter-TOG linkers are important for MT

lattice binding (Currie et al., 2012, Widlund et al., 2011) however little is known about how they interact with tubulin. Is this interaction direct or is it facilitated by other binding factors? As a first step, purified TOG constructs that contain linker regions can be tested for MT-binding using cosedimentation assays with taxol stabilized MTs and for binding to free tubulin by gel filtration. It would also be interesting to investigate whether TOG domains and/or their linkers have a preference for differential tubulin structure. In addition to taxol-stabilized MTs, cosedimentation assays can be performed with dynamic MTs, GTPγS MTs, GMPCPP-stabilized MTs or curled MT protofilaments to assess a structural preference. Gel filtration can also be performed with GDP tubulin or in the presence of colchicine, which induces a kink in tubulin heterodimers.

An XMAP215 mechanism involving a polarized TOG array bound to a polymerizing MT plus-end likely engages differential TOG binding functions. These function can range from MT lattice binding activity and nucleation, to the binding of free tubulin and potentiating its stable incorporation into the MT lattice by templating and/or lowering the tubulin heterodimer's off-rate of at the MT plus end. We showed using cellular MT polymerization assays that TOG domains work in an array: mutating predicted tubulin binding determinants in a TOG1-4 array results in diminished rescue activity observed with wild type constructs. Of note, mutating TOG4 in the array was the least dramatic mutation again highlighting the importance of a functional, continuous, TOG array, that polymerization activity is polarized from the N-terminal TOG domains, and that larger, contiguous functional TOG arrays enhance MT polymerization rates. Repeating this mutational analysis in the context of the full-length protein is a future direction pursued by the lab. Key experiments in the future could include constructs that replace or rearrange the

TOG domains. We hypothesize that disturbing the polarized, tuned array would be detrimental to the function of the protein and would result in a completely different effect on MT dynamics than the wild type array.

When compared to other models in the XMAP215 field, our model favors those proposed by the Rice and Hyman labs. The Rice lab proposes a "conformation selective" mechanism in which TOG domains can sense tubulin conformations: Stu2 TOG1 binds free, unpolymerized tubulin and loses affinity once it is incorporated into the lattice while TOG2 may bind a plus-end specific conformation (Ayaz et al., 2012). Based on our biochemical data TOGs 1-2 can recognize free tubulin similar to Stu2 TOG1 whereas TOGs 3-4 could be recognizing and stabilizing a MT plus-end specific population. The Hyman lab also showed the necessity for multiple TOG domains in an array to efficiently promote MT polymerization as shown in our cellular assays (Widlund et al., 2011). They show that polymerization requires a lattice-binding region in the linker between 4 and 5. This lattice binding could be enhanced by the presence of TOGs 3 and 4 and their recognition of a plus-end specific feature. Our structure of TOG4 from *Drosophila* and human XMAP215 members suggests that TOG domains bind tubulin in a similar fashion based on the conserved contacts with β-tubulin and at the α/β interface. This would rule out a 'wrap-around' mechanism of XMAP215: tubulin binding. In that model, multiple TOG domains (hypothesized to be four) bind around a single tubulin heterodimer and incorporate it into the lattice (Al-Bassam and Chang, 2011). This model would require the latter TOG domains, specifically TOGs 3 and 4, to bind a completely different face of the tubulin heterodimer. Our model of Msps TOG4 bound to tubulin suggests this is not in fact happening and that TOG domains bind tubulin in the same orientation as observed in the Stu2: tubulin structure.

In conclusion, our work here highlights key features of the XMAP215 TOG array that further our mechanistic understanding of this critical MT regulator. First, TOG domains function in an array to promote MT polymerization. Second, TOG domains in the array have different structures but are positionally conserved. Third, TOG domains in the array have different affinities for tubulin heterodimers and different MT nucleation activities. Collectively, this suggests that TOG domains, in general, mobilize an array-based mechanism to regulate MT dynamics and that differential TOG architecture in the array is likely positioned to differentially interact with free tubulin and the MT lattice to collectively drive MT polymerization.

The DTACC TACC domain is a dimer that confers MT plus-end and centrosome localization

TACC family proteins are important structural components of the mitotic spindle apparatus contributing to MT organization and stabilization. Disruption of TACC function causes disorganized and unstable spindle microtubules leading to multiple biological consequences including chromosome instability, developmental problems, and cancer (reviewed in Thakur et al., 2013). The mechanism in which TACC functions at the centrosome is poorly understood. Our study aims to further the field of centrosome biology by understanding how TACC interacts with its binding partners, specifically XMAP215 family members.

Here we have shown that similar to previously published data, the *Drosophila* TACC domain alone can robustly localize to centrosomes (Figure 4-2D, bottom; Gergely et al., 2000; Peset et al., 2005) and localized to the MT plus-end (Lee et al., 2001). The entire N-terminal region (residues 1-1063), however, was cytoplasmic with no observed localization

patterns in interphase or mitosis. This does not rule out function in the N-terminal region as this domain could contribute to the regulation of TACC domain localization. Recent studies on the human homolog TACC3 and its binding partner ch-TOG showed an intra-molecular interaction between the central repeat region in the variable N-terminal domain and the second subdomain of the TACC domain (CC2, residues 530-630; Thakur et al., 2013). This data suggests an intra-molecular interaction prior to binding by other factors such as ch-TOG (Thakur et al., 2013). Sequence analysis of the N-terminal region of DTACC reveal a set of two repeats (residues 406-505 and 746-847). These repeat sequences contain approximately 32% identity and are highly charged with multiple glutamic and aspartic acid residues present. It would be interesting to examine whether this intra-molecular interaction is a conserved function of TACC proteins by testing the ability of these repeats to interact with the *Drosophila* TACC domain. Experiments could include purification of purified components and analysis by SEC-MALS or biochemical analysis by immunoprecipitation.

Here, we have identified a minimal domain of the *Drosophila* TACC family member, DTACC, that confers TACC localization to spindle poles in mitosis and tracks along the MT plus-end potentially through an interaction with the XMAP215 family member Msps in interphase. While endogenous DTACC expression is specific to mitosis and is involved in Msps centrosome recruitment (Bellanger and Gonczy, 2003; Srayko et al., 2003; Sato et al., 2004; Conte et al., 2003; O'Brien et al., 2005; Kinoshita et al., 2005; Peset et al., 2005; Lee et al., 2001) we hypothesize that over-expression during interphase redirects DTACC's TACC domain constructs to growing MT plus-ends where Msps localizes. We show through Msps depletion that the TACC MT plus-end localization is downstream of Msps and our mutational analysis of DTACC residues 1177-1304 shows a large region that spans upwards

of 60 amino acids that is necessary for tip-tracking localization (Figure 4-5). To test whether this interaction is valid, SEC-MALS experiments with purified components are necessary to test for complex formation. Preliminary experiments were performed using the TACC domain (residues 1064-1304) or the minimal Msps interaction domain (residues 1177-1304) and the putative TOG6 domain from Msps (residues 1596-1940), which showed no interaction (Figure 4-S1). However, recent data from the Piekorz lab indicate that the ch-TOG region responsible for TACC binding is a fragment C-terminal of the putative TOG6 domain that was not included in our Msps construct. We are designing Msps constructs that include this fragment and will test for interaction with both the whole TACC domain and the minimal tip-tracking domain 1177-1304. It is also important to test our mutant constructs *in vitro* to determine whether we are disrupting factoring binding or protein dimerization. Currently, penetrant mutants that ablate TACC MT plus end tracking activity have been cloned into bacterial expression vectors and we are in the process of expressing and purifying these constructs. Once purified, we will perform CD analysis to determine if these mutations disrupt domain structure and thermostability as well as SEC-MALS to determine if homodimerization state has been compromised.

In addition to future structural and biochemical experiments, there are multiple questions that can be addressed using cell biology. Our cellular analysis to date has just looked at DTACC localization patterns and hasn't fully addressed function during mitosis. Work in the lab has begun quantifying mitotic phenotype associated with DTACC knock down in *Drosophila* S2 cells. We know our truncation constructs are sufficient for localization, however it would be interesting to assay whether they can rescue aberrant spindle phenotypes. There is conflicting data in the literature about Aurora A

phosphorylation and its necessity in recruitment and/or factor binding (Booth et al., 2011, Thakur et a, 2013). Our constructs do not contain the Aurora A phosphorylation sites, suggesting phosphorylation is not necessary for localization but it could still play a role in function. We have generated extended TACC domain constructs that include the Aurora A site and will test them in the context of mitotic phenotype rescue. Another outstanding question arises from the observation that the TACC domain decorates the entire spindle whereas the minimal domain only goes to centrosomes. Residues within the first half of the TACC domain may contribute this observed localization and will need further experimentation to determine what is responsible for this localization pattern. There is also little known of TACC's centrosome binding factors. Yeast two hybrid analysis can be performed to test for DTACC interactions with known centrosome proteins and would further our understanding of TACC recruitment to the centrosome. In addition, Msps function at the centrosome is poorly understood and tying in what we learned of the XMAP215 mechanism in our structural studies will be vital to this understanding. We know that the MT polymerization action of TOG domains is important to spindle morphology, particularly the pole-to-pole length (Brittle and Ohkura, 2005). We can begin to analyze Msps function at the centrosome using a similar mutational analysis as performed in interphase. We can artificially localize TOG domains to the centrosome by creating fusion constructs with the TACC domain or other centrosome binding domains, introduce our mutations, and analyze spindle morphology including spindle length and organization.

Concluding remarks

XMAP215 and DTACC family members are important regulators of MT dynamics.

Microtubules play essential roles in basic cellular functions, especially in cell migration and cell division. Cell migration is a complex process involved in embryonic development, repair and regrowth of damaged tissue, and progression of disease. In the early stages of life, cell migration is necessary for the development of the heart and circulatory system and failure of migration can lead to congenital heart defects. Later in life, cell migration can cause atherosclerotic plaques, a defining feature of a common fatal disease in Americans, atherosclerosis. Cancers can also be caused by the misregulation of MT dynamics or disruption of cell division as apparent with the human member of the XMAP215 family, ch-TOG that was identified as a gene that was over-expressed in colonic tumors (Charrasse, 1995) and the human member of the TACC family, TACC1 that was identified as a gene overexpressed in breast cancer (Still et al., 1999). Aberrant cell division can result in genomic instability, therefore leading to cancerous cell types. Disrupted MT dynamics can lead to both unregulated cell division and unregulated cellular migration, collectively contributing to metastatic cancer. A structural understanding of XMAP215 and TACC family function will be key in determining how MAPs mechanistically regulate MT dynamics in both mitosis and interphase, ultimately contributing to the overall understanding and treatment of such diseases.

REFERENCES

1. Al-Bassam, J., Larsen, N. A., Hyman, A. A., and Harrison, S. C. (2007). Crystal structure of a TOG domain: Conserved features of XMAP215/Dis1-family TOG domains and implications for tubulin binding. Structure, *15*(3), 355-362.

2. Al-Bassam, J., and Chang, F. (2011). Regulation of microtubule dynamics by TOG-domain proteins XMAP215/Dis1 and CLASP. Trends in Cell Biology, *21*(10), 604-614.

3. Ayaz, P., Ye, X., Huddleston, P., Brautigam, C.A., and Rice, L.M. (2012). A TOG:alphabeta-tubulin complex structure reveals conformation-based mechanisms for a microtubule polymerase. Science, *337*, 857-860.

4. Bellanger, J. M., and Gonczy, P. (2003). TAC-1 and ZYG-9 form a complex that promotes microtubule assembly in C. elegans embryos. Current Biology, *13*(17), 1488-1498.

5. Booth, D., G., Hood, F.E., Prior, I.A., and Royale, S.J. (2011). A TACC3/ch-TOG/clathrin complex stabilises kinetochore fibres by inter-microtubule bridging. The EMBO Journal, *30*, 906-919.

6. Brittle, A. L., and Ohkura, H. (2005). Minispindles, the XMAP215 homologue, suppresses pausing of interphase microtubules in drosophila. The EMBO Journal, *24*(7), 1387-1396.

7. Cassimeris, L., Becker, B., and Carney, B. (2009). TOGp regulates microtubule assembly and density during mitosis and contributes to chromosome directional instability. Cell Motililty and the Cytoskeleton, *66*, 535-545.

8. Charrasse, S., Schroeder, M., Gauthier-Rouviere, C., Ango, F., Cassimeris, L., Gard, D.L., and Larroque, C. (1998). The TOGp protein is a new human microtubule-associated protein homologous to the Xenopus XMAP215. Journal of Cell Science, *111* (Pt 10), 1371-1383.

9. Conte, N., Delaval, B., Ginestier, C., Ferrand, A., Isnardon, D., Larroque, C., Prigent, C., Seraphin, B., Jacquemier, J., and Birnbaum, D. (2003). TACC1-chTOG-aurora A protein complex in breast cancer. Oncogene, *22*(50), 8102-8116.

10. Cullen, C. F., Deak, P., Glover, D. M., and Ohkura, H. (1999). Mini spindles: A gene encoding a conserved microtubule-associated protein required for the integrity of the mitotic spindle in drosophila. The Journal of Cell Biology, *146*(5), 1005-1018.

11. Currie, J.D., Stewman, S., Schimizzi, G., Slep, K.C., Ma, A., and Rogers, S.L. (2011). The microtubule lattice and plus-end association of Drosophila Mini spindles is

spatially regulated to fine-tune microtubule dynamics. Molecular Biology of the Cell, *22*, 4343-4361.

12. Desai, A., and Mitchison, T. J. (1997). Microtubule polymerization dynamics. Annual Review of Cell and Developmental Biology, *13*, 83-117.

13. Gard, D. L., and Kirschner, M. W. (1987). A microtubule-associated protein from xenopus eggs that specifically promotes assembly at the plus-end. The Journal of Cell Biology, *105*(5), 2203-2215.

14. Howard, J., and Hyman, A. A. (2003). Dynamics and mechanics of the microtubule plus end. Nature, *422*(6933), 753-758.

15. Kawamura, E., and Wasteneys, G.O. (2008). MOR1, the Arabidopsis thaliana homologue of Xenopus MAP215, promotes rapid growth and shrinkage, and suppresses the pausing of microtubules in vivo. Journal of Cell Science, *121*, 4114-4123.

16. Kinoshita, K., Noetzel, T. L., Pelletier, L., Mechtler, K., Drechsel, D. N., Schwager, A., Lee, M., Raff, J.W., and Hyman, A. A. (2005). Aurora A phosphorylation of TACC3/maskin is required for centrosome-dependent microtubule assembly in mitosis. The Journal of Cell Biology, *170*(7), 1047-1055.

17. Kosco, K.A., Pearson, C.G., Maddox, P.S., Wang, P.J., Adams, I.R., Salmon, E.D., Bloom, K., and Huffaker, T.C. (2001). Control of microtubule dynamics by Stu2p is essential for spindle orientation and metaphase chromosome alignment in yeast. Molecular Biology of the Cell, *12*, 2870-2880.

18. Kronja, I., Kruljac-Letunic, A., Caudron-Herger, M., Bieling, P., and Karsenti, E. (2009). XMAP215-EB1 interaction is required for proper spindle assembly and chromosome segregation in Xenopus egg extract. Molecular Biology of the Cell, *20*, 2684-2696.

19. Lee, M. J., Gergely, F., Jeffers, K., Peak-Chew, S. Y., and Raff, J. W. (2001). Msps/XMAP215 interacts with the centrosomal protein D-TACC to regulate microtubule behavior. Nature Cell Biology, *3*(7), 643-649.

20. O'Brien, L. L., Albee, A. J., Liu, L., Tao, W., Dobrzyn, P., Lizarraga, S. B., and Wiese, C. (2005). The xenopus TACC homologue, maskin, functions in mitotic spindle assembly. Molecular Biology of the Cell, *16*(6), 2836-2847.

21. Pecqueur, L., Duellberg, C., Dreier, B., Jiang, Q.Y., Wang, C.G., Pluckthun, A., Surrey, T., Gigant, B., and Knossow, M. (2012). A designed ankyrin repeat protein selected to bind to tubulin caps the microtubule plus end. Proceedings of the National Academy of Science of the United States of America, *109*, 12011-12016.

22. Peset, I., Seiler, J., Sardon, T., Bejarano, L. A., Rybina, S., and Vernos, I. (2005). Function and regulation of maskin, a TACC family protein, in microtubule growth during mitosis. The Journal of Cell Biology, *170*(7), 1057-1066.

23. Sato, M., Vardy, L., Angel Garcia, M., Koonrugsa, N., and Toda, T. (2004). Interdependency of fission yeast Alp14/TOG and coiled coil protein Alp7 in microtubule localization and bipolar spindle formation. Molecular Biology of the Cell, *15*(4), 1609-1622.

24. Slep, K. C., and Vale, R. D. (2007). Structural basis of microtubule plus end tracking by XMAP215, CLIP-170, and EB1. Molecular Cell, *27*(6), 976-991.

25. Srayko, M., Quintin, S., Schwager, A., and Hyman, A. A. (2003). Caenorhabditis elegans TAC-1 and ZYG-9 form a complex that is essential for long astral and spindle microtubules. Current Biology*, 13*(17), 1506-1511.

26. Still, I. H., Hamilton, M., Vince, P., Wolfman, A., and Cowell, J. K. (1999). Cloning of TACC1, an embryonically expressed, potentially transforming coiled coil containing gene, from the 8p11 breast cancer amplicon. Oncogene, *18*(27), 4032-4038.

27. Thakur, H. C., Singh, M., Nagel-Steger, L., Prumbaum, D., Fansa, E. K., Gremer, L., Ezzohoini, H., Abts, A., Schmitt, L., Raunser, S., Ahmandian, M.R., and Piekorz, R. P. (2013). Role of centrosomal adaptor proteins of the TACC family in the regulation of microtubule dynamics during mitotic cell division. Biological Chemistry, *394*(11), 1411-1423.

28. Tournebize, R., Popov, A., Kinoshita, K., Ashford, A.J., Rybina, S., Pozniakovsky, A., Mayer, T.U., Walczak, C.E., Karsenti, E., and Hyman, A.A. (2000). Control of microtubule dynamics by the antagonistic activities of XMAP215 and XKCM1 in Xenopus egg extracts. Nature Cell Biology, *2*, 13-19.

29. Vasquez, R.J., Gard, D.L., and Cassimeris, L. (1994). XMAP from Xenopus eggs promotes rapid plus end assembly of microtubules and rapid microtubule polymer turnover. The Journal of Cell Biology, *127*, 985-993.

30. Widlund, P.O., Stear, J.H., Pozniakovsky, A., Zanic, M., Reber, S., Brouhard, G.J., Hyman, A.A., and Howard, J. (2011). XMAP215 polymerase activity is built by combining multiple tubulin-binding TOG domains and a basic lattice-binding region. Proceedings of the National Academy of Science of the United States of America, *108*, 2741-2746.

31. Zanic, M., Widlund, P.O., Hyman, A.A., and Howard, J. (2013). Synergy between XMAP215 and EB1 increases microtubule growth rates to physiological levels. Nature Cell Biology, *15*, 688-693.